# Proceedings of the I·R·E

AUGUST 1942

VOLUME 30 NUMBER 8



Institute of Radio Engineers


## There are many ways of choosing a transformer ...there are *even more ways of making one*

Where a stock item can do the job, by all means standardize. (The UTC catalogue covers over four hundred types.) *But*, the ideal transformer for a specific job doesn't just happen...it's designed. For example, after extensive development, UTC reduced the weight of an important aircraft item over 90%. *Let UTC design a unit to your specific problem.*

## *There is no substitute for engineering skill*

# UNITED TRANSFORMER CO.

150 VARICK STREET ★ NEW YORK, N. Y.

EXPORT DIVISION: 100 VARICK STREET NEW YORK, N. Y. CABLES: "ARLAB"

# Proceedings *of the* I·R·E

*Published Monthly by*
The Institute of Radio Engineers, Inc.

VOLUME 30 — *August, 1942* — NUMBER 8





Entered as second-class matter October 26, 1927, at the post office at Menasha, Wisconsin, under the Act of February 28, 1925, embodied in Paragraph 4, Section 538 of the Postal Laws and Regulations. Publication office, 450 Ahnaip Street, Menasha, Wisconsin. Editorial and advertising offices, 330 West 42nd St., New York, N. Y. Subscription, $10.00 per year; foreign, $11.00.

# THE INSTITUTE OF RADIO ENGINEERS
INCORPORATED

## New York Meeting—September 2, 1942

### SECTIONS

**ATLANTA**—Chairman, J. M. Comer; Secretary, G. V. Waldo, 3166 Peachtree Dr., N. E., Atlanta, Ga.

**BALTIMORE**—Chairman, V. D. Hauck; Secretary, G. J. Gross, Pa. Water & Power Co., 1611 Lexington Bldg., Baltimore, Md.

**BOSTON**—Chairman, J. M. Henry; Secretary, R. O. Oberg, Northeastern Univ., Boston, Mass.

**BUENOS AIRES**—Chairman, J. P. Arnaud; Secretary, Alexander Nadosy, Florida St. 1065, Dept. C-6, Buenos Aires, Argentina.

**BUFFALO-NIAGARA**—Chairman, F. H. Scheer; Secretary, Arnold Bartels, Colonial Radio Corp., 254 Rano St. Buffalo, N. Y.

**CHICAGO**—Chairman, R. A. Kay; Secretary, Walter Kenworth, 5505 Potomac Ave., Chicago, Ill.

**CINCINNATI**—Chairman, W. L. Schwesinger; Secretary, Howard Leppele, 4432 Raceview Ave., Cincinnati, Ohio.

**CLEVELAND**—Chairman, P. L. Hoover; Secretary, A. S. Nace, 3209 Archwood Ave., Cleveland, Ohio.

**CONNECTICUT VALLEY**—Chairman, F. G. Webber; Secretary, C. I. Bradford, 187 Glenarden Dr., Fairfield, Conn.

**DALLAS-FORT WORTH**—Chairman, Truett Kimzey; Secretary, P. C. Barnes, Radio Station WFAA-WBAP, Grapevine, Texas.

**DETROIT**—Chairman, M. Cottrell; Secretary, Paul Frincke, 26686 Kenwood Ave., Royal Oak, Michigan.

**EMPORIUM**—Chairman, R. K. Gessford; Secretary, H. D. Johnson, Hygrade Sylvania Corp., Emporium, Pa.

**INDIANAPOLIS**—Chairman, S. E. Benson; Secretary, B. H. Rinehart, 1920 Park Ave., Indianapolis, Ind.

**KANSAS CITY**—Chairman, H. K. Morgan; Secretary G. L. Taylor, Midland Radio School Power and Light Building, Kansas City, Mo.

**LOS ANGELES**—Chairman, C. F. Wolcott; Secretary, E. S. Sievers, Room 567, 417 S. Hill St., Los Angeles, Calif.

**MONTREAL**—Chairman, J. A. Ouimet; Secretary, J. R. Bain, Dept. 912, Northern Electric Co., 1231 Shearer St., Monteal, Que., Canada.

**PHILADELPHIA**—Chairman, C. C. Chambers; Secretary, R. L. Snyder, 103 Franklin Rd., Glassboro, N. J.

**PITTSBURGH**—Chairman, D. A. Myer; Secretary, A. P. Sunnergren, West Penn Power Co., 14 Wood St., Pittsburgh, Pa.

**PORTLAND**—Chairman, R. W. Deardorff; Secretary, B. R. Paul, 5960 S. W. 41st. Ave., Portland, Ore.

**ROCHESTER**—Chairman, O. L. Angevine, Jr.; Secretary, G. R. Town, Stromberg-Carlson Tel. Mfg. Co., Rochester, N. Y.

**ST. LOUIS**—Chairman, O. S. McDaniel; Secretary, H. D. Seielstad, 1017 S. Berry Rd., St. Louis, Mo.

**SAN FRANCISCO**—Chairman, H. E. Held; Secretary, W. G. Wagener, Heintz and Kaufman, South San Francisco, Calif.

**SEATTLE**—Chairman, K. H. Ellerbeck; Secretary, J. F. Johnson, 4316 Whitman Ave., Seattle, Wash.

**TORONTO**—Chairman, T. S. Farley; Secretary, L. C. Simmonds, A. C. Simmonds and Sons, 301 King St., E., Toronto, Ont., Canada.

**TWIN CITIES**—Chairman, R. E. Allison; Secretary, A. G. Peck, Twin-Cities Studios, Columbia Broadcasting System, 625 Second Ave., S., Minneapolis, Minn.

**WASHINGTON**—Chairman, E. M. Webster; Secretary, J. D. Wallace, Radio Division U. S. Naval Research Laboratory, Anacostia Station, D. C.

# Recording and Reproducing Standards*

LYNNE C. SMEBY†, MEMBER, I.R.E.

***Summary***—*The general absence of standards for transcription recording and reproducing for broadcasting has resulted in the use of as many as 10 equalizing networks by some stations. The National Association of Broadcasters has co-ordinated the work of a special committee, consisting of representatives of interested organizations, which has prepared and adopted a series of standards covering recording characteristics, mechanical dimensions of turntables, records, and grooves; rotational speeds, and minimum data for labels.*

As broadcasting has developed, the problem of reproducing transcriptions with uniform results has become of much concern to broadcast stations. Quite a number of different characteristics have been used by the various manufacturers of transcriptions, recording equipment, and reproducing equipment. Most of these characteristics produce good results by themselves with the proper playback equalization. The Engineering Committee of the National Association of Broadcasters early last year sent a questionnaire on recording to all stations. Among other interesting data obtained was the fact that some stations use as many as ten different equalizers. The NAB Engineering Committee recommended to its Board of Directors that NAB co-ordinate the work of a committee to be formed for the purpose of establishing recording and reproducing standards. The Board of Directors approved of this procedure and early in June, 1941, Neville Miller, President of the NAB, invited all companies interested in recording to a meeting to be held on June 26, 1941, in Detroit. Some twenty companies responded by sending representatives to the meeting. The Recording and Reproducing Standards Committee was formed at that time. The committee drew up a set of rules and regulations for conduct of the work. The committee also at that time formulated a list of the items that should be considered for standardization. In order to supervise and expedite the work, an Executive Committee of five members was appointed.

The Executive Committee was instructed to recommend standards on items that require little or no special study. It also was instructed to recommend a line of procedure for standardization on all other items. Between the first and second meetings of the main committee the Executive Committee held numerous meetings and made good progress with its work. The Executive Committee reported to the main committee at a meeting held in New York City on October 23, 1941. The main committee with minor changes adopted as standards or recommended good engineering practice sixteen of the items proposed by the Executive Committee. The committee decided to divide the remaining items between four subcommittees for further study. Since October 23 the Executive Committee and the subcommittees have held numerous meetings and have made good progress. The war effort, however, has seriously decreased the speed of the work. It was felt by the committee that it should not delay application of the sixteen standards already adopted, and therefore they are being submitted to the industry at this time.

There are presented below the sixteen standards as already adopted by NAB. The membership of the Recording and Reproducing Standards Committee, totaling 77 individuals, is practically all inclusive so far as those who are interested in recording is concerned. It is of interest to note that the Research Council of the Academy of Motion Picture Arts and Sciences, and the Canadian Broadcasting Corporation have exhibited interest in this project to the extent that they are members of the committee. Also of interest is the fact that the British Broadcasting Corporation and the Amalgamated Wireless (Australasia), Limited, of Australia have requested information on the project.

The Recording and Reproducing Standards Committee is working to complete additional standards. A supplement to the attached standards will be issued at such time as additions are made. The members of the committee have exhibited a fine spirit of co-operation, and many of them have devoted a considerable amount of time to the project. Several companies, which have standards of their own that produce excellent results, have modified their practices to adhere to the standards at considerable expense to themselves. This spirit of co-operation has produced excellent results so far, and undoubtedly will lead to further standardization of remaining items still under study by the committee.

## Technical Standards and Good Engineering Practices of the National Association of Broadcasters for Electrical Transcriptions and Recordings for Radio Broadcasting

### 1. Outer Diameters

It shall be standard that the outer record diameter fall within the limits specified in the following table:

| Nominal | Finished Records (Pressings or Instantaneous) | Lacquer Originals for Process |
|---|---|---|
| 16″ | 15-15/16″ ± 3/32″ | 17 1/4″ ± 1/16″ |
| 12″ | 11 7/8″ ± 1/32″ | 13 1/4″ ± 1/16″ |
| 10″ | 9 7/8″ ± 1/32″ | 11 1/4″ Minimum |

* Decimal classification: 621.385.97×R550. Original manuscript received by the Institute, May 11, 1942.

† Chairman, Recording and Reproducing Standards Committee; formerly, Director of Engineering, National Association of Broadcasting, Washington, D. C.

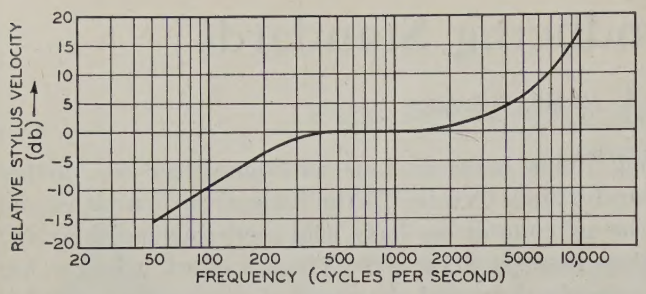


Fig. 1—Recording characteristics for vertical transcriptions. Stylus velocity—frequency. Tolerance, ±2 decibels.

2. Center Hole Diameter

It shall be standard that the record center hole diameter be 0.286″ ±0.001″.

3. Turntable Center Pin Diameter

It shall be standard that the diameter of the center pin of a transcription turntable be 0.2835″ ±0.0005″.

4. Outermost Groove Diameter

It shall be standard that the diameter of the outermost groove be within the limits specified in the following table:

16″—outside start 15 1/2″ ±1/16″
16″—inside start 15 9/16″ maximum
12″—outside start 11 1/2″ ±0.020″
10″—outside start 9 1/2″ ±0.020″

5. Innermost Groove Diameter

It shall be standard that the diameter of the innermost groove shall be not less than 7 1/2″ in the case of 33 1/3 revolution-per-minute records and not less than 3 3/4″ in the case of 78-revolution-per-minute records.

6. Uniformity of Groove Spacing

It shall be standard that the recorded grooves on a record shall be so spaced that at no point (except the concentric stopping groove) does the pitch deviate from the mean groove pitch by more than 5 per cent.

7. Stopping Groove

It shall be standard that at the termination of the recording groove spiral a locked concentric stopping groove shall be provided.

8. Number of Blank Grooves

It shall be standard that the number of blank grooves before modulation occurs shall be not less than two complete revolutions nor more than four, exclusive of any starting spiral.

9. Recording Turntable Speed (Revolutions per Minute)

It shall be standard that the mean speed of the recording turntable be either 33 1/3 or 78.26 revolutions per minute ±0.5 per cent.

10. Wow Factor

It shall be standard that the maximum instantaneous deviation from the mean speed of the recording turntable, when making the recording, shall not exceed ±0.1 per cent of the mean speed.

11. Record Warp

It shall be standard that the maximum departure of the surface of a record from a true plane because of warping shall not be in excess of 1/16″.

12. Minimum Label Information

It shall be standard for the label of a recording to contain at least the following technical information:

a. Type of recording—vertical or lateral
b. Speed—78.26 or 33 1/3
c. Direction of feed (start)—outside-in or inside-out
d. Recording frequency characteristic

13. Frequency Characteristic for Vertical Recording

It shall be standard that the recorded frequency characteristic on vertically recorded records be as shown in Fig. 1.

14. Frequency Characteristic for Lateral Recording

It shall be standard that the recorded frequency characteristic on laterally recorded records be as shown in Fig. 2.

15. Starting Spiral Grooves per Inch

It shall be good engineering practice in recordings having a starting spiral to use a rate of eight grooves per inch for the spiral. (Tolerance ±2 grooves per inch.)

16. Recording Grooves per Inch

It shall be good engineering practice to use numbers of grooves per inch in recording as follows: 96, 104, 112, 120, 128, 136, etc., in increments of eight. (Tolerance ±2 grooves per inch.)

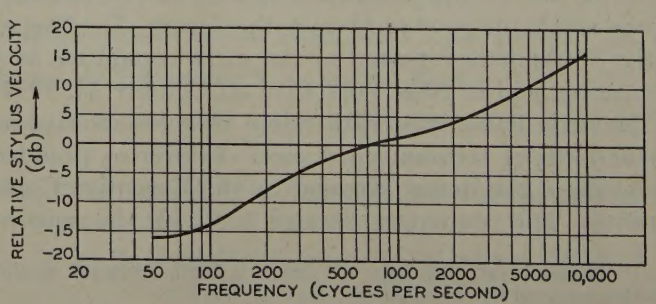


Fig. 2—Recording characteristic for lateral transcriptions. Stylus velocity—frequency. Tolerance, ±2 decibels.

# Aircraft Antennas*

GEORGE L. HALLER†, MEMBER, I.R.E.

***Summary***—*This paper is a review of the general problem of aircraft antennas used for communication in the frequency range of 2 to 20 megacycles. Fixed antennas, shunt-fed wing antennas, and trailing-wire antennas are discussed and several typical curves of resistance and reactance are included. The icing problem is considered. The characteristics of several types of wire suitable for aircraft antenna are compared. Also included is a description of the army model-airplane set-up for measuring radiating characteristics of various types of antennas under flight conditions.*

THIS PAPER is intended as a general discussion of aircraft radio communication antennas for use on frequencies between 2 and 20 megacycles. There are several differences between the demands of radio communication for military aircraft and those of civil aircraft. In the first place, military communication requires a coverage of a wide band of frequencies and any frequency may be required to be shifted in flight while antennas on civil aircraft are limited to several fixed frequencies. Then the military aircraft may require two or more communications systems operating simultaneously while the civil aircraft is usually limited to a single communication system. It is thought if the problems are discussed from a military viewpoint most of the problems of civil aircraft will also be considered.

In any antenna system, we must consider the actual antenna wire and possible wire rigging. The wire must be strong and low radio-frequency resistance is especially important due to the low values of radiation

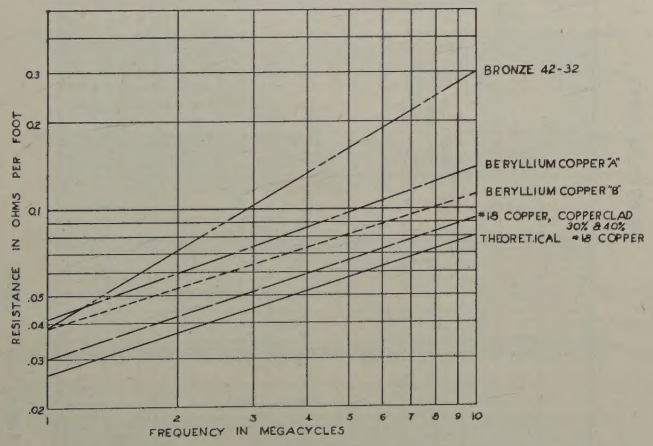


Fig. 1—Radio-frequency resistance of wires suitable for aircraft antennas.

resistance obtained. Tests of different alloys and types of wire have shown that a copper-clad steel wire has considerable advantage over other types. Curves shown in Fig. 1 indicate resistance of wire physically suitable for aircraft antennas. A 30 per cent direct-current-conductivity wire has practically the same resistance above 2 megacycles as pure copper wire and has a tensile strength of 180 pounds in a diameter of 0.040 inch. A phosphor-bronze wire of 42 strands of No. 32 wire much used for aircraft antenna has a resistance of three times that of the copper-clad wire at 10 megacycles.

In regard to rigging of antenna wire, possible icing must be considered.[1] Antenna wires can and do pick

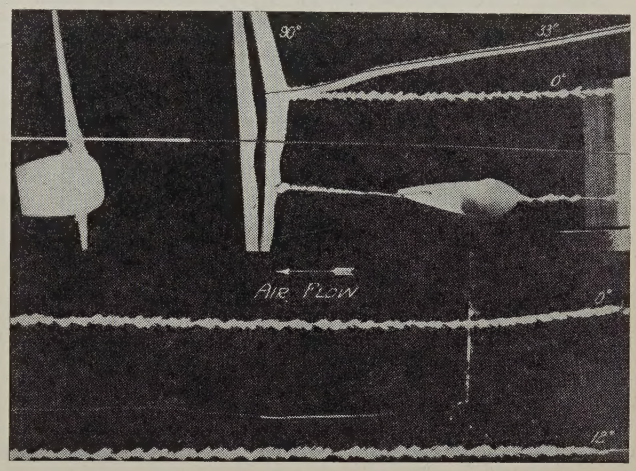


Fig. 2—Icing of aircraft antenna wires.

up heavy ice loads under some conditions which cause breakage and consequent loss of antenna. It is to be expected that a wire which is rigged transversely or at a right angle to the wind stream will pick up more ice than one which is rigged longitudinally or with the wind stream. Some methods have been devised to heat antenna wires electrically but considerable power must be used. Experiments have been conducted in an icing wind tunnel on the relation between the angle of the wire to the wind stream and the ice load picked up. The results of the work done to date indicate that there is a critical angle of icing below which the ice formed is much less in volume and more fragile. This critical angle is in the region of 15 to 20 degrees and, consequently, an attempt is made to keep the antenna wires below this angle. Fig. 2 shows photographs of wire ice at various angles of wind flow taken in a wind tunnel at an air speed of 80 miles per hour. Fig. 3 is a curve of ice diameter and ice volume versus wire angle relative to the wind stream. The critical angle region shows up very definitely on this curve of relative volume.

The actual antennas can be classified under three general types; the fixed-wire, the trailing-wire, and the shunt-fed wing. In the fixed-wire antenna, the size of the airplane will largely determine the length

* Decimal classification: R525. Original manuscript received by the Institute, October 15, 1941. Presented, Fifteenth Annual Convention, Boston, Massachusetts, June 28, 1940.

† War Department, Aircraft Radio Laboratory, Wright Field, Dayton, Ohio.

[1] G. L. Haller, "Icing of aircraft antenna wires," *Jour. Aeronaut. Sci.*, vol. 6, pp. 27–28; November, 1938.

of antenna which can be used and considerable loading is usually necessary to tune these antennas. The fundamental, quarter-wave frequency on the largest airplanes is above 3.0 megacycles while in smaller air-

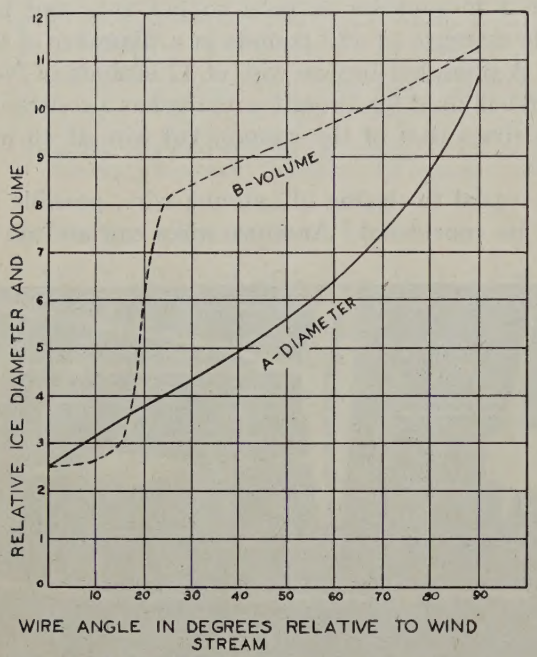


Fig. 3—Wire icing versus wire angle.

planes it may be as high as 12 to 15 megacycles. The effective height of fixed antennas is necessarily low and the total resistance on the lower frequencies 2 to 4 megacycles is seldom greater than 1 to 2 ohms.

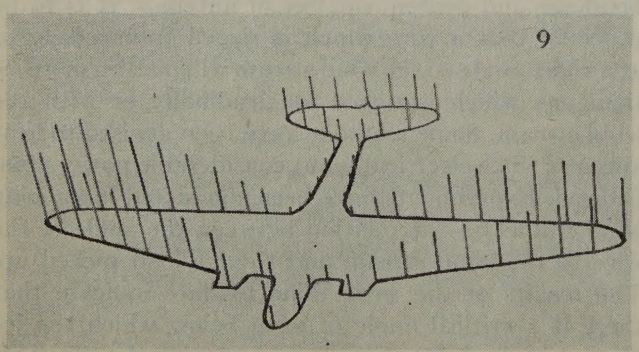


Fig. 4—Shunt-fed half-wave voltage distribution.

The shunt-fed wing antenna has recently been used with some success on the larger, all-metal airplanes. A feeder is taken through the skin of the fuselage and

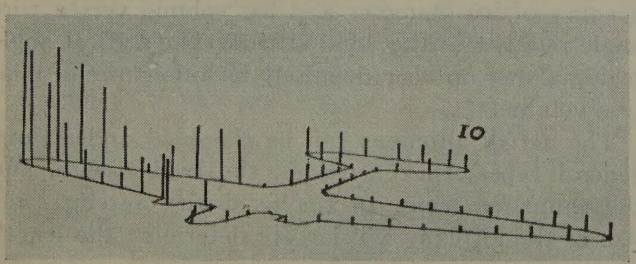


Fig. 5—Shunt-fed full-wave voltage distribution.

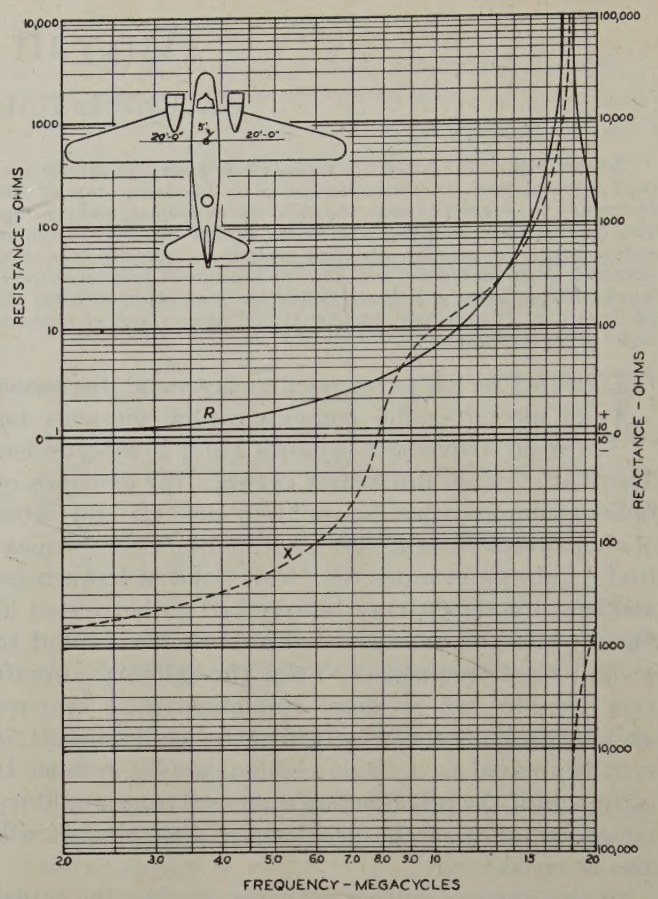


Fig. 6—Impedance characteristic, transverse antenna.

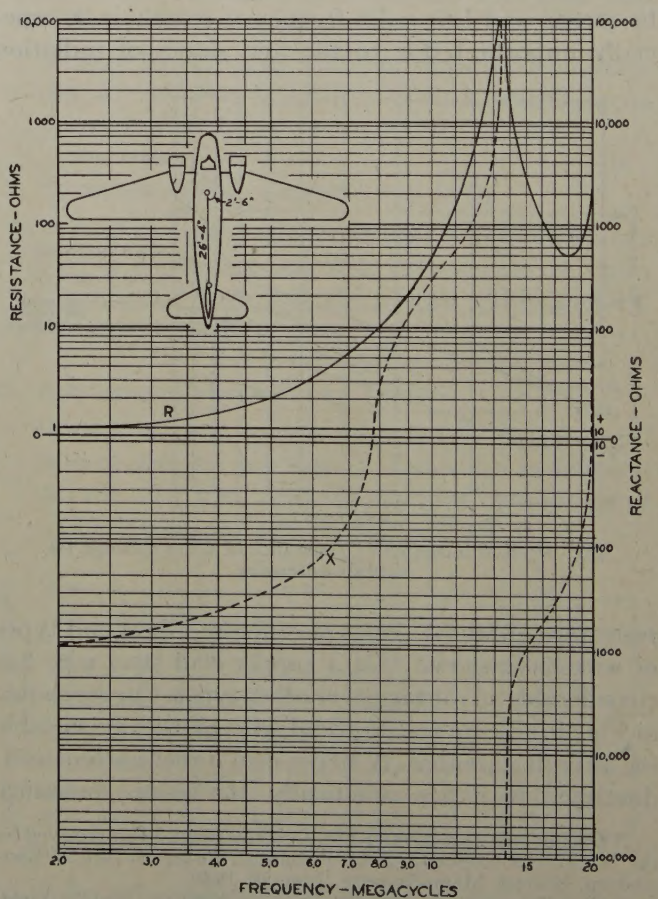


Fig. 7—Impedance characteristic, longitudinal antenna.

grounded a short distance out on the wing, usually directly behind the motor nacelle on a two-motor airplane. This causes the wing to become excited similar to a shunt-fed broadcast antenna. The frequency limitation of such an antenna appears from experimental results to be such that any frequency may be used if the wing spread of the airplane is 40 per cent or more of the working wavelength. Fig. 4 shows a representation of voltage measurements taken on an airplane at a frequency such that the wing spread was

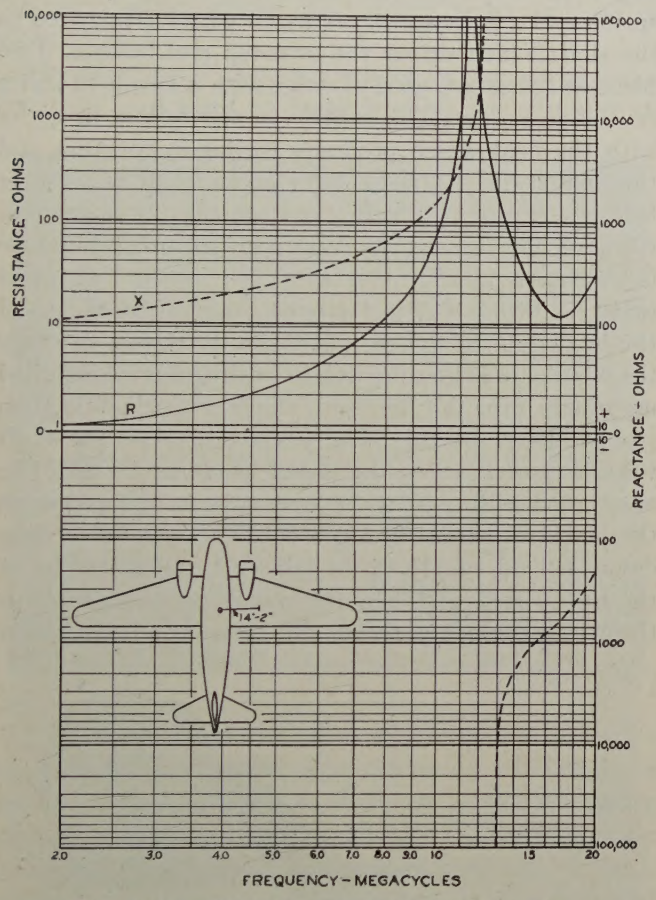


Fig. 8—Impedance characteristic, shunt-fed wing.

one-half wavelength long. Fig. 5 is the same except the frequency is twice as great, that is, the wing spread is now one full wavelength. The results obtained on wing antennas compare favorably with a fixed-wire antenna and sometimes are better. Phone communication ranges of several hundred miles can be expected consistently with about 50 watts of antenna power and telegraph communication across the continent has been accomplished between an airplane and its home base. On one test at 6 megacycles, an airplane on the ground had phone communication with its base more than 1000 miles away.

The impedance curves[2] of any antenna system are interesting, especially to the one who designs the radio equipment and several typical curves are included. Fig. 6 shows a transverse antenna on a medium-range

[2] G. L. Haller, "Constants of fixed antennas on aircraft," PROC. I.R.E., vol. 26, pp. 415–420; April, 1938.

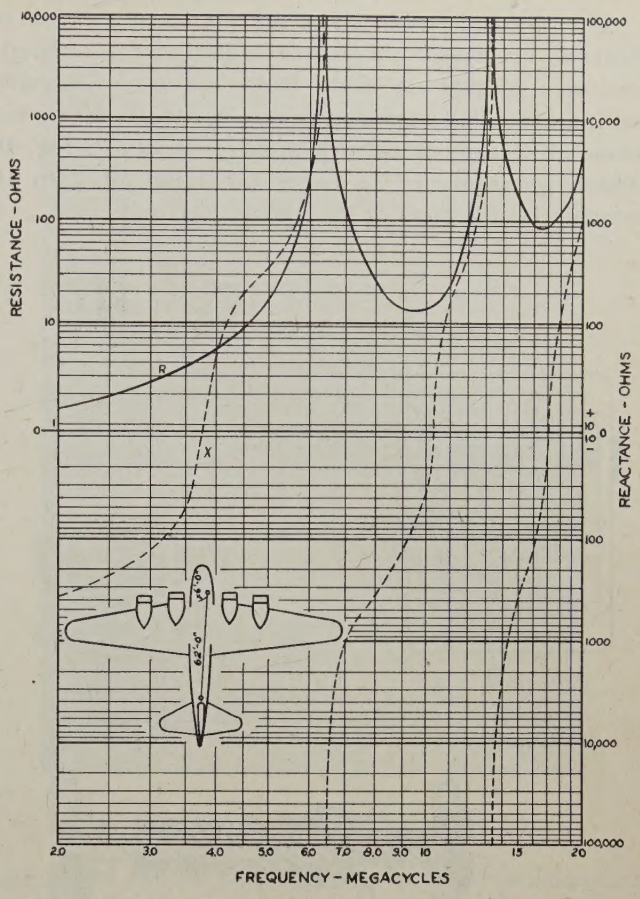


Fig. 9—Impedance characteristic, longitudinal antenna.

bomber with a wing spread of 90 feet. Fig. 7 shows a longitudinal antenna on the same airplane. Fig. 8 shows a shunt-fed wing antenna on the same airplane and Fig. 9 shows a longitudinal antenna on a large bomber with a wing spread of about 160 feet. The points of special interest on these curves are the low total resistance at the lower frequencies and the wide range of reactance which must be accommodated in any radio equipment which covers a wide band of frequencies.

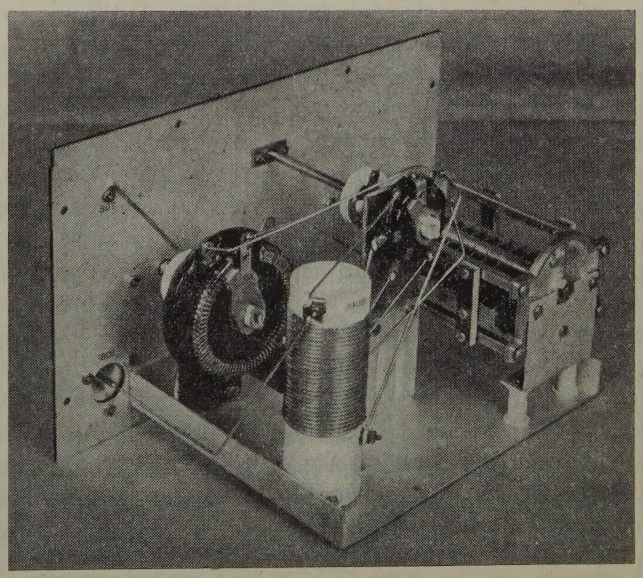

Fig. 10—Phantom aircraft antenna.

The physical problem of construction of a phantom antenna involves more than a single resistor, or single resistor and reactor, if the radio set is to be tested with a simulated aircraft antenna. Some phantoms become quite elaborate. Such a one is shown in Fig. 10 which was designed to cover the range of 2 to 10 megacycles for most of the above antennas.

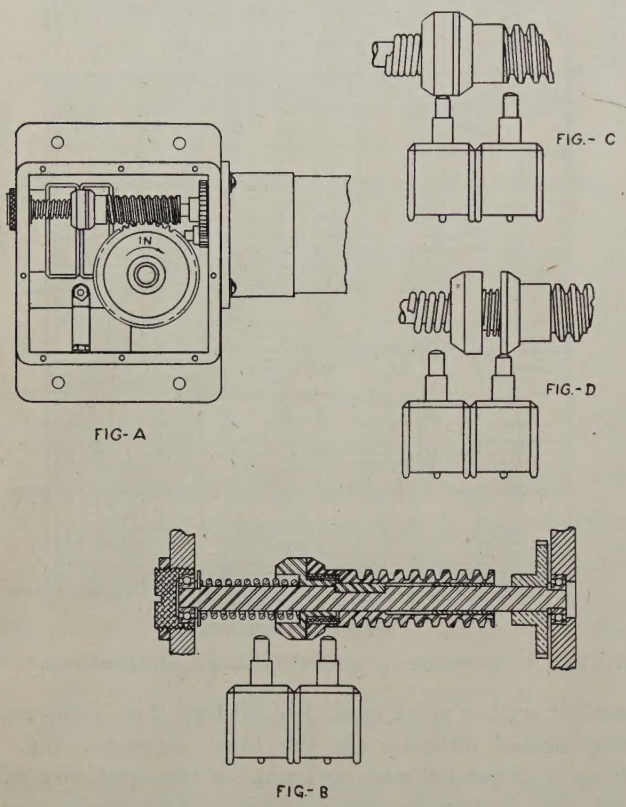


Fig. 11—Automatic antenna reel mechanism.

The trailing-wire antenna is probably the most efficient antenna, but brings in several physical problems. When adjusted to resonance, one-quarter wave, it has a resistance of between 10 and 20 ohms or more depending on the size of the airplane. Trailing-wire antennas are usually terminated by either a weight or a wind-sock drag device, although some trailing-wire antennas are used without either. The trailing wire with the wind sock or without any device hangs out almost horizontally and has poor directional effects, while the weighted trailing wire has considerable vertical component with a resultant circular field. One great advantage of the adjustable trailing wire is that it may be tuned by varying the length and consequently eliminates much of the tuning and loading apparatus otherwise needed. This tuning at the antenna allows the use of a transmission line which is a great advantage and which is almost impossible with a fixed antenna covering a wide frequency band. The antenna reels used are mostly hand-operated with a mechanism which, when turned by the operating handle in one direction winds the wire in on a ratchet; when turned the other way the spool is free to reel out wire, and when the handle is free the reel is locked for use. Several electric automatic reels have been used but have not found much favor. There has recently been developed an electric automatic antenna reel which may become more generally adopted.[3] The mechanism of this reel is novel enough to warrant a brief description. Fig. 11 is a cross-sectional view of the reel mechanism. Shown in the cross section is the motor pinion meshed with the cam-shaft pinion. On the cam shaft is a combined sliding worm and cam which is keyed to the shaft and another cam and a strong spring and a light spring. A worm wheel is fastened to the shaft which drives the antenna reel bobbin. Two Microswitches are used in series with a two-field series reversible motor. The switch to the left is in series with the field which produces reeling-in rotation and the switch to the right is in series with the motor field which produces reeling-out rotation. In operation, when reeling in wire, the cam and worm combination is as shown in Fig. 11B with the worm and cams being held from sliding farther to the left by means of the heavy spring which is sufficiently strong to carry the wire load. When the weight or drag device is pulled up snugly into the fair-lead, the worm wheel is then stopped from rotating. The worm travels on the shaft toward the left using the worm wheel as a rack. The worm pushes the cam which opens the switch and stops the motor as shown in Fig. 11C. The weight or drag device is held snugly in its fair-lead under tension of the heavy spring. When the motor contact switch is thrown to the out position, the motor receiving power

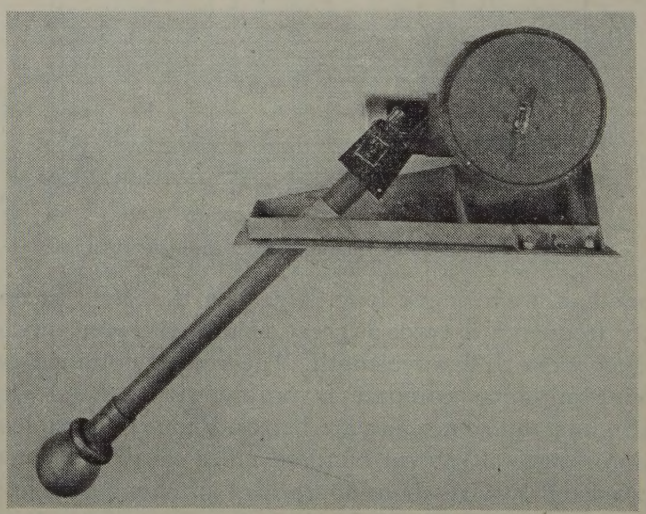

Fig. 12—Typical antenna reel mounting.

through the other switch reverses its rotation and reels out wire until the wire is all out, at which time as the end of the wire passes the dead center of the out position, the pull of the wire on the reel bobbin, and consequently the rotation of the worm wheel, is reversed, and the worm and cam travel toward the right and open the out switch as shown in Fig. 11D. Another

[3] J. K. DeArmond and G. L. Haller, United States Patent No. 2,204,579, issued June 18, 1940.

feature of the mechanism is that in case the wire should jam in the fair-lead and fail to pay out, the light spring will push the out-stop cam and worm to the right and stop the motor, which will prevent the reel from unspooling the wire and the possible fouling of control wires. The reel as commercially developed has a magnetic clutch between the motor and gear mechanism which allows fine adjustments of lengths by mechanically disconnecting the motor when the current is turned off. Fig. 12 shows a view of the automatic antenna reel with the fair-lead in a removable mounting, the use of which allows the antenna to be replaced in flight.

The directional characteristic of an aircraft antenna does not lend itself to mathematical analysis due to

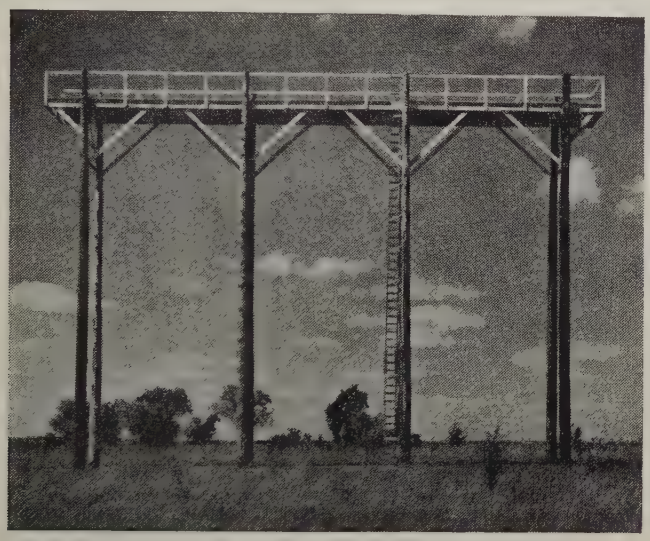

Fig. 13—Radiation test towers.

the complex physical structure of the airplane which is the ground, although a study of such characteristics using the principle of similitude is being made.[4,5] Scale models of the airplane under consideration are used, and the frequency is scaled up as the size is scaled down. Tests were first attempted on the ground and serious errors due to ground effects were noted. A tower system was then designed and built which would reduce the error to a few per cent. The errors encountered were the interference of the reflected wave with the direct wave and the difference in attenuation between the horizontal and vertical polarized waves. Fig. 13 shows a view of the radiation test tower which is 50 feet high and 70 feet long. The model is mounted as shown in Fig. 14 at one end of the tower, the field-strength-measuring equipment is mounted 30 feet from the model, and the observers stay at the other end of the tower and read the meters with telescopes.

[4] Ernst Harmening and Wolfgang Pfister, "Model measurements on fixed aircraft antennas to obtain radiation patterns in the short-wave region," *Hochfrequenz. und Elektroakustik*, vol. 53, pp. 41–45; February, 1939.

[5] G. L. Haller, "Free space propagation measurements at 75 megacycles," *Jour. Frank. Inst.*, vol. 229, pp. 165–180; February, 1940.

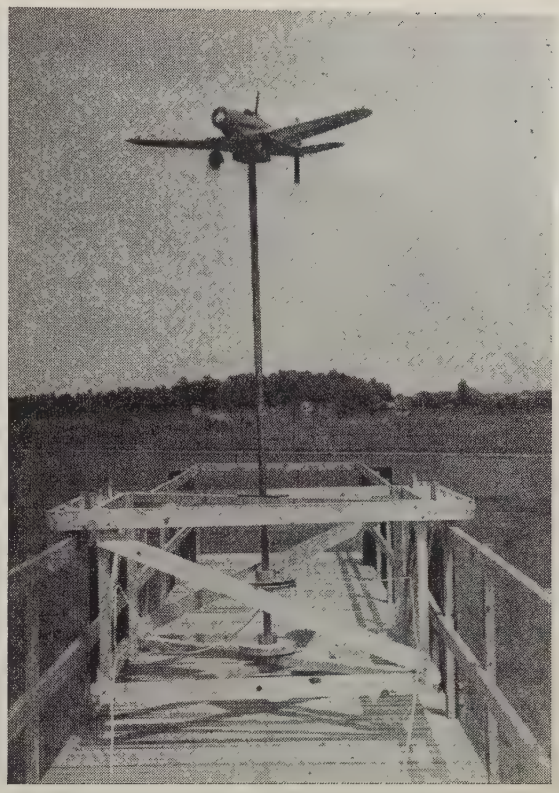

Fig. 14—Airplane model on tower.

The model can be placed in any of three positions on the support, that is, normal flying position as shown, with nose down, or with one wing down. From any of

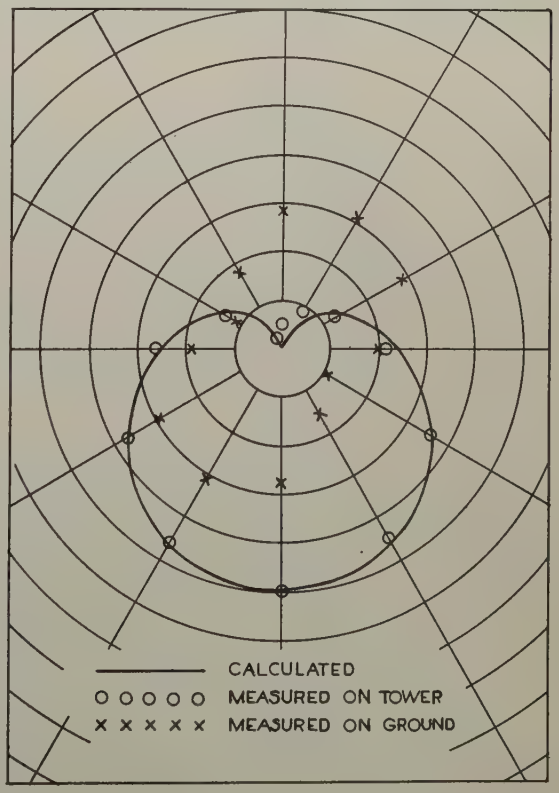


Fig. 15—Test pattern for tower measurements.

these positions the model may be rotated by means of ropes around the axis of the support. Tests made on the tower indicated that there was no difference between the horizontal- and vertical-wave attenuation,

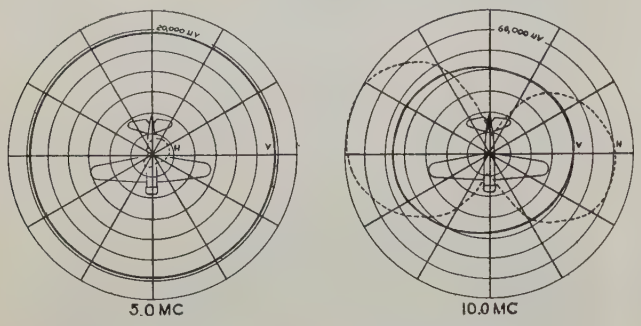


Fig. 16—Typical model measurements.

and a test pattern was made with a dipole transmitter and receiver. The pattern was a combination of vertical and horizontal polarized waves produced with the transmitting dipole mounted at an angle of 45 degrees with the ground and rotated about a vertical axis. The receiving dipole was mounted at the same angle and so that the coupling would vary from zero to maximum in 180 degrees. The calculated pattern was a cardioid as shown in Fig. 15. The actual pattern measured in the air and on the ground is also indicated, showing the ground error eliminated on the tower measurements. Fig. 16 shows a sample measurement made on a one-tenth-scale model of a low-wing monoplane at frequencies of 50 and 100 megacycles, simulating a frequency of 5 and 10 megacycles. It is to be noted that most of the energy at the lower frequency is in the vertical wave, while at the higher frequency considerable energy is present in the horizontal wave.

Those patterns which it has been possible to obtain from an actual airplane check with those obtained from the models, and the model patterns give information which it is impractical to obtain from the full-size airplane.

# Impedance-Measuring Instrument*

CARL E. SMITH†, MEMBER, I.R.E.

***Summary***—*Following a brief discussion of impedance-measuring methods, the theory underlying the operation of this instrument is presented with the development of useful equations. The merit of the scheme lies in the fact that measurements can be made while the impedance is in operation without disturbing the current distribution of the network. Practical arrangements of the parts are then considered along with the necessary adjustments. The paper ends with some results and conclusions.*

## I. Introduction

IMPEDANCE measurements at radio frequencies can in general be classified under resonance or null methods. Both methods depend upon the application of Ohm's law to compare unknown impedances with known impedances, but they differ fundamentally in the indicating method. Resonance methods depend upon the tuning of resonant circuits for maximum voltage or current while bridge methods depend upon balancing circuits to give a null voltage or current.

Most of the more common measuring schemes using these methods are of little or no value if it is desired to measure an impedance while it is operating in a network and not disturb the current distribution of the network. A typical example of this character is in a directional antenna system. It may be desired to match the impedances through transmission lines to minimize power loss and to prevent standing waves which may cause voltage flashover. The impedances in such a network are a function of the current distribution, hence, it is imperative not to alter this distribution while measuring the impedance.

* Decimal classification: R241. Original manuscript received by the Institute, September 23, 1941; revised manuscript received, November 12, 1941.

† Chief Engineer, United Broadcasting Company, and President, Smith Practical Radio Institute, Cleveland, Ohio.

## II. Theory of Operation

The operation of this instrument depends upon the measurement of voltages created by inserting a series-resonant circuit in series with the unknown load. If the series-resonant circuit is physically small, and free of resistance, its insertion will not affect the current distribution in the network. The desired voltages can then be measured with a very high-impedance vacuum-tube voltmeter.

Consider the pure resistance load $R_0$ connected to a generator of voltage $E$ as illustrated in Fig. 1(a). In

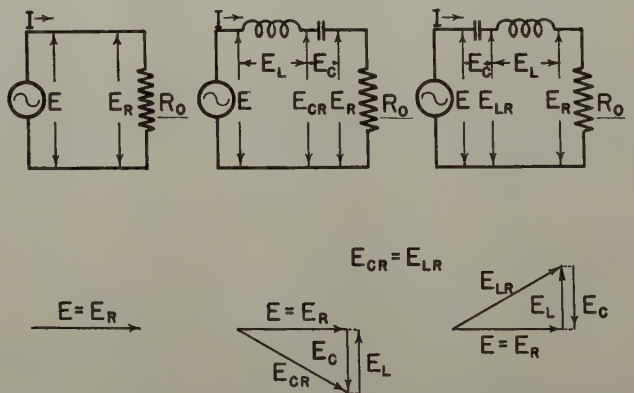


(a) Normal circuit (b) Series-resonant inductance-capacitance inserted (c) Series-resonant capacitance-inductance inserted

Fig. 1—Circuit and vector diagrams for a pure resistance load.

this circuit a current $I$ will flow and the magnitude of the resistance can be measured by taking the ratio of the voltage and current as indicated

$$R_0 = \frac{E}{I} \text{ ohms.} \tag{1}$$

Now connect a series-resonant inductance-capacitance in series with the load. With pure elements the magnitude of the input impedance by taking the voltage-current ratio will be equal to the load impedance. The voltage across the load resistance in series with the series condenser will be noted as $E_{CR}$ in Fig. 1(b). Now, reverse the positions of the inductance and capacitance as shown in Fig. 1(c). The voltage-current ratio should remain unaltered, hence, the magnitude of the voltages will be equal, thus,

$$E_{LR} = E_{CR} \text{ volts.} \tag{2}$$

Equations (1) and (2) give the desired magnitude and phase for the proper matching of transmission lines while they are in operation. Usually the characteristic impedance of the transmission line is known. The voltage-current ratio as given in (1) should be adjusted until it is equal to the magnitude of the characteristic impedance of the line. When (2) is also satisfied, there will be no reactive component, hence, a pure resistance of the proper magnitude.

If the load has an inductive component as indicated in Fig. 2(a) the series-resonant circuit as shown in Fig. 2(b), with the capacitance toward the load, will give a smaller value of voltage $E_{CZ}$ than when the series-resonant circuit is connected, with the inductance toward the load, giving a voltage $E_{LZ}$ as shown in Fig. 2(c). The reason for this is obvious. The inductive reactance of the load cancels a part of the capacitive reactance facing the load resulting in an impedance triangle with a hypotenuse less than if the load were a pure resistance. Similarly, when the inductance is toward the load the inductive reactance adds to the inductive reactance of the load to make the impedance-triangle hypotenuse greater than it would be for a pure resistive load.

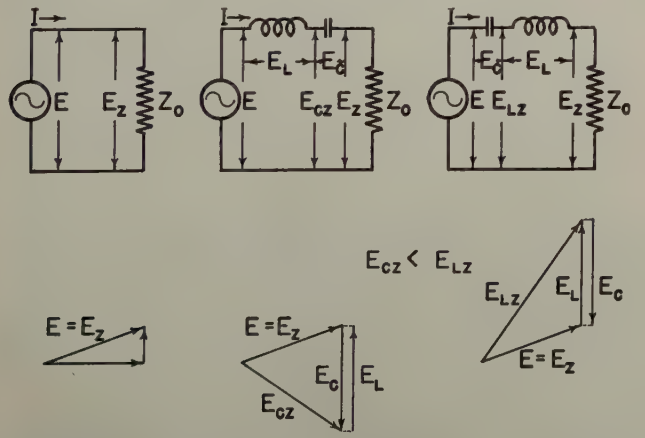


(a) Normal circuit (b) Series-resonant inductance-capacitance inserted (c) Series-resonant capacitance-inductance inserted

Fig. 2—Circuit and vector diagrams for an inductive load.

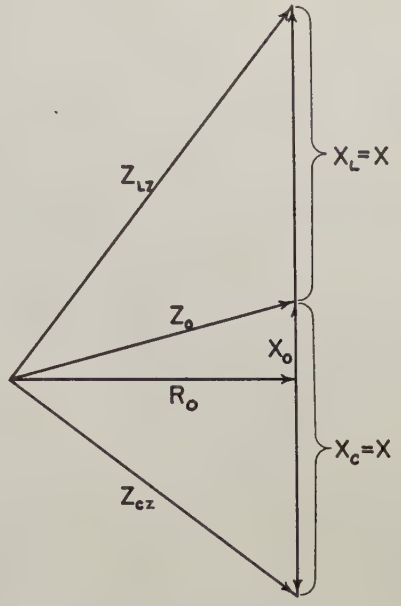


Fig. 3—Vector diagram of impedance triangles for an inductive load.

When the values of the series-resonant circuit are adjusted for series resonance, let,

$$X = X_L = X_C \text{ ohms.} \tag{3}$$

For best accuracy in making measurements $X$ should be made equal to the magnitude of the impedance to be measured.

Now, if the various impedances are defined by the measured voltage-current ratios,

$$Z_{LZ} = \frac{E_{LZ}}{I} \text{ ohms} \tag{4}$$

$$Z_{CZ} = \frac{E_{CZ}}{I} \text{ ohms} \tag{5}$$

$$Z_0 = \frac{E}{I} \text{ ohms.} \tag{6}$$

Then in the vector diagram of Fig. 3,

$$Z_{LZ}^2 = R_0^2 + (X_0 + X)^2 \tag{7}$$

$$Z_{CZ}^2 = R_0^2 + (X_0 - X)^2. \tag{8}$$

Subtracting (8) from (7),

$$Z_{LZ}^2 - Z_{CZ}^2 = X_0^2 + 2X_0X + X^2 - X_0^2 + 2X_0X - X^2$$
$$= 4X_0X.$$

Hence,

$$X_0 = \frac{Z_{LZ}^2 - Z_{CZ}^2}{4X} \text{ ohms.} \tag{9}$$

And, in the load-impedance triangle of Fig. 3,

$$R_0 = \sqrt{Z_0^2 - X_0^2} \text{ ohms.} \tag{10}$$

These last two equations give the resistive and reactive components of the load impedance. These

equations are useful for determining the components of the impedance of an antenna while it is in operation.

If the load has a capacitive component as indicated in Fig. 4(a) the series-resonant circuit as shown in Fig. 4(b) with the capacitance toward the load will give a larger value of $E_{CZ}$ than when the series-resonant circuit is reversed so that the inductance is toward the load to give $E_{LZ}$. When figuring the impedance, (9) and (10) still hold but $X_0$ will come out negative.

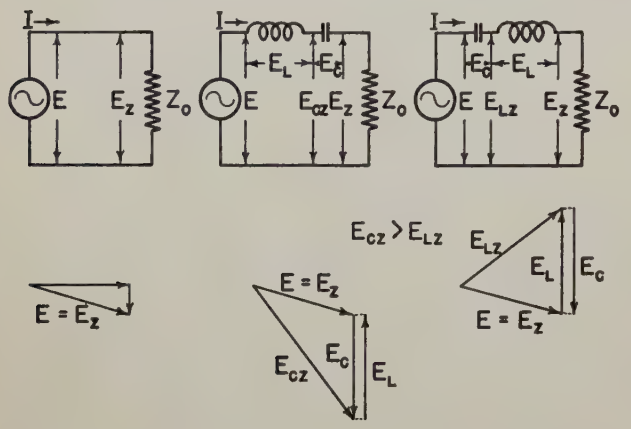


(a) Normal circuit (b) Series-resonant inductance-capacitance inserted (c) Series-resonant capacitance-inductance inserted

Fig. 4—Circuit and vector diagrams for a capacitive load.

## III. Practical Arrangements of Parts and Necessary Adjustments

In order to facilitate measurements it is desirable to make up a suitable switching arrangement such as shown in Fig. 5. The double-pole double-throw switch should make before break; the three positions give the voltages necessary to calculate the impedances in (4), (5), and (6). The ammeter in the instrument should be of the thermal type of rather low resistance; hence a 250- or even 500-milliampere range is more desirable than a 125-milliampere meter which has several ohms resistance. In practice it has been found that with the very high-impedance General Radio type 726A vacuum-tube voltmeter no appreciable error is encountered due to leaving the voltmeter connected between the coil and condenser when measuring with the switch in the short-circuited position for securing the result given in (6). This can be readily checked by actually placing the voltmeter from one side of the ammeter to the opposite side of the line. Of course a more complicated switch could be used to do this in one of its positions.

Care must be exercised in balancing $L_0$ and $C_0$. The inductance and capacitance of the lead wires from the elements to the reversing switch may have considerable effect if not properly balanced for the two positions. With the aid of a radio-frequency bridge it is not difficult to minimize this effect by properly adjusting the wiring.

Since $L_0$ necessarily contains some resistance, the voltage will be larger when the inductance is connected toward a resistance load as shown in Fig. 5(a) in the $E_{LZ}$ position. This effect can be balanced out by short-circuiting the condenser with the proper leakage resistance to give a similar impedance triangle. This would increase the resistive component of the series-resonant circuit. Rather than increase this undesired resistive component, calibrating readings can be made with the instrument connected to a pure resistance $R_0$ as shown in Fig. 5(a). A noninductive carbon resistor is quite satisfactory for this standard. If the desired value is not on hand a carbon resistor, slightly below value, can be selected and the carbon filed off until the desired value is reached. With the calibrating $R_0$ equal to the characteristic impedance of the transmission line, these calibrating readings must be reproduced when the instrument is actually connected in the transmission line as shown in Fig. 5(b).

## IV. Results and Conclusions

The use of this instrument was keenly appreciated when adjusting the three-tower directional array for radio station WHK. The transmission lines were so near a half wavelength that a deliberate 100 per cent mismatch would cause less than 1 per cent variation in the meter readings at the opposite ends of the several transmission lines. As soon as this instrument was placed in the lines, low power could be used and the condition of the impedance match immediately determined. The matching networks could then be readily adjusted to give a perfect impedance match in all the transmission lines while maintaining the proper current magnitude and phase relations in the various antennas of the system.

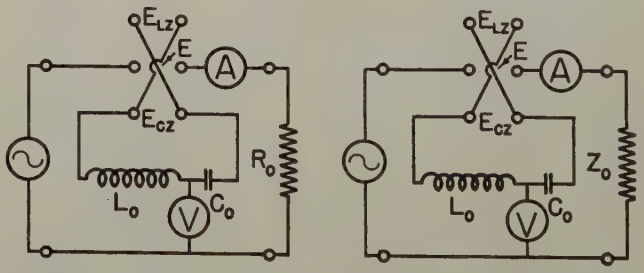


(a) Calibrating circuit (b) Measuring circuit

Fig. 5—Circuit diagram of impedance-measuring instrument.

Experience with the use of this instrument makes one appreciate its simplicity and usefulness for matching transmission lines of any length. Furthermore, its application need not be confined to transmission lines, but can be used to measure or check the driving-point impedance of antennas while they are in operation.

## Acknowledgment

The author wishes to thank Mr. J. S. Hill of the United Broadcasting Company for preparing the drawings for this article in their final form.

# The Zero-Beat Method of Frequency Discrimination*

C. F. SHEAFFER†, ASSOCIATE, I.R.E.

***Summary***—*A method of frequency discrimination in which the frequency of balance is determined solely by the frequency of the controlling oscillator is explained. The method utilizes the phase turnover, which occurs at zero beat, between two beat sources when one of the beating signals is dephased by 90 degrees before it is applied to one of the beat detectors. A network is inserted in one of the beat sources which shifts its phase an additional 90 degrees and makes its output a direction function of the frequency. The beats are then amplified and supplied to a balanced rectifier, from which a direct voltage is available which changes polarity with the direction of frequency deviation.*

SINCE the advent of the practical frequency-modulation system of radio transmission, there has been a constant search for a method of frequency stabilization which would be both simple and effective.

Each system in present use has its particular advantages and weak points. It seems that the most effective systems either require a multitude of frequency-doubler stages, or a multitude of frequency-divider stages, which renders either of these systems rather cumbersome for use in portable equipment.

The Crosby circuit,[1] which makes use of a reactance-tube-controlled oscillator, stabilized by a discriminator, approaches the ideal but has several fundamental weaknesses. Perhaps the predominating one is the fact that, in this method, the discriminator must be a phase-shifting device whose elements are subject to temperature, mechanical, and other variations which require the use of temperature control and precautionary design considerations in order to secure adequate stability.

If a system of discrimination could be devised which would not depend upon tuned circuits, this weak point could be hurdled. If, further, the discriminator output could be made as high as desired without affecting the frequency of balance, the problem of securing adequate stabilization would not be difficult. Such a system[2] has been devised and is the subject of this paper.

The various elements involved in the device, and their arrangement, are indicated in Fig. 1. The frequency modulation, as well as the automatic frequency control, is accomplished by utilizing the control of the so-called reactance tube over the frequency of a tuned-circuit oscillator. In the arrangement of Fig. 1, the oscillator operates at a frequency of 2650 kilocycles, and is followed by a buffer amplifier which drives a frequency-doubler stage. The discriminator voltage stability is acquired by utilizing a highly stable crystal-controlled oscillator adjusted to give an output frequency of 5300 kilocycles. In detector 1, the output of the frequency doubler is mixed with that of the crystal oscillator and the resulting beat is selected in the plate circuit. The phase of the crystal output is shifted by 90 degrees and mixed with the doubler output in detector 2 to provide a second source of beat frequency. We must now consider the relationship between these sources of beat frequency. If the frequency of the doubler output is equal to that of the crystal oscillator, the beats will have zero frequency. If the doubler frequency is not equal to the crystal frequency, beats occur as a result of the falling in and out of step of the two radio-frequency voltages. Since the phase of the crystal-frequency supply fed to detector 2 lags that fed to detector 1 by 90 degrees, the two beats will have a phase separation of 90 degrees which is independent of the beat frequency. If the phase of the doubler output is advancing with respect to that of the crystal, that is, if its frequency is higher, the voltages applied to detector 2 fall in step one quarter of a beat cycle later than those applied to detector 1. In this case, therefore, the beat outputs of the detectors will have the relationship $E_{d1}=jE_{d2}$. If, however, the phase of the doubler frequency is retarding with respect to that of the crystal, the radio frequencies applied to detector 2 will fall out of step one quarter of a beat cycle after the voltages at detector 1 were in step. The phase relationship between the detector outputs in this case will be $E_{d1}=-jE_{d2}$. We thus see that a relative phase reversal between the beat supplies takes place as the frequency difference goes through zero, that is, at zero beat.

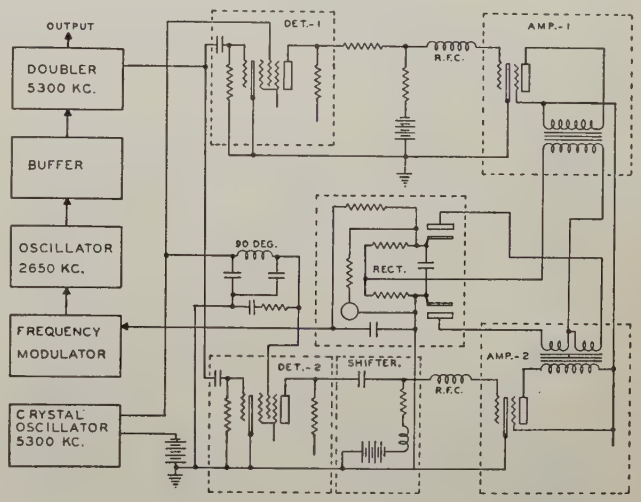


Fig. 1—Schematic diagram of the zero-beat frequency-discriminator system utilized as a control element in a frequency-modulation transmitter.

It now becomes apparent that if one of the beat supplies can be given an additional 90-degree shift which will hold for all beat frequencies of importance,

* Decimal classification: R355.6×R414. Original manuscript received by the Institute, November 13, 1941.

† U. S. Signal Corps, Oklahoma City, Oklahoma.

[1] M. G. Crosby, "Reactance tube frequency modulators," *RCA Rev.*, vol. 5, pp. 89–96; July, 1940.

[2] U. S. Patent No. 2,274,434, February 24, 1942.

and its output can be made a linear function of the frequency, we will have at hand the elements of a frequency discriminator. For all practical purposes this is accomplished by the network in the plate circuit of detector 2. The beat voltage at the output of detector 1 and that at the output of the shifter device, therefore, will be either in phase or out of phase, dependent upon whether the doubler frequency has deviated in a positive or negative direction. There remains, therefore, only the problem of amplifying and supplying the two derived beats to the balanced rectifier in a manner that will make available a rectified difference voltage proportional to the deviation and direction of deviation of the doubler frequency. This is accomplished by the two amplifiers and their associated output transformers which are connected so as to provide voltages at the plates of the two diodes which represent, respectively, the sum and difference of the two beat voltages.

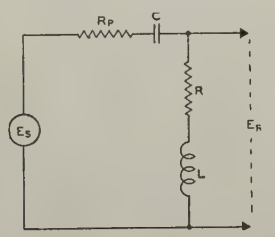


Fig. 2—An equivalent circuit of the 90-degree beat shifter.

Since the output of amplifier 2 is directly proportional to the beat frequency, the equations for the voltages applied to the diodes of the balanced rectifier may be written as

$$E_1 = E_{a1} + Kf_dE_{d2}/2$$
$$E_2 = E_{a1} - Kf_dE_{d2}/2.$$

We shall call the resulting rectified voltages $E_{r1}$ and $E_{r2}$. The output of the duodiode rectifier from cathode to cathode will be

$$E_{r1} - E_{r2} = (E_{a1} + Kf_dE_{d2}/2) - (E_{a1} - Kf_dE_{d2}/2)$$
$$= Kf_dE_{d2}.$$

In these equations the frequency deviation $f_d$ is either a positive or negative quantity, dependent upon the direction of deviation.

The output, when filtered, is therefore a positive or negative direct voltage whose amplitude and polarity are dependent upon the deviation and direction of deviation of the doubler frequency from that of the crystal oscillator. The voltage is zero only at zero beat and any deviation from the zero-beat value automatically produces a frequency-correcting voltage, for application to the reactance-tube grid, which acts to limit the deviation of the oscillator frequency.

This discriminator has two very important advantages over the tuned-circuit type. The first, of course, is that its balance frequency is fixed by the crystal, and therefore does not in any way depend upon unstable, temperature-sensitive, tuned circuits for stability. The correct adjustment for the oscillator tuning is always the setting which gives zero discriminator-rectifier output, and therefore a means is continuously available for readjusting the oscillator frequency during operation, which makes possible a maximum of accuracy at all times. A meter may be provided for this purpose and can be calibrated to indicate the frequency deviation covering the tolerance range.

The second advantage is that the two beat sources may be amplified to any desired extent without affecting the frequency of balance, and therefore the sensitivity of the device is limited only by practical circuit components.

It is required that the two amplifiers be flat throughout the modulation band of the frequency-modulated signal, and that their phase characteristics be identical. The output transformers must, therefore, be high-quality devices with electrostatic shielding between the primary and secondary windings. Discrimination at relatively low deviation level is indicated if transformers are used as coupling devices, but this imposes no serious restriction on the amount of control which can be attained.

A further requirement is that the 90-degree network in the plate of detector 2 shift the phase by 90 degrees for all frequencies important to the system. The means whereby this is accomplished is therefore an important part of the device. An equivalent circuit of the network is shown in Fig. 2. The output/input voltage ratio may be written as

$$\frac{E_r}{E_s} = \frac{(R + j\omega L)}{(R + R_p) + j(\omega L - 1/\omega C)}. \qquad (1)$$

Rationalizing this expression we obtain

$$\frac{E_r}{E_s} = \frac{R(R + R_p) + \omega L(\omega L - 1/\omega C)}{(R + R_p)^2 + (\omega L - 1/\omega C)^2}$$
$$+ j\frac{(R + R_p)\omega L - R(\omega L - 1/\omega C)}{(R + R_p)^2 + (\omega L - 1/\omega C)^2}. \qquad (2)$$

If the numerator of the first term of (2) can be equated to zero for all frequencies, the network will then shift the phase of any frequency passed through it by exactly 90 degrees. This, of course, is impossible. However, suppose that, within the frequency band of importance, values are selected so that $1/\omega C \gg \omega L$. The numerator could then be written as approximately $R(R+R_p)-L/C$, which contains no frequency term and therefore may be equated to zero.

It is also required that the voltage ratio be a linear function. This is realized if the second term of equation (2) is a direct function of the frequency. Suppose that in addition to the above $(R+R_p)^2 \ll (1/\omega C)^2$. Equation (2) then reduces to $E_r/E_s = j\omega CR$.

Design procedure is, therefore, based upon the selection of circuit components which meet, to a sufficient extent, the above conditions.

An experimental unit based on Fig. 1 was built up

in the workshop and experiment indicated that the discriminator operation was entirely satisfactory. A sensitivity of the order of 20 volts per kilocycle was possible throughout a band of plus or minus 15 kilocycles, even though small tubes and limited supply voltage was used. Symmetry of output with respect to positive and negative frequency deviation is a characteristic of this discriminator, as is also linearity.

The device is completely electronic in principle and can be made sufficiently compact for use in portable and semiportable transmitters. It forms the basis for a control system which can quite capably maintain the stability well within the requirements of the Federal Communications Commission for frequency-modulation broadcast transmitters.

# Cosmic Static*

GROTE REBER†, ASSOCIATE, I.R.E.

***Summary***—*Cosmic static is defined as electromagnetic radiation which may be detected by radio receiving equipment and which has extraterrestrial origin. A highly directive system for detecting and recording these radiations is described and analyzed.*

*Data are given on the variations in intensity of cosmic static in relation to various regions of the galaxy. The effects of interference are discussed.*

*It is suggested that cosmic static is the equivalent of thermal agitation in which all space is the conductor and the input terminals of the detecting equipment are projected by means of an antenna system to same far-distant part of space.*

## Introduction

"COSMIC STATIC" is used throughout this paper to designate those electromagnetic radiations, the sources of which are not associated with the earth or its atmosphere, and which have wavelengths such that they are detectable by ordinary radio receiving equipment. Some time ago the initial results[1] and a short description of the apparatus[2] used in this work were published. Since then the performance of this equipment has been closely scrutinized to understand better what the requirements for the measurement of this phenomenon are and how to meet them. Since both cosmic static and thermal-agitation noise generated in the receiver are continuous spectra of constant amplitude over the limited frequency range within the acceptance band of the receiver, there is only a single parameter to distinguish one from the other, namely magnitude. These two disturbances are continuous spectra from separate sources and will add together on a power basis. Fortunately the absolute magnitude of thermal-noise energy has been well established and may be used as a reference level for estimating the magnitude of cosmic static.

## Collector System

The major piece of apparatus used in this work is shown in Figs. 1, 2, and 3. The electromagnetic energy from space is collected by a mirror and captured by a drum which acts as a black body. No direct measurement has been made of the angular resolving power of this combination. At 160 megacycles, the mirror has an aperture of 5.1 wavelengths and a focal length of 3.25 wavelengths. Experiments with models and theoretical investigation indicate the half-amplitude points on polar curves of power sensitivity are about 6 degrees apart in the plane of the magnetic vector and 8 degrees apart in the plane of the electric vector. These values are somewhat larger than estimated in a previous paper. Fig. 4 shows the antenna wire inside of the drum and the transmission line going to the receiver. This

Fig. 1—Collector pointed to declination +40 degrees. Small drum at focal point for operation at 900 megacycles. Mirror diameter, 31.4 feet, focal length, 20 feet.

* Decimal classification: R114. Original manuscript received by the Institute, August 27, 1941: revised manuscript received, May 8, 1942.

† 212 W. Seminary Ave., Wheaton, Illinois.

[1] G. Reber, "Cosmic static," *Astrophys. Jour.*, vol. 91, p. 621; June, 1940.

[2] G. Reber, "Cosmic static," PROC. I.R.E., vol. 28, pp. 68–71; February, 1940.

Fig. 2—Collector pointed to declination −32.5 degrees. Large drum at focal point for operation at 160 megacycles.

Fig. 3—Turning mechanism for changing declination.

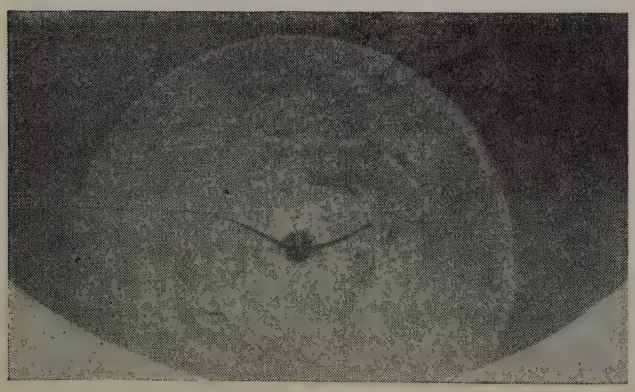

Fig. 4—View through aperture of drum showing antenna wire and transmission line.

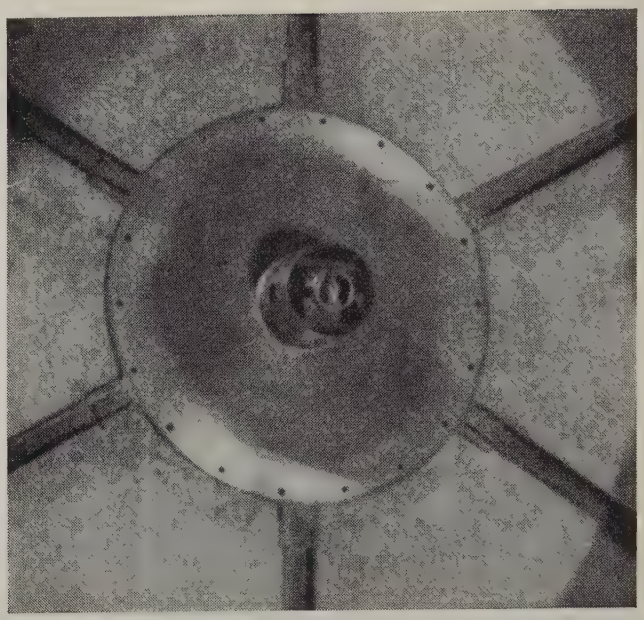

Fig. 5—Mount for receiver on end of drum. Antenna trimmers adjusted through holes in side of shield tube.

Fig. 6—Elevation of high-frequency amplifier. Power cable connects at side. Concentric-line tuned circuits adjusted to resonance by screws in upper band. Antenna trimmers adjusted by inserting wrench through hole in lower band, shown filled by rubber stopper.

transmission line is tuned and terminated in a single-turn loop shown in Fig. 5. The receiver or high-frequency amplifier which mounts on this fitting on the

end of the drum has within its center cavity a small pickup coil which couples to the loop at the end of the transmission line.

### High-Frequency Amplifier

The amplifier shown in Figs. 6 to 8 is the fourth and first successful one in a series of designs. Early tests gave the erroneous impression that this amplifier had a pass band of about 1 megacycle. Actually the half-amplitude points on the response curve were found to be much closer together than expected and are a function of the screen voltage. Fig. 9 gives the gain characteristics for maximum and minimum screen voltages of Table I. It will be observed that not only does the bandwidth decrease but the gain increases rapidly with screen voltage. Such performance is indicative of regeneration. Actually the effect is principally caused by the decrease of the input electron loading as the accelerating potential of the screen increases. Cascading the five stages magnifies the effect greatly and makes the accurate control of screen voltage imperative. Since the electron-loading conductance is proportional to the square of the frequency, the gain should rise as the frequency decreases. Table II gives data to demonstrate this effect. Thermal-noise voltage provided constant input level.

TABLE I

| Screen Voltage | Output Voltage $V_o$ | Bandwidth in Megacycles 6 Decibels Down |
|---|---|---|
| 92 | 0.14 | 0.44 |
| 96 | 0.22 | |
| 98.5 | 0.27 | |
| 102 | 0.37 | 0.19 |

TABLE II

| Frequency in Megacycles | Output Voltage |
|---|---|
| 168 | 0.4 |
| 167 | 0.5 |
| 166 | 0.6 |
| 163 | 0.8 |
| 159 | 1.4 |

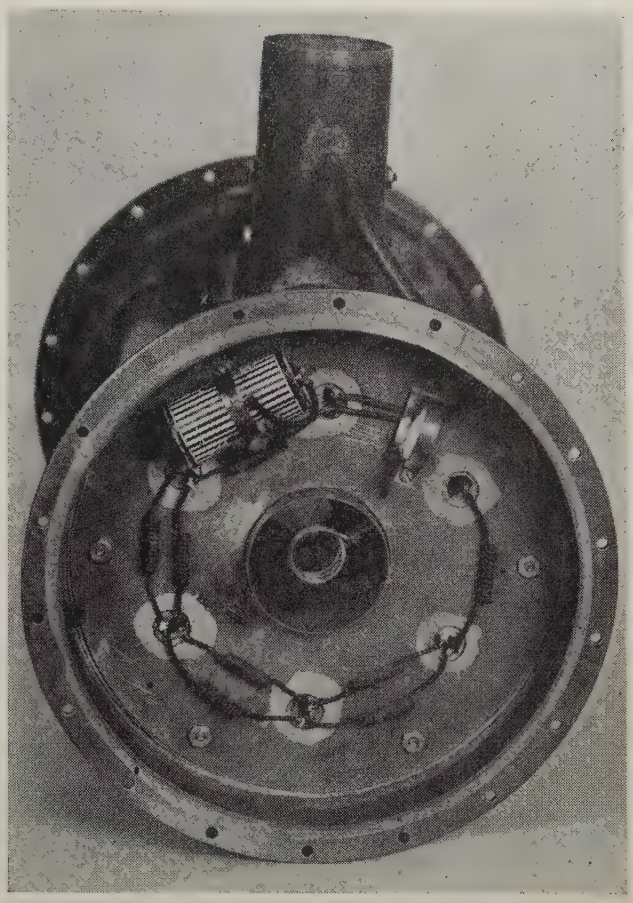

Fig. 8—Bottom view of high-frequency amplifier. Coupling coil for transferring cosmic-static energy from antenna to first grid circuit in center cavity.

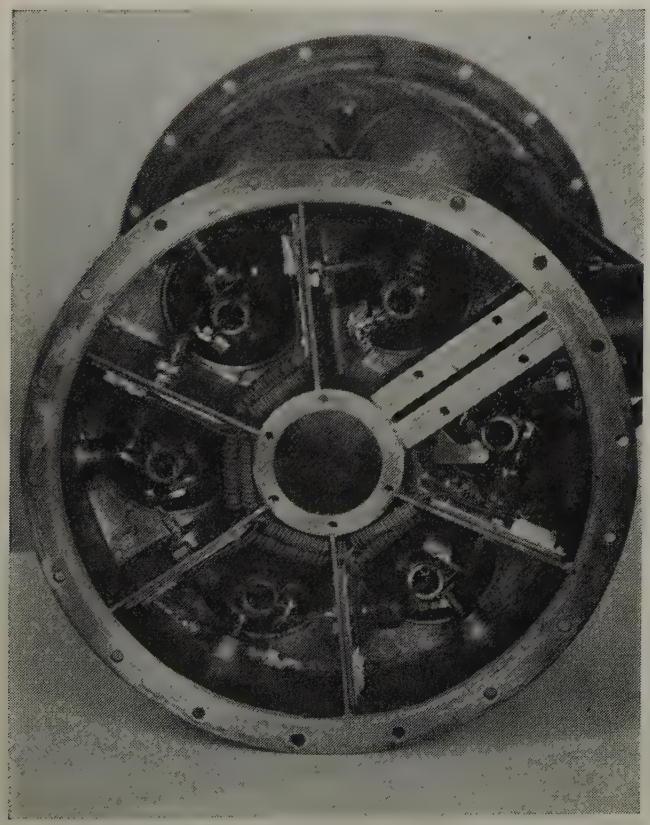

Fig. 7—Top view of high-frequency amplifier. First grid circuit is at upper right. Successive stages are in counterclockwise direction to diode compartment at right.

### Diode Rectifier

When the frequency is very high, a diode peak voltmeter will read low because of the electron inertia

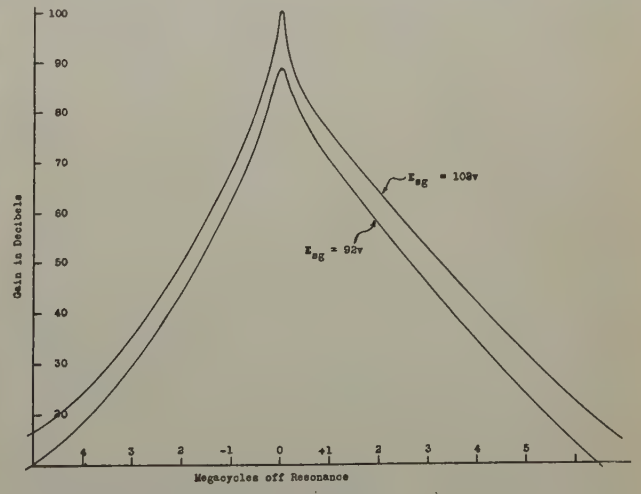


Fig. 9—Over-all gain of high-frequency amplifier at 160 megacycles for two different screen voltages

effects. Megaw[3] has analyzed the situation and found with only a small error the transit-time loss to be

$$(1 - K) = \frac{0.068 f x_a}{\sqrt{V}} \tag{1}$$

where $f$ = frequency in megacycles per second
$x_a$ = anode-cathode spacing in centimeters
$K = V_0/V$
$V_0$ = observed peak volts
$V$ = true peak volts

If a great waste of amplification is to be avoided it is apparent that $x_a$ must be kept small. Consequently a relatively large direct-current potential exists across the diode produced by the thermal velocity of electrons emitted from the cathode. This will cause no harm provided the potential remains constant. Therefore the diode heater voltage must be accurately controlled. Likewise, minute changes in mechanical clearance between the anode and the cathode will cause small changes in diode thermal voltage. Some of the charts in Figs. 10 and 11 to 14 show discontinuity points where the line shifts slightly one way or the other and proceeds with the original slope. Often these jumps are associated with surges of voltage. Apparently they are produced by a slight relative movement of the anode and cathode caused by direct mechanical shock or mechanical shock as a result of strong electrostatic fields which may affect the distribution of the emissive material on the cathode surface and thereby the effective clearance. The output of the diode rectifier is fed down a concentric cable to a direct-current amplifier and recorder.

## Auxiliary Equipment

This apparatus is shown in Figs. 15 and 16. The cable from the diode terminates at the input terminals of a direct-current amplifier in the center panel. The meter at the left of the direct-current amplifier indicates the direct voltage built up across the diode resistor and the knobs below are set for zero. Sometimes it is desirable to listen to the sounds being collected by the apparatus and for this purpose the headphone connection and the volume control at the right of the direct-current amplifier are convenient. The recorder on the top panel is operated from this direct-current amplifier. Full-scale deflection is obtained on 0.1, 0.2, 0.5, and 1.0 volt at the input terminals of the direct-current amplifier. A variety of chart speeds from 3/4 of an inch per hour to 12 inches per minute are available of which 6 inches per hour is most commonly used. The bottom panel contains the power supply with voltage regulators on screen and diode heater potentials. On top of the cabinet is a signal generator of range 140 to 200 megacycles for measuring the receiver performance.

[3] E. C. S. Megaw, "Voltage measurement at very high frequency," *Wireless Eng.*, vol. 13, p. 65; February, 1936.

## Circuit Analysis

Fig. 17 shows a block diagram of the entire system. Three resistors and their associated noise generators are in parallel forming the input circuit. Proceeding according to methods outlined by Moullin[4] we have, when $R_a = R_f \ll R_g$, the mean-square voltage at the first grid with the antenna at temperature $T_a$,

$$V^2 = k f_w R_f \left[ T_a + T_f + T_g \frac{R_f}{R_g} \right]. \tag{2}$$

When $T_a$ is zero the mean-square background voltage is

$$V_n^2 = k f_w R_f \left[ T_f + T_g \frac{R_f}{R_g} \right]. \tag{3}$$

The increase in input voltage caused by the signal voltage from cosmic static is $V - V_n = V_s$.

$$V_s = [k f_w R_f]^{1/2} \left[ \left( T_a + T_f + T_g \frac{R_f}{R_g} \right)^{1/2} - \left( T_f + T_g \frac{R_f}{R_g} \right)^{1/2} \right]. \tag{4}$$

The significance of the above notation may be obtained from the figure and $k$ = Boltzmann constant $= 1.37 \times 10^{-23}$ watt second per absolute degree. When fluctuation noise is impressed on a diode rectifier in series with a filter circuit, $R_d$ in parallel with $C_d$ (the usual diode resistor and condenser), a direct-current potential will be built up across the condenser. Superimposed on this direct-current potential will be a small ripple voltage. Passing through an amplifier of gain $G$ to a linear detector we find the ripple voltage to have a root-mean-square value of

$$V_r = G \left( \frac{Sq}{2C_d} \right)^{1/2} V^{1/2} = G \left( \frac{Sq}{2C_d} \right)^{1/2} (k f_w R_f)^{1/4} \left( T_a + T_f + T_g \frac{R_f}{R_g} \right)^{1/4} \tag{5}$$

where $S = \dfrac{\text{indicated direct voltage}}{\text{root-mean-square random voltage}} = \dfrac{V_o}{GV}$

$q$ = mean charge of random fluctuation energy. Likewise the direct signal voltage $V_{os}$ will be the difference between the direct voltage generated with signal $V_o$ and that from the thermal-agitation background noise $V_{on}$ or $V_o - V_{on} = V_{os}$. The value $S$ is rather uncertain as the indicated voltage $V_o$ depends not only on the effective voltage $GV$ applied to the rectifier but also its waveshape. If $GV$ were sinusoidal and $C_d$ large, then $S = 1.414$. If $GV$ is random and $C_d$ zero, then $S = 0.798$ according to Landon.[5] The diode will act as a peak voltmeter provided the peak voltages do not occur too infrequently compared to the time constant $R_d C_d$ or contain too little energy. While the number of

[4] E. B. Moullin, "Spontaneous Fluctuations of Voltage," Oxford University Press, Oxford, England, 1938, p. 194.

[5] V. D. Landon, "Distribution of amplitude in fluctuation voltage," Proc. I.R.E., vol. 29, pp. 50–55; February, 1941.

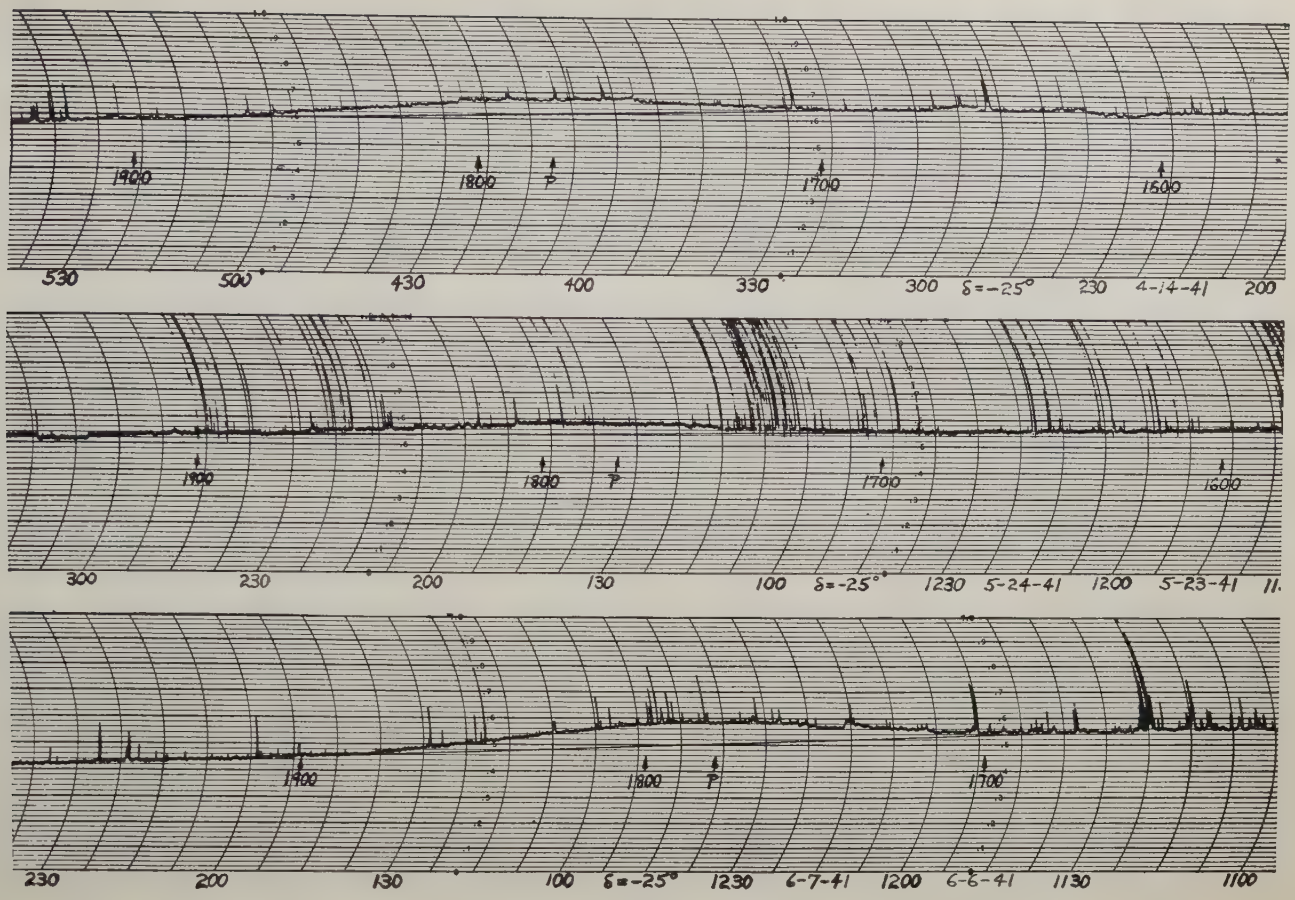


Fig. 10—Charts demonstrating the forward movement of cosmic static with the elapse of mean solar time.

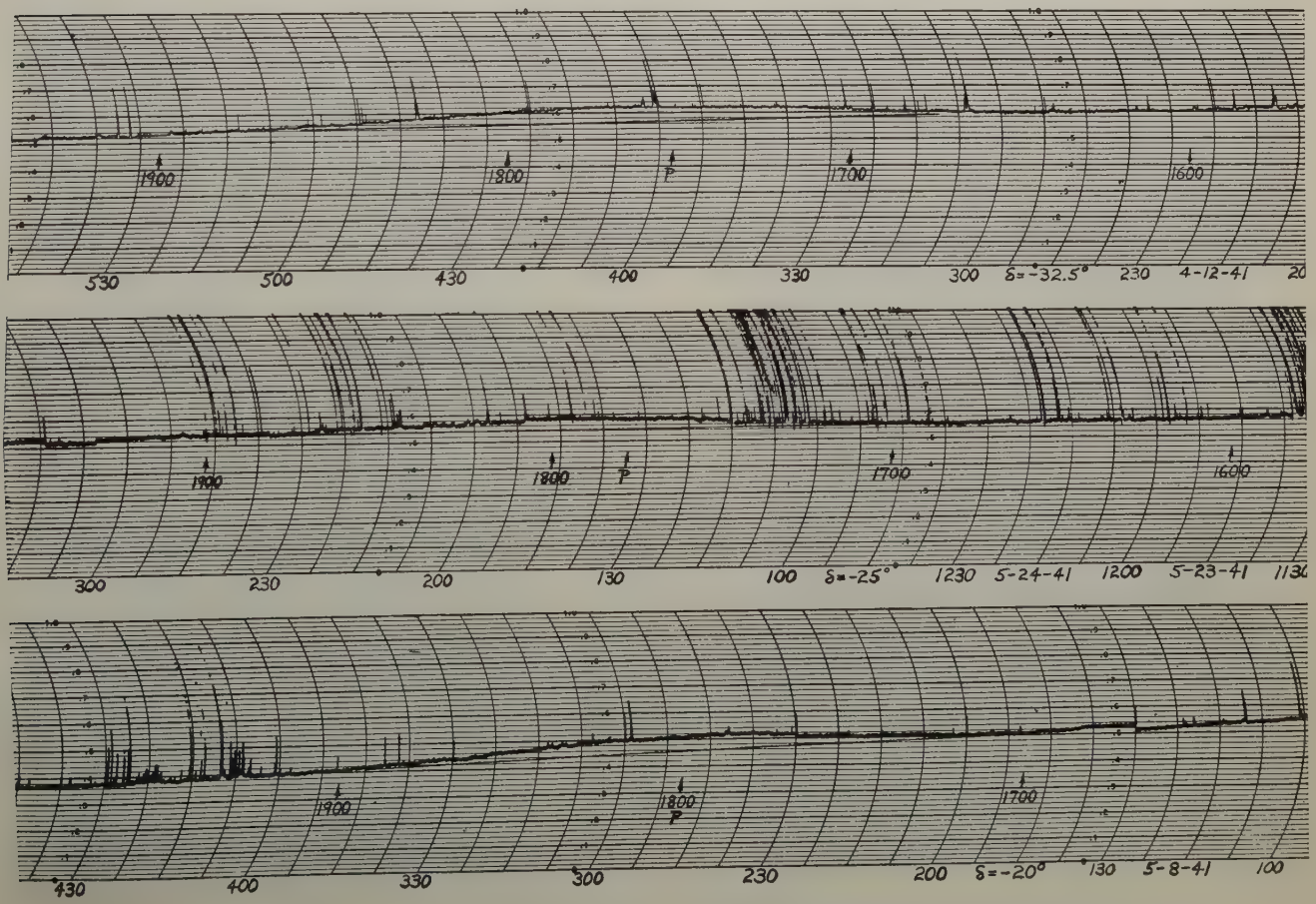


Fig. 11—Sample charts of cosmic-static record.

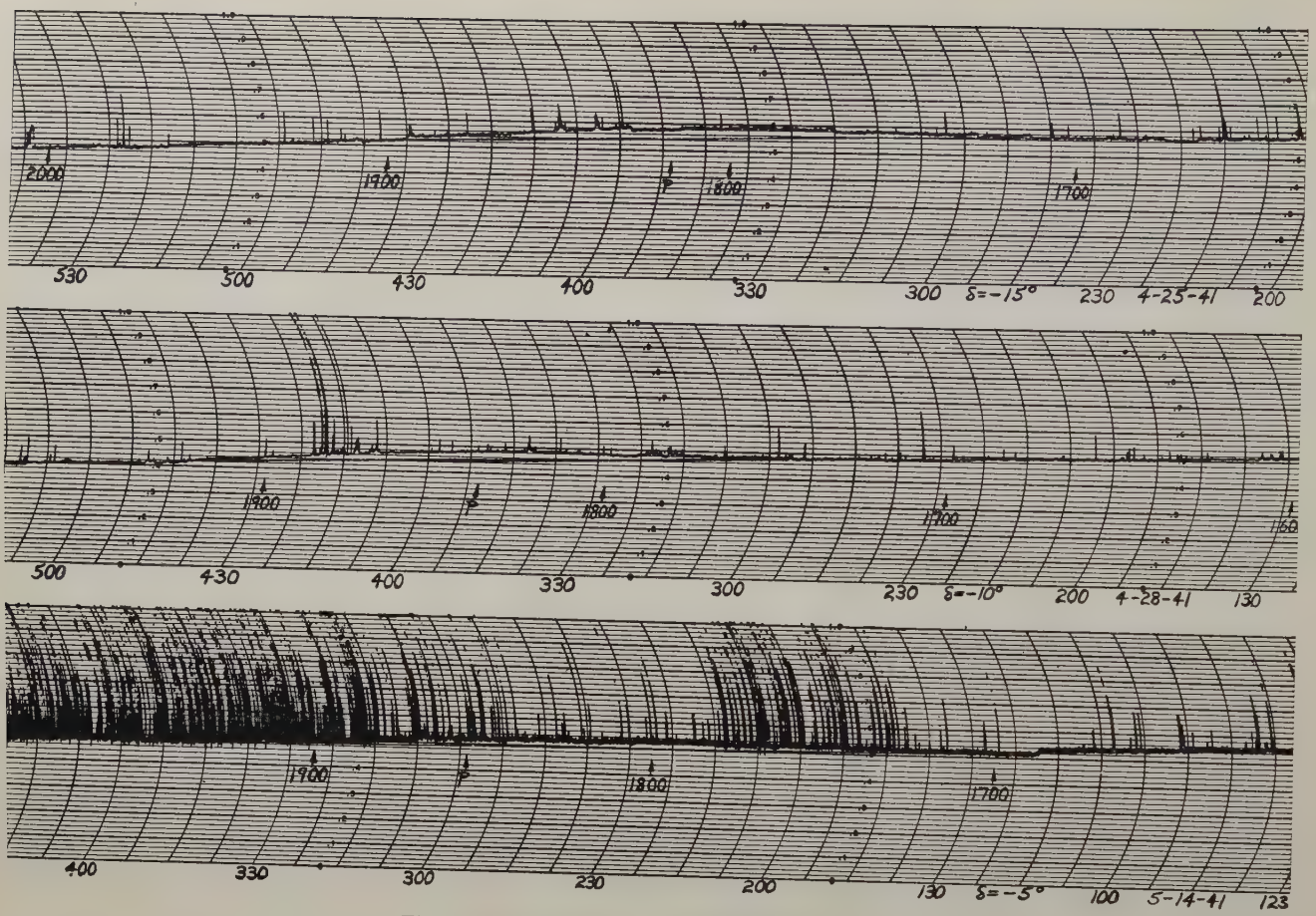


Fig. 12—Sample charts of cosmic-static record.

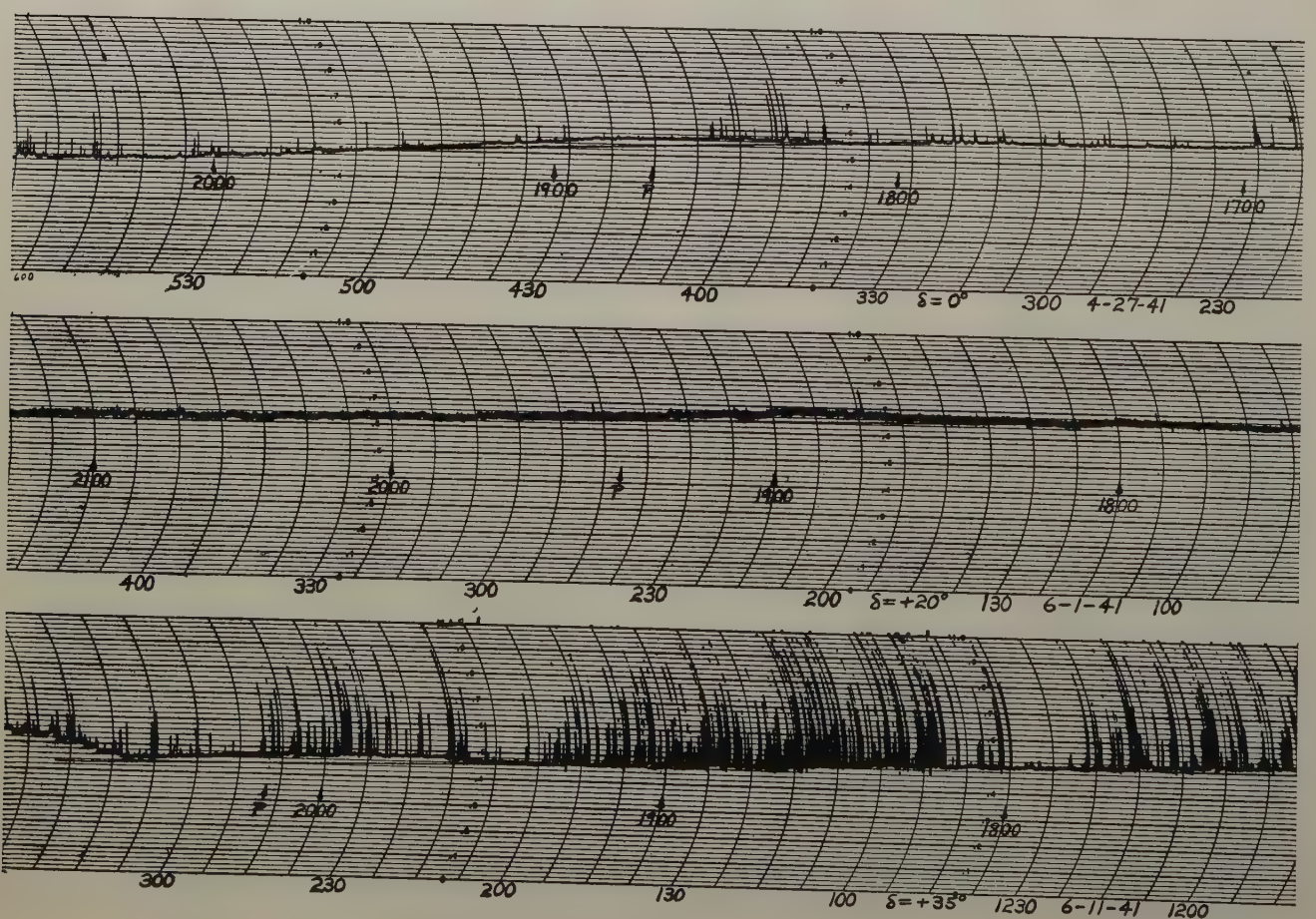


Fig. 13—Sample charts of cosmic-static record.

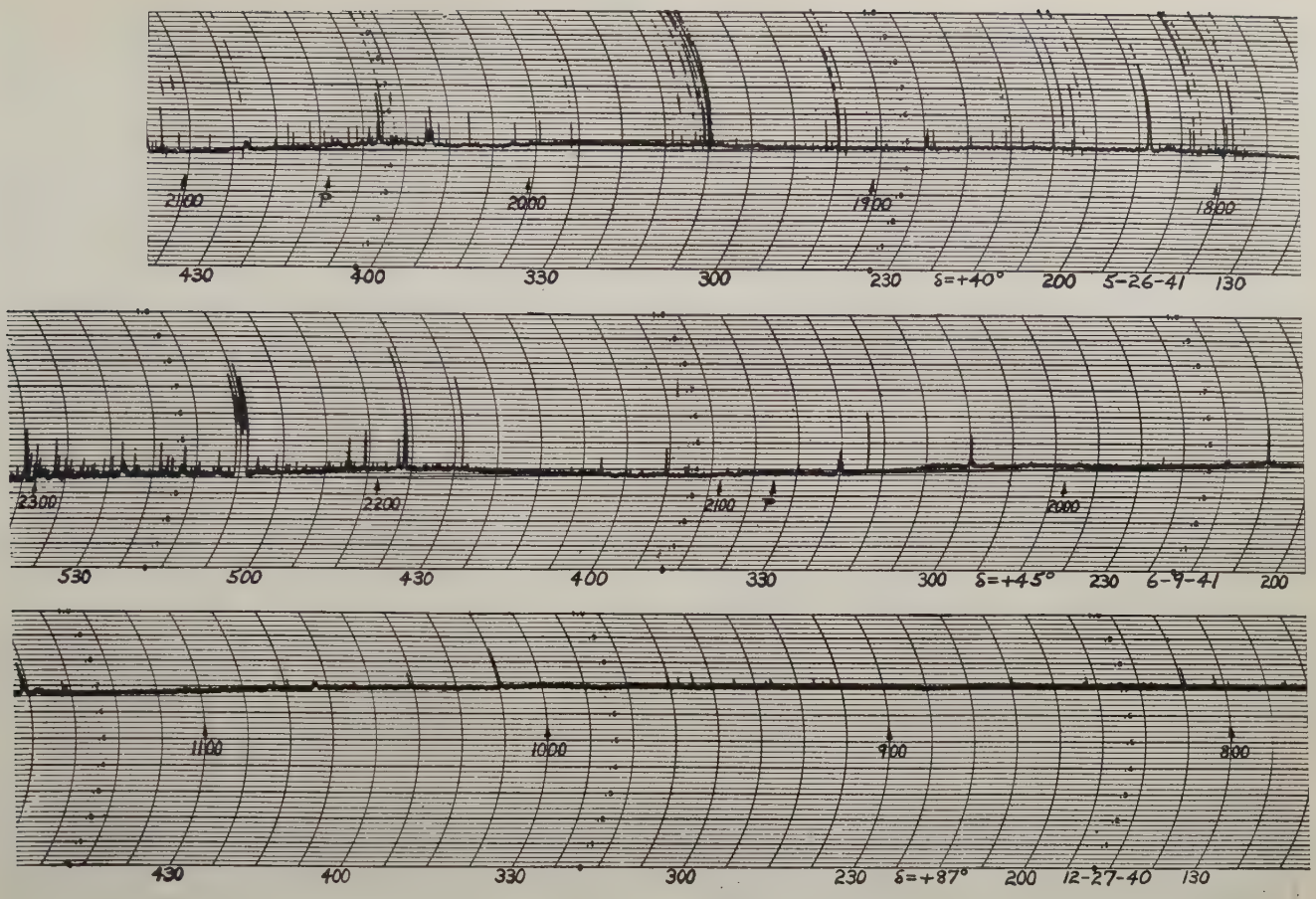


Fig. 14—Sample charts of cosmic-static record.

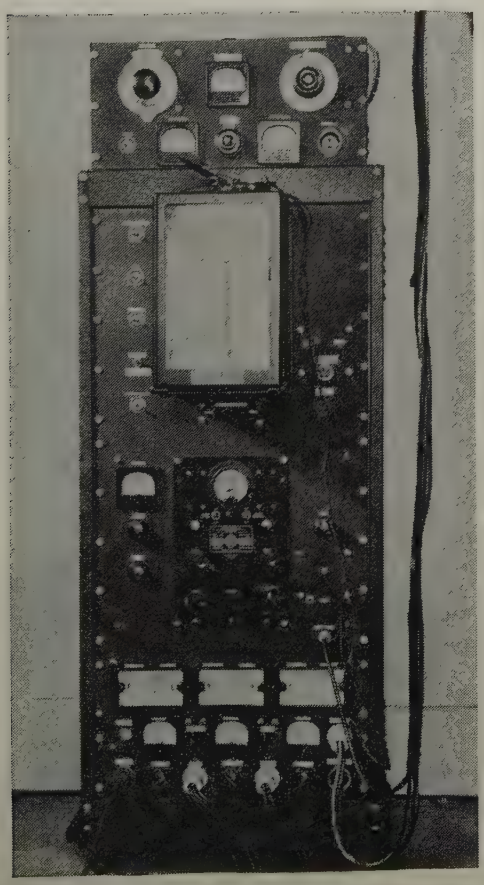

Fig. 15—Front view of recorder and power supply.

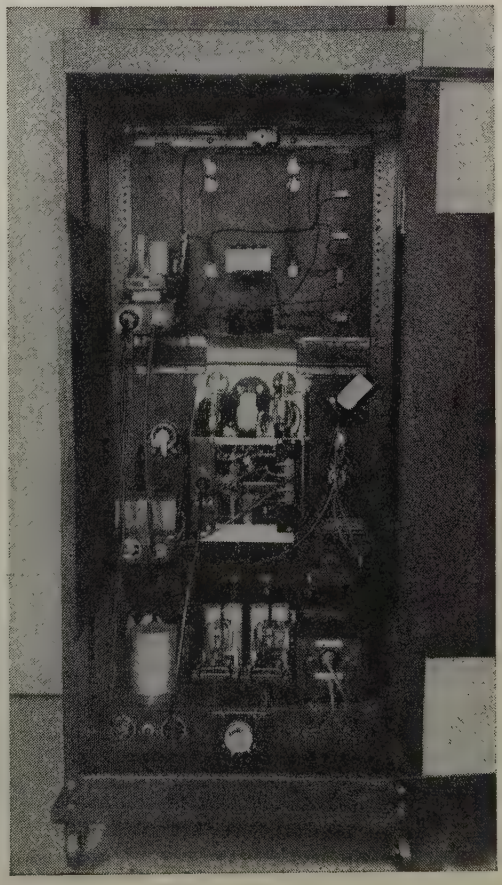

Fig. 16—Rear view of recorder and power supply.

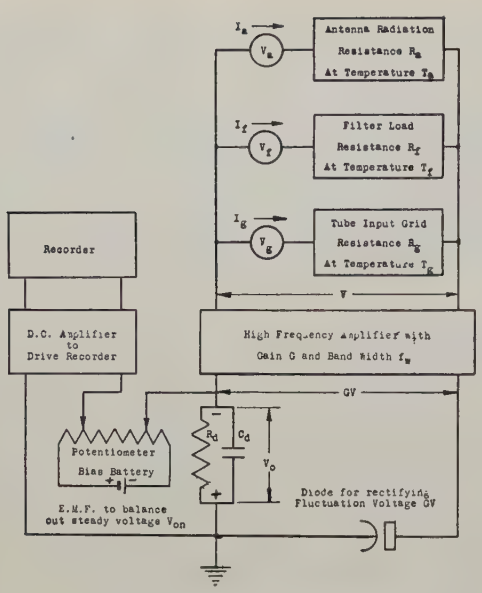


Fig. 17—Block diagram of the entire system with the exception of power supply.

peaks in a given time exceeding $4GV$ is proportional to the bandwidth, the duration of the peaks is inversely proportional to the bandwidth. Consequently if $S$ is not a constant it will not change rapidly with $f_w$. For practical purposes a rounded value of $S=1$ may be assumed. The ratio of direct signal voltage to ripple voltage is

$$\frac{V_{os}}{V_r} = \left(\frac{2SC_d}{q}\right)^{1/2} (kf_wR_f)^{1/4} \left(T_a + T_f + T_g\frac{R_f}{R_g}\right)^{1/4} \left[\left(1 - \left(\frac{T_fR_g + T_gR_f}{T_aR_g + T_fR_g + T_gR_f}\right)^{1/2}\right)\right]. \tag{6}$$

So far the input circuit has been assumed to contain only resistance. However in practice some shunt capacitance is always present. Wheeler[6] concludes that the maximum uniform impedance which can be built up is limited to

$$R_f = \frac{1}{\pi Cf_w} \text{ ohms.} \tag{7}$$

By inserting this into (6) the limiting value of signal-to-noise ratio is found:

[6] H. A. Wheeler, "Wide-band amplifiers for television," Proc. I.R.E., vol. 27, pp. 429–438; July, 1939.

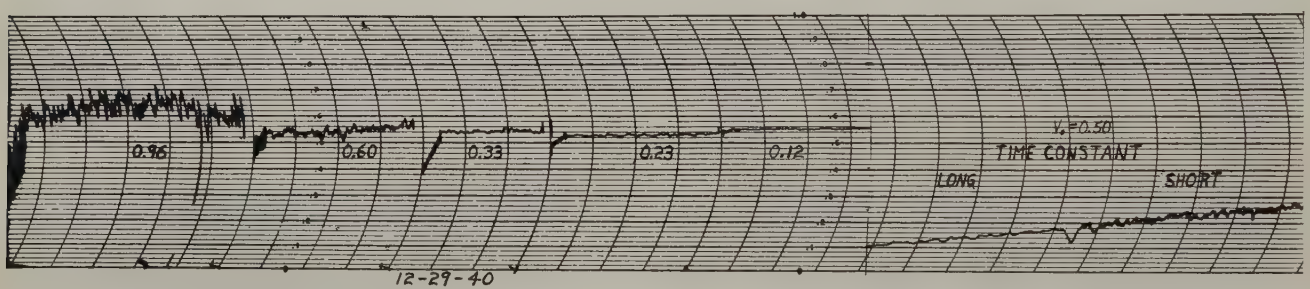


Fig. 18 (a)—Ripple voltage as a function of $V_o$. The random variation increased a bit more rapidly than $V_o$ because as $E_{sg}$ was increased the effective bandwidth decreased slightly.

Fig. 18 (b)—Decrease of ripple voltage caused by increase of time constant of recorder. Chart speed 6 inches per minute. $V_o$=0.5 volt.

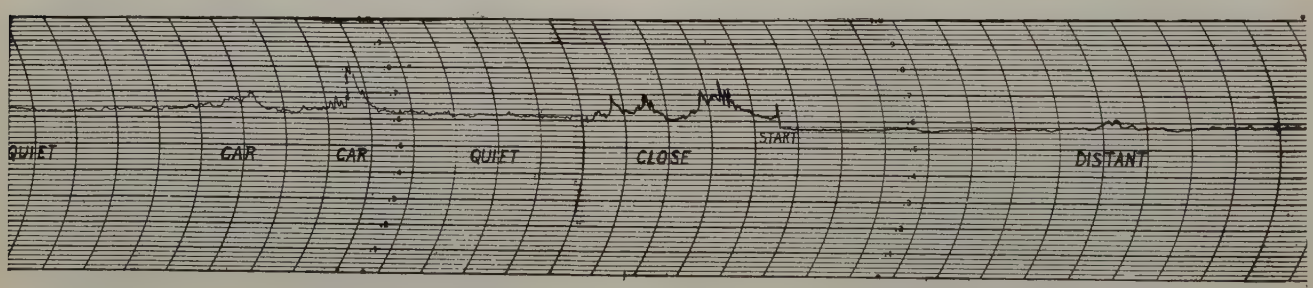


Fig. 19—Sample of auto ignition noise. Receiver at rather low sensitivity as indicated by small width of line.

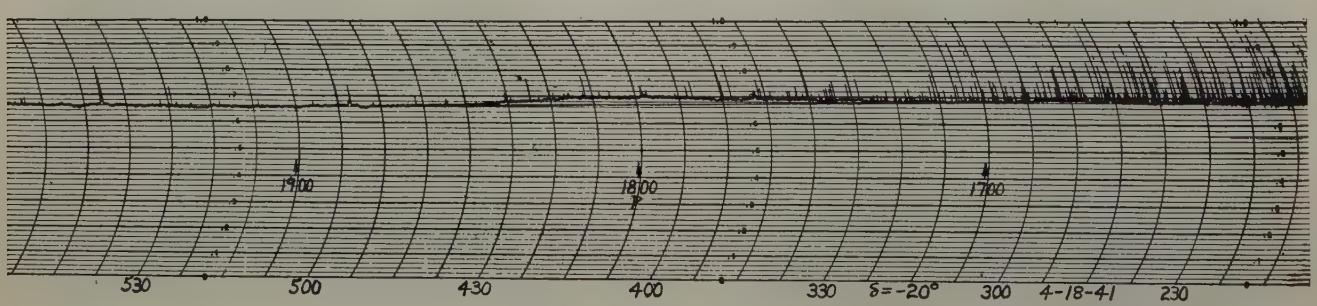


Fig. 20—Record of cosmic static at declination −20 degrees.

$$\frac{V_{os}}{V_r} = \left(\frac{2SC_d}{q}\right)^{1/2} \left(\frac{k}{\pi C}\right)^{1/4} \left(T_a + T_f + T_g\frac{R_f}{R_g}\right)^{1/4} \cdot \left(1 - \left(\frac{T_fR_g + T_gR_f}{T_aR_g + T_fR_g + T_gR_f}\right)^{1/2}\right). \quad (8)$$

The amount of gain required in the amplifier may be obtained by evaluating (1) for $V$ and (3) for $V_n$. Division of the former by the latter gives the gain $G$ necessary.

To determine $q$ we have without antenna and with the electron damping acting as a filter load resistance

$$q = 4SC_d\left(\frac{V_r}{V_o}\right)^2 (kf_wR_fT_f)^{1/2}. \quad (9)$$

By experiment

$S=1.0$ $\quad V_r/V_o=2\cdot10^{-3}$ $\quad f_w=4.4\cdot10^5$ $\quad T_f=1.4\cdot10^3$
$C_d=4\cdot10^{-9}$ $\quad k=1.37\cdot10^{-23}$ $\quad R_f=7\cdot10^3$.

so $q=5\cdot10^{-19}$ ampere per second. Therefore 3 electrons are contained in the average random charge.

## Signal-to-Ripple Ratio

The limit of sensitivity is reached when the rise produced by cosmic static is of the same magnitude as the ripple voltage. Increased gain will be of no avail as indicated by (6) and verified by Fig. 18(a). Each level was taken at 6 inches per minute to show the fine structure of the random voltage and 6 inches per hour to show the width of the resulting line. The rather steep drop at the low chart rate is caused by the gradual warm-up of the amplifier. The sensitivity may be increased by increasing $C_d$ as shown in Fig. 18(b); or the product $R_ff_w$ may be increased out to a limit of $1/\pi C$. Then either $C$ or the effective temperature of the input circuit $(T_f+T_gR_f/R_g)$ may be decreased. While not obvious from (8), it will be found upon evaluation when $T_a<T_f\gg T_gR_f/R_g$ that $V_{os}/V_r$ is about proportional to $(1/T_f)^{1/2}$. Ferris[7] has shown that the effective temperature associated with thermal-agitation noise from electron loading is 1.4 times the true cathode temperature $T_k$ or $T_g=1.4T_k$. So to increase sensitivity it is necessary not only to reduce $T_f$ but also to keep $T_gR_f/R_g$ small compared to $T_f$.

## Thermodynamic Relations

From Fig. 17 we find the energy of the input system is

$$\begin{aligned} &2V_n^2/R_f \quad \text{when} \quad T_a = 0 \\ &2V^2/R_f \quad \text{when} \quad T_a = T_a. \end{aligned} \quad (10)$$

The gain in energy becomes

$$U = \frac{2}{R_f}(V^2 - V_n^2) = 2kT_af_w \text{ watts}. \quad (11)$$

[7] D. O. North and W. R. Ferris, "Fluctuations in vacuum-tube grids," Proc. I.R.E., vol. 29, pp. 49–50; February, 1941.

Now define the incremental rise of voltage from cosmic static as

$$\Delta = \frac{V_s}{V_n} = \frac{V - V_n}{V_n}. \quad (12)$$

Consequently, $V^2 - V_n^2 = 2\Delta V_n^2$. Substitution of this into (11) gives for the energy captured from space

$$U = 4\Delta kf_w\left(T_f + T_g\frac{R_f}{R_g}\right) \text{ watts}. \quad (13)$$

Equating (11) and (13) gives the effective temperature of the antenna radiation resistance as

$$T_a = 2\Delta\left(T_f + T_g\frac{R_f}{R_g}\right). \quad (14)$$

It must be noted that this is not the temperature of space in the direction toward which the apparatus is pointed but a good many times space temperature depending upon the size of mirror, resolving power, and efficiency of the drum.

Consider the question of transfer of energy by letting the power sent into resistor $R_a$ from the network be $U_1$

$$U_1 = \frac{V^2}{R_f}kf_w\left(T_a + T_f + T_g\frac{R_f}{R_g}\right). \quad (15)$$

Similarly let the power generated in resistor $R_a$ and transferred to the network be $U_2$

$$U_2 = 2kT_af_w. \quad (16)$$

When $U_1=U_2$ then $T_a=T_f+T_gR_f/R_g$ and the system is in equilibrium.

When $U_1<U_2$ then $T_a>T_f+T_gR_f/R_g$ and the system absorbs energy from space.

When $U_1>U_2$ then $T_a<T_f+T_gR_f/R_g$ and the system radiates thermal-agitation-noise energy or sends out a beam of hiss noise into space. This is the case actually existing.

For calibrating the apparatus we have on the bench without dummy antenna

$$\begin{aligned} V^2 &= 4kf_wR_fT_f\left(1 + \frac{T_gR_f}{T_fR_g}\right) \\ \text{and} \quad V_o &= 2SG(kf_wR_fT_f)^{1/2}\left(1 + \frac{T_gR_f}{T_fR_g}\right)^{1/2}. \end{aligned} \quad (17)$$

On the bench with dummy antenna of $R_a=R_f$ and $T_a=T_f$

$$\begin{aligned} V^2 &= kf_wR_fT_f\left(2 + \frac{T_gR_f}{T_fR_g}\right) \\ \text{and} \quad V_o &= \sqrt{2}SG(kf_wR_fT_f)^{1/2}\left(1 + \frac{T_gR_f}{2T_fR_g}\right)^{1/2}. \end{aligned} \quad (18)$$

On the drum and pointed to empty space $R_a=R_f$ and $T_a$ is zero

$$V^2 = kf_wR_fT_f\left(1 + \frac{T_gR_f}{T_fR_g}\right)$$

and

$$V_o = SG(kf_wR_fT_f)^{1/2}\left(1+\frac{T_gR_f}{T_fR_g}\right)^{1/2}. \qquad (19)$$

## Automobile-Ignition Noise

It is quite well known[8,9] that the radiation or acceptance pattern of an opening for electromagnetic waves which is small compared to a wavelength is $r=(\cos\theta)^2$ in the plane of the electric vector and $r=(\cos\theta)^{3/2}$ in the plane of the magnetic vector. Now the mirror when viewed from the focal point (aperture of drum) subtends a solid angle of 43 degrees. Consequently the major part of the drum acceptance pattern is covered by the mirror. However beyond the edge of the mirror and out to $\theta=90$ degrees the drum is still, though rather inefficiently, capable of receiving electromagnetic energy. It is in this region that the ignition disturbance leaks in. The noise from one car is merely a series of popping sounds and might be dealt with successfully; however the noise in the aggregate from many cars approaches a continuous spectrum which has a variable intensity from moment to moment and consequently disrupts any attempts at delicate measurements. By reason of the urban location where this work is being carried on the only useful hours are from midnight to about 6 A.M.

## Results

Data are obtained by measuring output versus time for a given declination setting of the mirror. The results then appear as intensity versus right ascension. When no electromagnetic energy is captured from space the recorder will draw a straight line. Because the various balances used in the apparatus are generally imperfect, the slope of the line is seldom zero. This situation is of little consequence provided the line remains on scale the required length of time. When energy from the heavens is intercepted the line will rise slightly from its normal position. The amount of this deflection in terms of reference level (thermal-agitation noise) gives the absolute amount of cosmic-static energy at the input terminals of the amplifier. In order to reduce this energy back to intensity from the sky, the characteristics of the drum, mirror, and acceptance pattern of the entire collector must be known. The charts reproduced in Figs. 10 to 14 are samples of those obtained at a frequency of 160 megacycles per second. Chart speed in all cases is 6 inches per hour and Central Standard Time is noted at the bottom. Direction in terms of right ascension at the meridian is indicated by arrows marked with the sidereal time. The arrow marked $P$ indicates the accepted plane of the milky way.

Sidereal time gains about 4 minutes per day on mean solar time. Therefore a given source of cosmic-static disturbance should move forward at this rate if the energy really is coming from a fixed position in space. The charts shown in Fig. 10 were taken at $-25$ degrees declination on the dates noted and demonstrate the expected regular advance with time. Comparison between Fig. 11 and Fig. 20 will show the same result for data taken at $-20$ degrees declination. In the latter case during the early morning hours considerable rain static was present from local thunderstorm which gradually disappeared by 3:30 A.M.

Figs. 11 to 14 show charts taken at various declinations across the milky way from Scorpio to Cygnus. It will be observed that in the direction of Scorpio the energy arrives from a broad band in the sky which closely agrees with the accepted center of the galaxy. As traces are scanned at more northern declinations the center of the disturbance becomes weaker and gradually moves off to the west of the accepted plane of the galaxy. Finally in the region of Cygnus a split seems to originate somewhere between galactic longitude 40 and 45 degrees. This is first apparent at $\delta=+40$ degrees where the center of the disturbance had divided into two maxima of equal amplitude at right ascensions 1945 and 2025. At $\delta=+45$ degrees the west branch has continued in about the same direction (RA2010) while the east branch has crossed to the other side of the plane of the galaxy and has become entirely separate (RA2150) and stronger. In other words there is some evidence that a split occurs in this cosmic-static disturbance similar to the well-known split in the milky way. Unfortunately, the present method of scanning along declination lines makes it quite difficult to obtain good data beyond $\delta=+45$ degrees. Table III gives a résumé of all the automatically recorded data at hand. The additional information necessary for reducing the data is drum efficiency $E_d=50$ per cent, mirror efficiency $E_m=85$ per cent, area of mirror $A=7\times10^5$ square centimeters. As determined from Tables I and II the electron loading of the first grid is the main damping on the input circuit. Therefore in computing $U$ from (13) the value of $T_g$ is 1400 degrees; $R_f=R_g$ and the first term within the brackets is dropped as nonexistent. The acceptance pattern of the collector is an ellipse 6 degrees high ($\phi_M$) and 8 degrees wide ($\phi_E$). Since only the horizontally polarized radiation is received, the total energy available is $2U$ on the assumption that cosmic static is of random polarization. Therefore, the absolute intensity in watts per square centimeter, per circular degree, per kilocycle band is

$$I=\frac{2U}{E_dE_mA\phi_E\phi_Mf_w}=\frac{8\Delta kT_g\cdot10^3}{E_dE_mA\phi_E\phi_M}. \qquad (20)$$

Data from the region Perseus to Puppis were taken in the autumn of 1940 and are not particularly good. However comparison will show the results to be in substantial agreement with the initial survey as

[8] G. Reber, "Electric resonance chambers," *Communications*, vol. 18, p. 5; December, 1938.

[9] W. L. Barrow and F. M. Greene, "Rectangular hollow-pipe radiators," Proc. I.R.E., vol. 26, pp. 1498–1520; December, 1938.

previously[1] described. The last chart taken at declination $\delta = +87$ degrees is one of three taken to check upon whether or not this disturbance might possibly be of local origin. As these three runs all give no response it may be assumed the extraterrestrial origin is correct.

Charts taken on 4-18-41 ($\delta = -20$), 5-14-41 ($\delta = -5$), and 6-11-41 ($\delta = +35$) were made during local thunderstorms. Even under these unfavorable conditions the response from cosmic static can be seen. During the morning of 6-11-41 shortly before the cosmic static had moved out of range at 3:15 A.M. a severe wind arose and the resulting vibration upset the tuning adjustments causing the pen to run off scale. At these short radio wavelengths, rain static does not have the crash and rumble characteristic of long radio wavelengths but rather is a series of loud snaps, one for each lightning flash. Because the directivity of the collector limits the recorded flashes to a small chosen direction, relatively few appear on the chart. Consequently the receiver has time to clear itself and return to normal between flashes even though the surges are of tremendous amplitude. How automobile-ignition noise differs from this and its disruptive characteristics were discussed in a preceding section. The few small spikes and peaked rises shown on some of the charts are caused by, respectively, the opening or closing of contacts in electrical devices and the passing of a single car. The real solution of these difficulties would be to move the apparatus out in the desert somewhere far from any man-made electrical disturbances. Then, and then only could data be taken over the entire 24 hours and critical measurement made on several important points. Radiation from the corona of the sun has been estimated as of sufficient magnitude to be detectable but so far this has been impossible of substantiation or denial. Likewise a very desirable check on the possible absorption from ionization of the earth's upper atmosphere would be obtained by making duplicate measures of the intensity at selected directions during the daylight hours as well as at night.

Returning to (14) and the next to the last column of Table III, we find that the maximum value of $\Delta$ is 2.6 per cent of the reference level. Applying the same reasoning set out for the calculation of the intensity we find the maximum value of $T_a$ to be 73 degrees which is the maximum effective temperature of the antenna radiation[10] resistance $R_a$.

Quoting from Johnson,[11] "The electric charges in a conductor are found to be in a state of thermal agitation, in thermodynamic equilibrium with the heat motion of the atoms of the conductor. The manifestation of the phenomenon is a fluctuation of potential difference between the terminals of the conductor which can be measured by suitable instruments." Moullin[4] on pages 66 and 67 outlines Bell's[12] derivation of thermal-agitation noise which starts out with the number of free electrons per cubic centimeter, the

TABLE III

| Galactic longitude in degrees | Declination in degrees | Date of record | Volts deflection | Volts reference level | Per Cent | Intensity in watts per square centimeter, circular degree, kilocycle band |
|---|---|---|---|---|---|---|
| 322.5 | −32.5 | 4-10-41 | 0.0037 | 0.22 | 1.7 | |
| | | 4-11-41 | 0.0063 | 0.21 | 3.0 | |
| | | 4-12-41 | 0.0058 | 0.21 | 2.8 | |
| | | 5-10-41 | 0.0060 | 0.27 | 2.2 | |
| | | | | average | 2.4 | $2.9\times10^{-25}$ |
| 331.5 | −25 | 4-14-41 | 0.0048 | 0.16 | 3.0 | |
| | | 4-17-41 | 0.0024 | 0.16 | 1.5 | |
| | | 5-24-41 | 0.0043 | 0.29 | 1.5 | |
| | | 6- 6-41 | 0.0068 | 0.22 | 3.1 | |
| | | 6- 7-41 | 0.0085 | 0.22 | 3.9 | |
| | | | | average | 2.6 | 3.1 |
| 337.2 | −20 | 4-18-41 | 0.0029 | 0.25 | 1.2 | |
| | | 4-19-41 | 0.0037 | 0.25 | 1.5 | |
| | | 5- 8-41 | 0.0055 | 0.27 | 2.0 | |
| | | | | average | 1.6 | 1.9 |
| 342.6 | −15 | 4-24-41 | 0.0046 | 0.24 | 1.9 | |
| | | 4-25-41 | 0.0038 | 0.24 | 1.6 | |
| | | 4-26-41 | 0.0040 | 0.24 | 1.7 | |
| | | | | average | 1.7 | 2.0 |
| 348.1 | −10 | 4-28-41 | 0.0035 | 0.24 | 1.5 | |
| | | 4-30-41 | 0.0035 | 0.24 | 1.5 | |
| | | | | average | 1.5 | 1.8 |
| 354.5 | −5 | 5-14-41 | 0.0027 | 0.28 | 1.0 | |
| | | 5-16-41 | 0.0025 | 0.28 | 0.9 | |
| | | | | average | 1.0 | 1.2 |
| 0.0 | 0 | 4-13-41 | 0.0030 | 0.22 | 1.4 | |
| | | 4-27-41 | 0.0030 | 0.24 | 1.2 | |
| | | 5- 5-41 | 0.0023 | 0.27 | 0.9 | |
| | | 5- 6-41 | 0.0045 | 0.27 | 1.6 | |
| | | | | average | 1.3 | 1.6 |
| 5.5 | +5 | 5-17-41 | 0.0053 | 0.28 | 1.9 | 2.3 |
| 10.9 | +10 | 5-20-41 | 0.0028 | 0.25 | 1.1 | 1.3 |
| 22.0 | +20 | 5-30-41 | 0.0035 | 0.27 | 1.3 | |
| | | 6- 1-41 | 0.0039 | 0.27 | 1.4 | |
| | | 6- 2-41 | 0.0041 | 0.25 | 1.6 | |
| | | | | average | 1.4 | 1.7 |
| 40.3 | +35 | 6-11-41 | 0.0033 | 0.22 | 1.5 | 1.8 |
| 45.5 | +40 | 5- 4-41 | 0.0047 | 0.27 | 1.7 | |
| | | 5-26-41 | 0.0028 | 0.27 | 1.0 | |
| | | 5-27-41 | 0.0026 | 0.27 | 1.0 | |
| | | 5-28-41 | 0.0020 | 0.27 | 0.7 | |
| | | | | average | 1.1 | $1.3\times10^{-25}$ |
| 52.3 | +45 | 6- 4-41 | 0.0046 | 0.25 | 1.8 | |
| | | 6- 5-41 | 0.0020 | 0.21 | 1.0 | |
| | | 6- 9-41 | 0.0018 | 0.22 | 0.8 | |
| | | west branch | | average | 1.2 | 1.4 |
| | | 6- 9-41 | 0.0029 | 0.22 | 1.3 | |
| | | east branch $\frac{1.3}{0.8}\times1.4\times10^{-25}$ | | | | 2.3 |
| 114.7 | +53½ | 10-10-40 | 0.0052 | 0.37 | 1.4 | |
| | | 10-11-40 | 0.0028 | 0.20 | 1.4 | |
| | | | | average | 1.4 | 1.7 |
| 120.7 | +50 | 10- 5-40 | 0.0047 | 0.37 | 1.3 | 1.6 |
| 125.9 | +46 | 10-18-40 | 0.0020 | 0.30 | 0.7 | |
| | | 10-19-40 | 0.0032 | 0.33 | 1.0 | |
| | | | | average | 0.8 | 1.0 |
| 139.3 | +35 | 10-20-40 | No evidence. Intensity less than | | | 0.3 |
| | | 10-21-40 | | | | |
| 151.3 | +24 | 10-13-40 | 0.0039 | 0.56 | 0.7 | |
| | | 10-16-40 | 0.0020 | 0.24 | 0.8 | |
| | | | | average | 0.8 | 0.9 |
| 171 | +7½ | 10- 6-40 | 0.0040 | 0.53 | 0.8 | 0.9 |
| 180 | 0° | 10-26-40 | No evidence. Intensity less than | | | 0.3 |
| | | 11- 3-40 | | | | |
| 191 | −10 | 11-10-40 | No evidence. Intensity less than | | | 0.3 |
| | | 11-11-40 | | | | |
| 216.7 | −32.5 | 12-26-40 | 0.0020 | 0.21 | 1.0 | |
| | | 12-31-40 | 0.0037 | 0.35 | 1.0 | |
| | | | | average | 1.0 | 1.2 |

[10] W. A. Harris, RCA Review, vol. 6, pp. 119–121; July, 1941.
[11] J. B. Johnson, *Phys. Rev.*, vol. 32, p. 97; July, 1928.
[12] D. A. Bell, *Jour. I.E.E.* (London), Vol. 82, p. 529; 1938.

mean free path, and the average time of flight. It ends up with the desired formula $V^2/R=4kTf_w$. Now it is well known that the material of space contains large numbers of free electrons, and that these electrons are in equilibrium with the energy density of the particular region. Consequently it appears a reasonable assumption that the magnitude of $R_a$ and $T_a$ can be determined by the measuring apparatus but the nature of $R_a$ is determined in the depths of space. In such a case, cosmic static is really thermal-agitation noise on a grandiose scale where all of the space is the conductor and the input terminals of the amplifier are projected by means of the antenna and collector system to some far distant part represented by $R_a$. The nature of the material encountered in the conductor can never be duplicated in the laboratory as the mean free path of the electrons is about $10^9$ kilometers or about the radius of the orbit of the planet Jupiter. Now if this speculation has any foundation, then the intensity-versus-frequency function of cosmic static should be the same as that of thermal-agitation noise; in other words the intensity per unit frequency bandwidth should be constant independent of frequency from any region in the sky. To determine whether or not this is really the case can best be learned by measurements at some other frequency several octaves from the present one of 160 megacycles. From the above point of view the whole device may be considered as a very special type of sensitive bolometer where the variable arm of the bridge consists of the material in space. The writer is of the opinion that, given proper apparatus, the study of this long-wave electromagnetic radiation will produce information important to the physical sciences.

# Transients in Frequency Modulation*

H. SALINGER†, ASSOCIATE, I.R.E.

***Summary***—*In a frequency-modulation system, a sudden jump in carrier frequency corresponding to a Heaviside unit signal will result in a transient depending on the receiving-filter bandwidth. If this bandwith exceeds twice the maximum frequency swing, the shape and duration of the transient is shown to be about the same as in an amplitude-modulation system with the same bandwidth; for narrower filters the transient lasts longer. These results are applied to several practical cases. The transient is favorably affected by using an amplitude limiter and by arranging the filter pass band so as to enclose the maximum frequency swing symmetrically.*

IT IS one of the fundamental facts of communication technique that to receive modulated waves, a certain filter bandwidth is necessary. For amplitude-modulated signals, this law can be stated either in terms of the useful sidebands which have to pass the receiving filters, or in terms of the transients which will originate in these filters due to a sudden change in carrier amplitude.

With the growing interest in frequency modulation, it is natural to study the same question in this case. The first method is readily applicable, for the position and intensity of the sidebands in frequency modulation are well understood. However, for certain applications which have been proposed, especially in the television field, it is more desirable to consider the transients which will develop in the receiver upon a sudden change in frequency. This problem will be dealt with in the present paper.

It is sometimes argued that, as the amplitude of a frequency-modulated wave stays constant, a sudden change in frequency will not change the energy content of the circuits involved; therefore, it is concluded that no transients should occur. But this claim will not stand examination. A sudden change in frequency is equivalent to switching off the original frequency while the new frequency is simultaneously switched on. This will generate in the receiving filter two transients, the envelopes of which are similar and add up to a constant value, but, as the carrier frequencies are different, beats will occur, and these would affect a frequency-modulation receiver.

## I. Theory

In the case of amplitude modulation, the standard method of attacking the problem is to consider an incident wave,

$$\begin{aligned} z &= A \sin \Omega t \cdots t < 0, \\ z &= (A + B) \sin \Omega t \cdots t > 0; \end{aligned} \tag{1'}$$

in a linear system, $A=0$ can be assumed without loss of generality. This wave is passed through an ideal filter, which has infinite attenuation outside a frequency range $\Omega_1$ to $\Omega_2$, and a constant or even zero attenuation inside this range. The carrier frequency $\Omega$ lies between $\Omega_1$ and $\Omega_2$ and usually $\Omega=\frac{1}{2}(\Omega_1+\Omega_2)$ is assumed. The phase constant of the filter is taken as varying linearly with the frequency inside the transmission band.

In our case, let us start with equally simple assumptions. The incident wave is

$$\begin{aligned} z &= \sin \omega_1 t \cdots t < 0, \\ z &= \sin \omega_2 t \cdots t > 0. \end{aligned} \tag{1}$$

The filter is again assumed to be an ideal one, with the transmission range lying between $\omega_1-\delta_1$ and

* Decimal classification: R 414. Original manuscript received by the Institute, September 22, 1941.

† Formerly, Farnsworth Television and Radio Corporation, Fort Wayne, Indiana; now 801 West Packard Avenue, Fort Wayne, Indiana.

$\omega_2+\delta_2$; but for the moment, we shall consider only the case $\delta_1=\delta_2=\delta$, so that the frequency swing lies symmetrically inside the filter transmission range. As in practical cases $\omega_2-\omega_1 \ll \omega_1$, we may introduce an average frequency $\Omega$ by letting $\omega_1=\Omega-\Delta$, $\omega_2=\Omega+\Delta$. No loss in generality will occur by assuming $\Delta>0$, i.e., $\omega_1<\omega_2$. These conditions are schematically represented in Fig. 1.

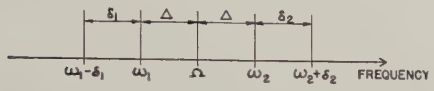


Fig. 1—Relative position of signal frequencies and filter limits.

The method of complex integration lends itself as readily to this case as to the corresponding amplitude-modulation problem.[1] The theory is developed in the Appendix and leads to a formula for the output current of the filter

$$y = \sin \Omega t \cos \Delta t + \frac{1}{\pi} \cos \Omega t \,(L \sin \Delta t + K \cos \Delta c), \quad (2)$$

where $K = \mathrm{Ci}(\delta+2\Delta)t - \mathrm{Ci}\delta t$, $L = \mathrm{Si}(\delta+2\Delta)t + \mathrm{Si}\delta t$; $\mathrm{Si}(x)$ and $\mathrm{Ci}(x)$ are the sine and cosine integrals.

As $\Delta \ll \Omega$ and $\delta \ll \Omega$, (2) can be considered as a wave of average frequency $\Omega$, but of varying phase $\phi$ and amplitude $A$; then

$$y = A \sin (\Omega t + \phi)$$

where

$$\phi = \tan^{-1} \frac{1}{\pi} (L \tan \Delta t + K). \quad (3)$$

If this wave is sent through an amplitude limiter and balanced frequency detector, a signal proportional to $d\phi/dt$ will be recorded. In forming $d\phi/dt$, it is useful to remember that

$$\frac{dL}{dt} \sin \Delta t + \frac{dK}{dt} \cos \Delta t = 0 \quad (4)$$

which can easily be proved. We finally get

$$\frac{d\phi}{dt} = \frac{\Delta}{\pi} \cdot \frac{L}{\cos^2 \Delta t + \frac{1}{\pi^2} (L \sin \Delta t + K \cos \Delta t)^2}. \quad (5)$$

This gives $d\phi/dt = \pm\Delta$ for $t = \pm\infty$, as it should, for at large negative values of $t$ we have a frequency $\omega_1 = \Omega - \Delta_1$ and for large positive values of $t$, $\omega_2 = \Omega + \Delta$. It is therefore advantageous to introduce a "reduced detected frequency" $\tilde{\omega}$ given by

$$\tilde{\omega} = \frac{1}{\Delta} \frac{d\phi}{dt}. \quad (6)$$

$\tilde{\omega}$ becomes $\pm 1$ for $t = \pm\infty$, vanishes at $t=0$, and is an odd function of $t$; that is, $\tilde{\omega}(-t) = -\tilde{\omega}(t)$. It is therefore necessary to plot $\tilde{\omega}(t)$ only for positive values of $t$. If we take $\Delta t$ as the abscissa, we get curves which are perfectly general, and depend only on the parameter $p = \delta + \Delta/\Delta$ = filter bandwidth/frequency swing.

This has been done in Fig. 2. It is at once seen that

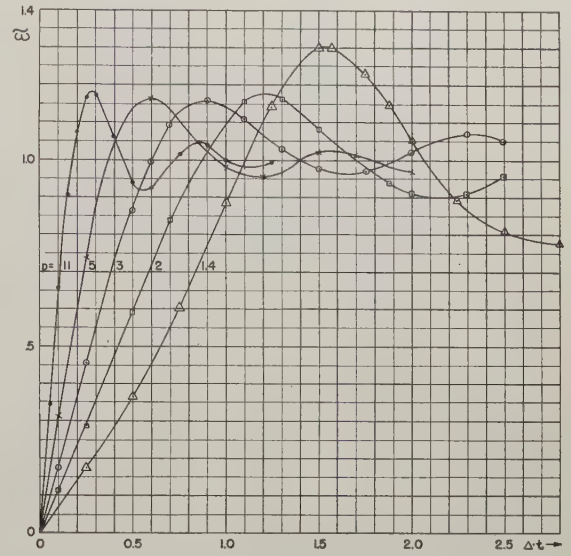


Fig. 2—Shape of transients. $p$ is the ratio of filter bandwidth/frequency swing.

the transition from $\omega_1$ to $\omega_2$ (that is, from $\tilde{\omega}=-1$ to $\tilde{\omega}=+1$) takes the more time, expressed in the scale of $\Delta t$, the smaller the parameter $p$ is.

The question suggests itself as to how this transition time compares with that of an amplitude-modulation system of equal filter bandwidth. To answer this question, the curves have been redrawn in Fig. 3 with $(\delta+\Delta)t$ as abscissa instead of $\Delta t$. $\delta+\Delta$ is half the filter bandwidth. This can be compared to the amplitude-

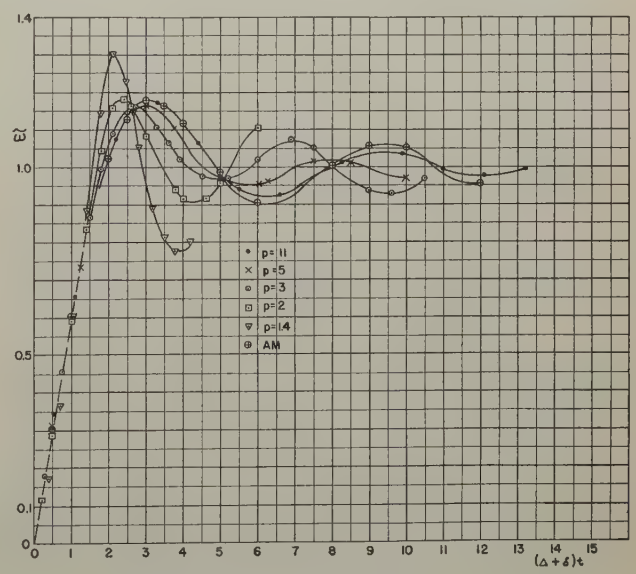


Fig. 3—Transients in frequency modulation and amplitude modulation, for equal filter bandwidth.

modulation transient for an equal bandwidth, for which the formula

$$y = \tfrac{1}{2} \sin \Omega t \left(1 + \frac{2}{\pi} \mathrm{Si}(\delta+\Delta)t\right) \quad (7)$$

[1] H. A. Wheeler's paper "The solution of unsymmetrical sideband problems with the aid of the zero-frequency carrier," PROC. I.R.E., vol. 29, pp. 446–458; August, 1941, in which an alternative method is proposed, appeared after this analysis was completed.

is easily derived. The amplitude of (7) (or rather the quantity $2/\pi \mathrm{Si}(\delta+\Delta)t$ which gives the upper half of the transition curve and is comparable to our frequency-modulation curves) is also plotted on Fig. 3 and marked $AM$.

These curves reveal the fact that the initial rise is identical for all the curves, and depends only on the filter bandwidth, at least as long as $p>2$; e.g., all the curves cut the line $\bar{\omega}=1$ initially at a time $\tau$ given approximately by $(\Delta+\delta)\tau=1.8$. $\Delta+\delta$ is half the bandwidth in radians. If $b=(\Delta+\delta)/\pi$ is the bandwidth in cycles per second, then the transition time is $2\tau=3.6/\pi b=1.1/b$; the factor 2 arising from the fact that our curves show only the upper half of the transient.

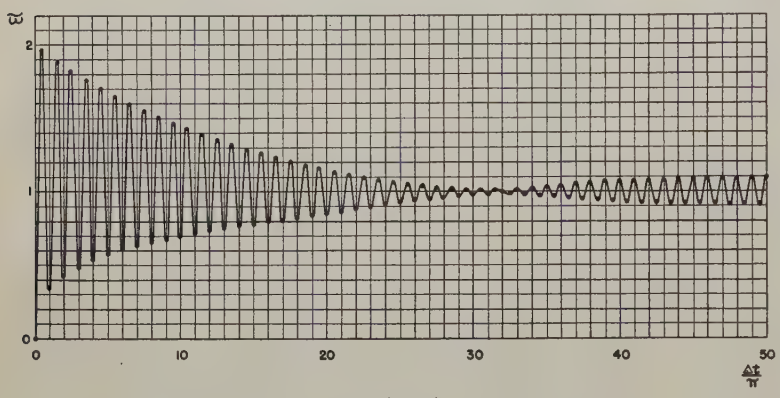


Fig. 4—Transient for $p=1.02$.

For larger values of $t$, the curves no longer coincide, but are still similar to one another.

The curve for $p=1.4$ is different from the other curves, and in view of the large transient fluctuations distinctly less favorable. It is desirable to know what will happen at still lower values of $p$. The tables of the functions Si and Ci which were available did not permit exact calculation of such a curve, but an estimate has been made for $p=1.02$ (that is, when the filter bandwidth exceeds the frequency swing by only 2 per cent) which is shown on Fig. 4. It is seen that the initial rise of the curve is rather unimportant as compared to the violent transient fluctuations which follow it. These fluctuations correspond to a transient frequency of $\Delta/\pi$ cycles per second, and their amplitude will have decayed to within about 10 per cent of the final value after $\delta t=4$ or in our case for $\Delta t\geqq 200$.

## II. Applications

Before we proceed with the general discussion, let us consider the practical import of our results for some typical cases.

1. Frequency-modulation broadcasting, on a carrier frequency of $\Omega=2\pi\cdot 40\cdot 10^6$, and with a swing of $2\Delta=2\pi\cdot 150{,}000$.

The transient should be appreciably shorter than one syllable; let us assume that it must be finished within 0.01 second, that is within $\Delta t=4700$. It is seen from Fig. 4 that this condition is easily fulfilled, even if the filter bandwidth exceeds the frequency swing by only 2 per cent. Thus, in this case, the practically obtainable precision and stability of the filters will determine the bandwidth, i.e., the number of channels per megacycle, rather than transient considerations.

2. Television synchronizing signals transmitted by frequency modulation while the video signals are amplitude-modulated.

We choose $2\Delta=2\pi\cdot 2\cdot 10^6$. The transient should be finished within about 0.005 of the duration of a horizontal line. For a 525-line, 30-frame, interlaced picture this means that the transient may last 0.32 microsecond, corresponding to a $\Delta t$ of 1. The necessary bandwidth is $b=1.1/0.32\cdot 10^6=3.45$ megacycles, for a frequency swing of 2 megacycles. The signal variations which follow the initial steep rise will hardly be of any consequence in this case.

3. Television, transmitted by frequency modulation on a high carrier frequency of several hundred megacycles.

The transition time should be one-half picture element or about 0.064 microsecond. The bandwidth would then have to be $b=1.1/0.064\cdot 10^6=17.2$ megacycles. But this figure is valid only if the frequency swing is not more than half this value, i.e., 8.6 megacycles. If a frequency swing of 20 megacycles is preferred, we should have at least $p=2$ (i.e., 40 megacycles bandwidth), in order to cut down the transient fluctuations which would put a relief structure into the picture. If the fluctuations which Fig. 3 shows for $p\geq 2$ are considered objectionable, it would be necessary that they occur within the time of $\frac{1}{2}\cdot 0.064$ microsecond. Thus from Fig. 3 we might choose $(\Delta+\delta)0.032\cdot 10^6=6$, i.e., $\Delta+\delta=\pi b=1.9\cdot 10^8$ or $b=60$ megacycles.

In all these cases the frequency swing corresponding to maximum signal amplitude was taken as the basis of our figures. If even for this case $p>2$, $p$ will be much larger for a smaller swing, but the time of transition will not be changed. On the other hand, if the filter bandwidth exceeds the maximum swing only slightly, the transient may be troublesome at maximum swing but negligible at smaller signal amplitudes. In this respect, frequency-modulation differs materially from amplitude-modulation operation, where the transient is proportional to the input signal but does not change its shape for different signal amplitudes.

## III. Extensions of the Theory

The remainder of this paper will be devoted to a discussion of some of the simplifications introduced into the theory.

1. A balanced frequency-modulation detector with amplitude limiter was assumed, so that the signal derived from (3) is given by forming $d\phi/dt$ which leads to (5). It is, of course, possible to dispense with this

complicated arrangement and use a coil or a resonant circuit, followed by an ordinary amplitude-modulation detector. This is equivalent to differentiating the first part of (3), or directly, (2), and determining the amplitude of the resulting wave. Thus from (2) and (5) we get

$$\frac{dy}{dt} = \cos \Omega t \left[ \Omega \cos \Delta t + \frac{\Delta}{\pi} (L \cos \Delta t - K \sin \Delta t) \right] - \sin \Omega t \left[ \Delta \sin \Delta t + \frac{\Omega}{\pi} (L \sin \Delta t + K \cos \Delta t) \right]. \quad (8)$$

This is a wave of frequency $\Omega$ with a variable amplitude $A_1$. All we shall do here is to compute its amplitude for $t=0$. As

$$L_{t=0} = 0, \qquad K_{t=0} = \log_e \frac{\delta + 2\Delta}{\delta} = \log_e \frac{p+1}{p-1}, \quad (9)$$

we get

$$(A_1)_{t=0} = \Omega \sqrt{1 + \left( \frac{1}{\pi} \log_e \frac{p+1}{p-1} \right)^2}. \quad (10)$$

For $p=2$, $(A_1)_{t=0} = 1.1\Omega$. Let us take, e.g., the case of frequency-modulation broadcasting with $\Omega/2\pi = 40$ megacycles and $\Delta/2\pi = 75$ kilocycles. The transient, as previously computed with an amplitude limiter present, will consist of a smooth transition from $\Omega-\Delta$ to $\Omega+\Delta$, with a slight overswing on both sides. Particularly at $t=0$, we found $\tilde{\omega}=0$, which means that the instantaneous frequency is $\Omega$. Without the limiter, at this instant the frequency will be higher by 10 per cent, that is, by 4 megacycles. It is at once seen that this method of reception would involve a large transient, and the importance of the amplitude limiter is thus clearly brought out.

This statement is thought to be valid and important even though the action of the amplitude limiter has been considered here in a purely formal way, by assuming that the detector will respond only to the variable phase $\phi$ in (3). A more detailed discussion of the response of an amplitude limiter to a transient, based on an assumed characteristic curve of the limiter, might be worthwhile.

2. The assumption that the frequency swing lies symmetrically within the filter pass band helped to simplify the formulas. Actually, the larger part of the computations in the Appendix was carried out without making use of this simplification. It is not particularly difficult to work out the formulas for the more general case which was shown in Fig. 1, but the formulas get rather unwieldy and will not be reproduced here. They have been worked out for some cases, and the results are plotted in Fig. 5, in which curve 1 represents the case $\delta_1 = \delta_2 = 2\Delta$, curve 2, $\delta_1 = 1.6\Delta$, $\delta_2 = 2.4\Delta$, and curve 3, $\delta_1 = \Delta$, $\delta_2 = 3\Delta$. Thus the total bandwidth is the same in these cases, corresponding to $p=3$. Even though the equation $\tilde{\omega}(-t) = -\tilde{\omega}(t)$ is no longer valid if $\delta_1 \neq \delta_2$, it seemed to be sufficient to draw the curves only for $t>0$.

The curves show that it is not favorable to make $\delta_1$ unequal to $\delta_2$; the transient fluctuations after the initial rise are much more pronounced in this case than for $\delta_1 = \delta_2$.

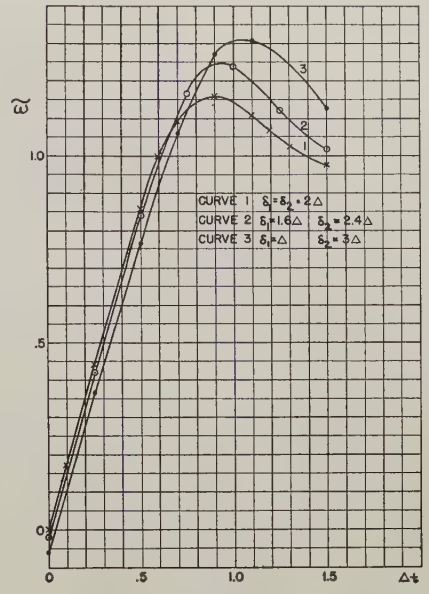


Fig. 5—Transients for unsymmetrical filter position.

3. It may be questioned whether (1) is general enough to form the starting point of our discussion. Therefore, the whole development has been rechecked for the case

$$z = \cos \omega_1 t \cdots t < 0,$$
$$z = \cos \omega_2 t \cdots t > 0. \quad (11)$$

In (11), both $z$ and $dz/dt$ are continuous at $t=0$, while (1) defines a function for which $dz/dt$ is discontinuous at $t=0$. Therefore, a different form of transient might be expected. Actually, (11) gives the same kind of transient; in particular, (5) remains unchanged. This shows that the phase of the carrier wave at the instant when its frequency is changed does not matter.

4. A still more general case which might be of some interest is the following one:

$$z = \sin \omega_1 t \cdots t < 0,$$
$$z = \sin (\omega_2 t + \phi_0) \cdots t > 0. \quad (12)$$

$z$ is, strictly speaking, discontinuous at $t=0$. But we may assume that $z$ changes continuously from the law which applies for $t<0$, to the one valid for $t>0$, within a time which is so short that we are not interested in the details of this transition; and thus (12) might be considered as an adequate idealization of the actual behavior. Of course, a sudden change of phase within a short time interval is equivalent to a high signal frequency, and thus a large transient may be expected. A computation along the methods used in this paper bears out this prediction.

If we want to discover what this means in practical cases, we must remember that a theory based on an idealization such as (1′) (for the amplitude-modulation

case) or (1) or (12) can only cover the influence of the receiving filter; it determines what filter bandwidth is necessary for a given type of signal, or how many channels may be located in a given frequency band. It does not determine the ability of a given communication system to transmit such signals, as we would have first to find out whether it is possible to emit the signal as given, e.g., by (1′). Therefore, our statement that (12) is less favorable than (1) means that we have to investigate the modulating method and ascertain that it does not introduce any permanent phase shifts as the modulating signal changes its amplitude.

## Appendix

### *Frequency-Modulation Transient Theory*

Consider the integral

$$J = \frac{1}{4\pi}\int_{P_1} e^{iut}\left(\frac{1}{u-\omega_1} - \frac{1}{u+\omega_1}\right)du, \qquad (13)$$

where the path of integration $P_1$ in the $u$ plane is shown in Fig. 6. It can be shown by standard methods

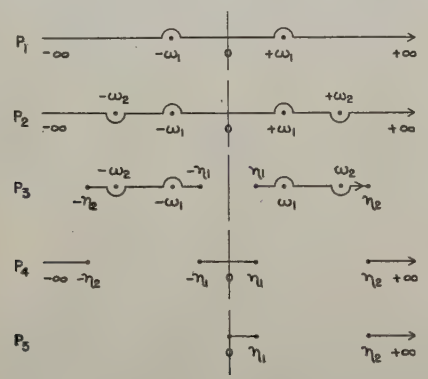


Fig. 6—Paths of integration $P_1$ to $P_5$.

that for $t>0$, $P_1$ can be transformed into a closed contour by adding a large semicircle in the upper half plane; and if this semicircle is large enough its addition will not change the value of $J$. Thus $J=0$ for $t>0$, as no singular points are enclosed by the contour. For $t<0$, we have to complete the contour by a semicircle in the lower half of the plane, and $J$ will be equal to the sum of the residues at the singular points $\pm\omega_1$. Thus

$$J = -\frac{2\pi j}{4\pi}(e^{j\omega_1 t} - e^{-j\omega_1 t}) = \sin\omega_1 t, \quad t<0;$$

the $-$ sign is due to the fact that we encircle the singular points clockwise, that is in the mathematically negative sense.

From this it follows that the incident wave assumed in (1)

$$z = \sin\omega_1 t, \quad t<0; \qquad z = \sin\omega_2 t, \quad t>0 \qquad (14)$$

can be represented by

$$z = \frac{1}{4\pi}\int_{P_2} e^{iut}\left[\frac{1}{u-\omega_1} - \frac{1}{u+\omega_1} - \frac{1}{u-\omega_2} + \frac{1}{u+\omega_2}\right]du, \qquad (15)$$

where $P_2$ is shown in Fig. 6.

We apply $z$ to the input of an ideal filter. We may neglect from the start the effect of its phase constant, as it is well known that a linear phase shift only causes a time delay in the output signal, which does not interest us. If the filter transmission range goes from $\eta_1$ to $\eta_2$, we shall get an output wave

$$y = \frac{1}{4\pi}\int_{P_3}\cdots \qquad (16)$$

where the integrand is the same as before, and $P_3$ is shown on Fig. 6. In order to avoid difficulties at the singular points, it is preferable to write

$$y = z - \frac{1}{4\pi}\int_{P_4}\cdots \qquad (17)$$

where $z$ is given by (14); for $P_4$, see Fig. 6. The bracket expression in the integrand of (15) is an even function of $u$; thus we arrive at our final expression

$$y = z - \frac{1}{2\pi}\int_{P_5}\cos ut\left[\frac{1}{u-\omega_1} - \frac{1}{u+\omega_1} - \frac{1}{u-\omega_2} + \frac{1}{u+\omega_2}\right]du; \qquad (18)$$

$P_5$, again, has to be taken from Fig. 6. The integrand splits into four parts, and $P_5$ is composed of two parts. Thus eight integrals have to be evaluated, the first of which is

$$\int_0^{\eta_1}\frac{\cos ut}{u-\omega_1}du = \int_{-\omega_1}^{\eta_1-\omega_1}\frac{\cos(v+\omega_1)t}{v}dv$$
$$= \cos\omega_1 t\int_{-\omega_1 t}^{(\eta_1-\omega_1)t}\frac{\cos v}{v}dv - \sin\omega_1 t\int_{-\omega_1 t}^{(\eta_1-\omega_1)t}\frac{\sin v}{v}dv. \qquad (19)$$

It we now introduce the sine and cosine integral[2,3]

$$\mathrm{Si}x = \int_0^x\frac{\sin x}{x}dx, \qquad \mathrm{Ci}x = -\int_x^\infty\frac{\cos x}{x}dx$$

with the properties

$$\mathrm{Si}(-x) = -\mathrm{Si}x, \qquad \mathrm{Ci}(-x) = \mathrm{Ci}x + j\pi,$$
$$\mathrm{Si}(\infty) = \frac{\pi}{2}, \qquad \mathrm{Ci}(\infty) = 0,$$

we get

$$\int_0^{\eta_1}\frac{\cos ut}{u-\omega_1}du = \cos\omega_1 t[\mathrm{Ci}(\omega_1-\eta_1)t - \mathrm{Ci}(\omega_1 t)] + \sin\omega_1 t[\mathrm{Si}(\omega_1-\eta_1)t - \mathrm{Si}(\omega_1 t)]. \qquad (20)$$

The seven other integrals can be handled similarly. If all the contributions are added together, terms like

[2] The notation follows E. Jahnke and F. Emde, "Tables of Functions," B. G. Teubner, Leipzig, Germany, 1938.
[3] E. T. Whitaker and G. N. Watson, "Modern Analysis," 1927, define Ci without the $-$ sign.

$\mathrm{Ci}(\omega_1 t)$ will be found to cancel, while in terms like $\mathrm{Ci}(\omega_1+\eta)t$ the argument may be safely replaced by $\infty$ for all interesting values of $t$. This has been checked repeatedly in numerical examples. The only terms that remain, then, are those containing differences of frequencies as arguments of the sine or cosine integral. The final formula will be given only for the case $\omega_1-\eta_1=\eta_2-\omega_2=\delta$, that is, when the interval $\omega_1 \cdots \omega_2$ lies symmetrically in the interval $\eta_1 \cdots \eta_2$. If all the integrals are evaluated and the results inserted into (18) and (14), we get

$$y = 1/2(\sin \omega_1 t + \sin \omega_2 t) + \frac{K}{2\pi}(\cos \omega_1 t + \cos \omega_2 t) - \frac{L}{2\pi}(\sin \omega_1 t - \sin \omega_2 t),$$

where

$$K = \mathrm{Ci}(\delta + 2\Delta)t - \mathrm{Ci}\delta t, \quad L = \mathrm{Si}(\delta + 2\Delta)t + \mathrm{Si}\delta t,$$

$$\Delta = \frac{\omega_2 - \omega_1}{2}. \tag{21}$$

If we write $\omega_1=\Omega-\Delta$, $\omega_2=\Omega+\Delta$, formula (2) of the paper results.

Equation (21) has been derived only for $t>0$. It is, however, possible by making the substitution $v=-u$ in (16), to show that

$$y(-t) = y(t) - \sin \omega_1 t - \sin \omega_2 t. \tag{22}$$

But the same relation follows from (21) if we simply replace $t$ by $-t$. This proves that (21) is also valid for $t<0$.

# The Characteristic Curves of the Triode*

E. L. CHAFFEE†, FELLOW, I.R.E.

***Summary***—*A method is described by which the entire static characteristic curves for the plate current of a power triode can be deduced from one experimentally determined curve. This experimental curve can be obtained at low power without danger of overheating the tube. Using the same procedure, the grid-current curves and the total space-current curves can be determined.*

*A new log-log chart is described on which the static characteristic curves of a triode are presented by means of straight lines, and two curves giving the division of space current between the grid and plate.*

THE static characteristic curves of a vacuum tube constitute the complete data from which the operation of the tube can be calculated. The complete static curves of a power tube are generally presented graphically. In fact, even if satisfactory analytical relations could be obtained for the curves, the graphical form would be the preferred form from which to make the calculations for the operating characteristics of the tube. It is simpler to draw on the characteristic chart the assumed path of operation and to read off directly the current values than to calculate them from analytical expressions for the path and the curves.

The complete static curves of large tubes cannot in general be taken by the ordinary direct-current method such as is used for small tubes because the power supplied to the tube while reading the potentials and currents in certain regions far exceeds the safe dissipation of the electrodes. The static curves must be obtained by some intermittent method[1–3] in which the potentials are applied for short intervals of time. Such methods require special apparatus which must be of sufficient capacity to supply the large currents and potentials when the curves of very large tubes are to be determined. Furthermore, the actual work of obtaining the complete characteristics of any tube is considerable because of the large number of observation points required.

One purpose of this paper is to present a simple scheme by which the complete static curves of a triode can be obtained by extrapolation from only three curves, i.e., one grid-current curve, one plate-current curve, and one total-current curve. These curves may be obtained by ordinary direct-current methods at low power. Another purpose is to describe a simplified method of presentation of the entire set of curves.

The static curves best suited[2,4,5] to the calculation of power-tube performance at radio frequencies are the constant grid-current and plate-current curves plotted with grid and plate voltages as co-ordinates such as those shown in Fig. 1. Curves of constant $i_p+i_g$ are also shown in Fig. 1 for three current values.

These total-current curves are simpler in shape, being straight over a greater range, than are the plate-current curves. They are simpler from a theoretical point of view because the total current determines the space charge between cathode and grid. It is well known that the total current can conveniently be considered as the plate current of an equivalent diode.

## Theoretical Discussion

Before discussing the general properties of the

* Decimal classification: R131. Original manuscript received by the Institute, August 27, 1940; revised manuscript received, January 8, 1942.

† Cruft Laboratory, Harvard University, Cambridge, Massachusetts.

[1] H. N. Kozanowski and I. E. Mouromtseff, "Vacuum tube characteristics in the positive grid region by an oscillographic method, PROC. I.R.E., vol. 21, pp. 1082–1096; August, 1933.

[2] E. L. Chaffee, "Power tube characteristics," *Electronics*, vol. 11, pp. 34–42; June, 1938.

[3] O. W. Livingston, "Oscillographic method of measuring positive-grid characteristics," PROC. I.R.E., vol. 28, pp. 267–268; June, 1940.

[4] I. E. Mouromtseff and H. N. Kozanowski, "A 'short cut' method for calculation of harmonic distortion in wave modulation," PROC. I.R.E., vol. 22, pp. 1090–1101; September, 1934.

[5] E. L. Chaffee, "Operating characteristics of power tubes," *Jour. Appl. Phys.*, vol. 9, pp. 471–482; July, 1938.

constant-current curves illustrated in Fig. 1, a theoretical background is useful.

The influence of velocity distribution of emission at the cathode upon the electron current through a high-vacuum tube is well known. The calculation of the space-charge distribution and the current for any ap-

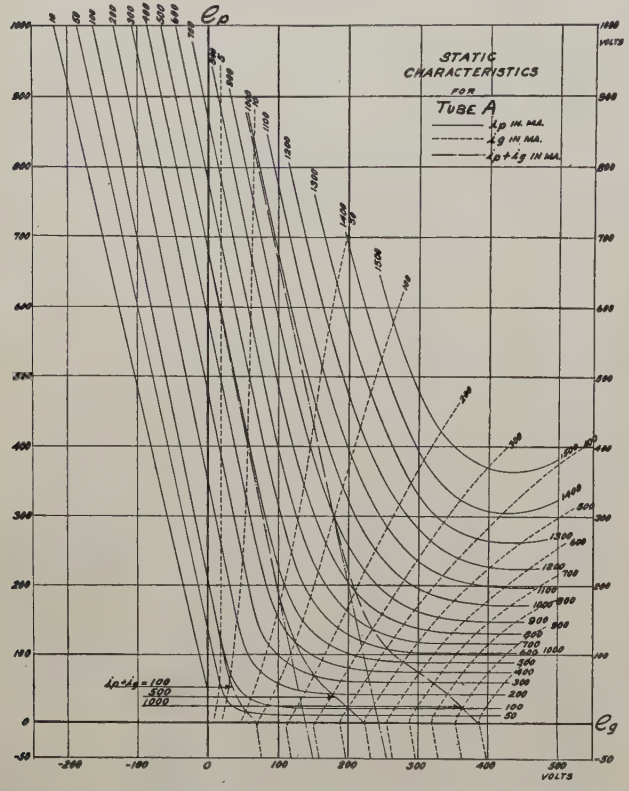


Fig. 1—Static-characteristic curves.

plied potential has been made by Epstein,[6] Fry,[7,8] and Langmuir[9] for the case of a plane diode, but the exact analysis for a cylindrical diode and for other shapes is difficult and, to the knowledge of the author, has not been completed.

The analysis of the plane diode provides the following approximate equation for the space current in amperes per square centimeter, given by Langmuir[9]

$$i=2.331\times10^{-6}\frac{(V_p-V_m)^{3/2}}{(d-x_m)^2}\left[1+1.33\left(\frac{kT}{e(V_p-V_m)}\right)^{1/2}-0.406\left(\frac{kT}{e(V_p-V_m)}\right)^{3/4}+\cdots\right]^2, \quad (1)$$

where $V_m$ is the potential at the potential minimum located $x_m$ centimeters from the cathode, $d$ is the distance from cathode to plate, $T$ is the absolute temperature of the cathode, $k$ is Boltzmann's constant, and $e$ is the electronic charge. The values of $V_m$ and $x_m$ depend upon the ratio of the space current to the saturation current of the emitter.[9]

If $i^{2/3}$ is plotted against $V_p$ for assumed values of saturation current, $T$ and $d$, the result is a line which is nearly straight except for low values of $V_p$. This plot is nearly parallel to the simple Child's equation

$$i = 2.331\times10^{-6}\frac{V_p^{3/2}}{d^2}\ \frac{\text{amperes}}{\text{centimeters squared}} \quad (2)$$

but is displaced toward negative potentials by an approximately constant distance except for low values of $V_p$ as shown in Fig. 2(a). This suggests that perhaps the space current can be expressed with an accuracy sufficient for practical purposes in the form

$$i = 2.331\times10^{-6}\frac{(V_p+V_t)^{3/2}}{d^2}, \quad (3)$$

where $V_t$ is the approximately constant voltage displacement. Comparing (3) with (1) we obtain for $V_t$ the series

$$V_t=\frac{4}{3}\frac{x_m}{d}V_p-V_m+1.78\left(\frac{kTV_p}{e}\right)^{1/2}\left(1+\frac{4}{3}\frac{x_m}{d}\right)-0.542\left(\frac{kT}{e}\right)^{3/4}V_p^{1/4}+\cdots \quad (4)$$

Equation (4) does not indicate that $V_t$ is independent of $V_p$ although it should be remembered that as $V_p$ increases, $x_m$ and $V_m$ decrease, $V_m$ being intrinsically negative. Experimentally determined graphs of $i^{2/3}$ against $V_p$ for various configurations, as shown in Fig. 3, are strikingly linear except for values of $V_p$ less than 10 or 15 volts and for values of $i_p$ approaching satura-

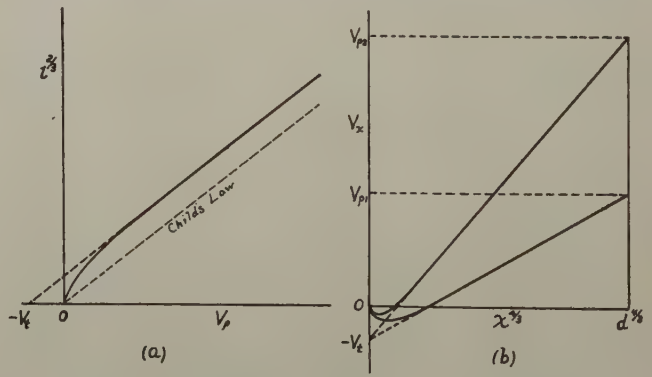


Fig. 2—Graphs of $i^{2/3}$ versus $V_p$ and $V_x$ versus $x^{4/3}$ for a plane diode.

tion current. The increase in $V_t$ as $V_p$ increases, demanded by (4) for the diode, may be compensated for by the progressive emission saturation at the cool ends of the cathode as the plate voltage is increased. The same effect may also operate to make $V_t$ nearly constant for other configurations. At any rate, some fortunate combination of circumstances operates to

[6] P. S. Epstein, "Zur Theorie der Raumladungserscheinungen," *Verh. der D. Phys. Ges.*, vol. 21, pp. 85–99, no. 5–6; 1919.
[7] T. C. Fry, *Phys. Rev.* vol. 17, pp. 441–452; April; 1921.
[8] T. C. Fry, "Potential distribution between parallel plane electrodes," *Phys. Rev.*, vol. 22, pp. 445–446; April, 1923.
[9] I. Langmuir, "The effect of space charge and initial velocities on the potential distribution and thermionic current between parallel plane electrodes," *Phys. Rev.*, vol. 21, pp. 419–435; April, 1923.

permit the effect of initial velocities to be incorporated in the one constant correction factor $V_i$. For practical purposes it is possible to express the space current for almost any configuration in the form

$$i = A(V_p + V_i)^{3/2}. \tag{5}$$

The value of $V_i$ depends upon $T$ and the geometrical relations of the electrodes. The value of $V_i$ must be determined experimentally and has a value of a few volts.

We shall now examine the value of $V$ at various distances from the cathode of a plane diode when $V_p$ is assumed constant. Child's law, giving the voltage $V_x$ at any distance $x$ from the plane cathode which emits electrons with zero velocity, is (2) when $V_x$ is substituted for $V_p$ and $x$ for $d$. Hence, $V_x$ plotted against $x^{4/3}$ is a straight line through the origin. The graph for the plane diode when initial velocities of emission are taken into account is as shown in Fig. 2(b) for two values of $V_p$. Except for small values of $x$ the line is practically straight but intersects the voltage axis at $-V_i$ corresponding to a particular value of $V_p$. Although this negative intercept is not theoretically independent of $V_p$ for a plane diode, if the experimental plot corresponding to Fig. 2(a), and shown in Fig. 3 for several cases, is straight for all values of $V_p$ except

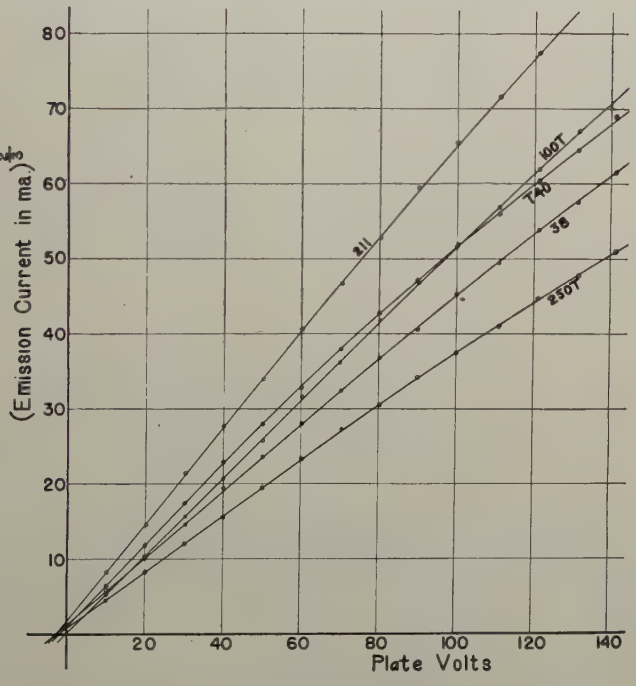


Fig. 3—Graph of $i^{2/3}$ versus $e_p$ for several commercial power tubes. $e_p = e_g$.

the low values, then the negative intercept of Fig. 2(b) for various values of $V_p$ is the same and equal to $V_i$ as shown in Fig. 2(a).

The theoretical values of the negative intercept of Fig. 2(b) for the plane diode can easily be obtained from Langmuir's $\xi$ and $\eta$ functions.[9] From Langmuir's paper we have

$$\eta_x - \eta_0 = \frac{e}{kT} V_x = \frac{11{,}600}{T} V_x. \tag{6}$$

The value of $\eta_0$ is given by the expression

$$\eta_0 = \log_e \frac{i_{sat}}{i_p} \tag{7}$$

where $i_{sat}$ is the saturation emission current.

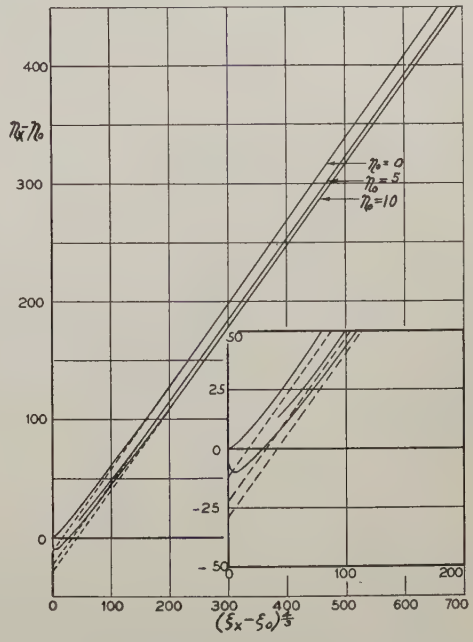


Fig. 4—Graph showing the distribution of potential within a plane diode.

Also from Langmuir's paper we can write

$$\xi_x - \xi_0 = \frac{29{,}037}{T^{3/4}} \times \left(\frac{i_p}{i_{sat}}\right). \tag{8}$$

Hence for any chosen values of $T$, $i_{sat}$, and $i_p$, $\eta_x - \eta_0$ is proportional to $V_x$, and $\xi_x - \xi_0$ is proportional to $x$. A graph of $\eta_x - \eta_0$ and $(\xi_x - \xi_0)$, as obtained from tabulated values of these functions, gives a graph of the type shown in Fig. 2(b). Such graphs, for three values of $\eta_0$, are shown in Fig. 4. These graphs are straight except for low values of $\xi_x - \xi_0$, but the negative intercepts on the voltage axis vary with $\eta_0$. We may take the values of $i_{sat}/i$ which are of practical importance to range from, say 1/3, where the linearity of the 3/2-power line begins to be affected by insipient saturation effects, down to say 1/30, below which the currents are so small as to contribute but little to the power output of the tube. This range of $i_{sat}/i_0$ corresponds to a range of $\eta_0$ from 1.1 to 3.4 as given by (7), and a theoretical range of negative intercept of from about 11.5 to 19.5. Assuming $11{,}600/T$ for a thoriated cathode to be about 6.5 and for a tungsten cathode about 4.5, the intercepts just given correspond to a $V_i$ of from 2.2 to 3 volts for thoriated cathodes, and from 3.2 to 4.3 volts for tungsten cathodes. The exact boundaries of each of these ranges are not to be

considered as exact since they depend upon the temperature at which the cathode is operated, but the extent of variation of $V_t$ corresponding to the assumed range of $i_{sat}/i$ is of significance.

The conclusion to be drawn from the preceding discussion is that, although theory for the plane diode does not support a $V_t$ which is entirely independent of $V_p$, theory does show that $V_t$ falls within a certain small range, the average value of which is different from zero and may serve as an approximate correction

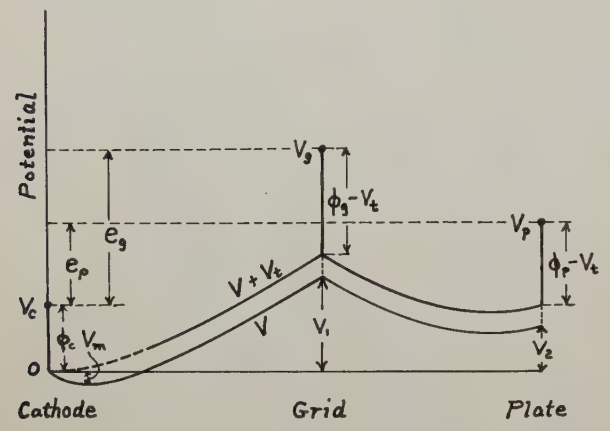


Fig. 5—Potentials within a triode.

for the effects of initial velocities of emission. Experimental results show that for various configurations of electrodes, $V_t$ may for practical purposes be taken as a constant. Then the straight lines of Figs. 2 (a) and (b) may be taken as a practicable approximation to the actual conditions, provided $V_p$ and $x$ are not small. The graphs of Fig. 2(b) would also apply to the cylindrical diode if the abscissa were the proper function of the radius. We may then write the following approximate equations for the equivalent diode:

$$\nabla^2(V + V_t) = 4\pi\rho \tag{9}$$

$$u = \rho v \tag{10}$$

$$(V+V_t)e = 1/2mv^2. \tag{11}$$

Where $V$ is the potential measured from the cathode; $\rho$ is the charge density taken as a positive quantity for electrons; $u$ is the current density; and $v$ is the velocity of the electrons. These equations give values of $V$, $\rho$, $u$, and $v$ which agree approximately with the actual values except for small values of $V_p$ and for points close to the cathode.

In effect we have replaced the actual cathode by an ideal cathode which emits electrons with zero initial velocity and dropped its potential $V_t$ volts below the potential of the actual cathode. The differences between the real and equivalent diodes are confined to a region close to the cathode. The potential sheet, current density, and space charge at points remote from the cathode are practically unchanged. It would then seem possible to apply 9, 10, and 11 to multielectrode tubes of almost any configuration by assuming the cathode replaced by the Child's cathode at a lower potential leaving conditions near the other electrodes practically unchanged.

Eliminating $\rho$ and $v$ from 9, 10, and 11 gives

$$u = \frac{1}{4\pi}\nabla^2(V + V_t)\sqrt{\frac{2e}{m}(V + V_t)}. \tag{12}$$

Suppose now that $(V+V_t)$ everywhere is changed to $(V'+V_t)=\lambda(V+V_t)$, where $\lambda$ is some constant factor. Equation (12) shows that $u'$ is everywhere $\lambda^{3/2}u$. This discussion was given by Langmuir[9,10] for the case of zero initial velocity of emission. Langmuir also shows that the paths of the electrons retain their same shape.

The general result just derived is as follows: *Within the limitations set by the approximations, the current density at every point varies as* $(V+V_t)^{3/2}$ *provided* $V+V_t$ *everywhere is altered proportionately.*

Since the total current to any electrode is the surface integral of the normal current density, the following corollary of the general theorem is evident:

*Each electrode current is altered by a factor* $\lambda^{3/2}$ *if the potential* $V+V_t$ *everywhere in the space surrounding all electrodes is altered by the factor* $\lambda$.

We must now determine how the electrode potentials $V_p$ and $V_g$ shall be varied so that the potential $V+V_t$ shall everywhere vary in the same ratio. (See Fig. 5.) Let the potential just outside the grid be $V_1$. Then $V_1+V_t=V_g-\phi_g+V_t$, where $\phi_g$ is the electron affinity of the material of the grid electrode. Let $V_g'$ be the grid potential corresponding to the condition that $V_1'+V_t=\lambda(V_1+V_t)$. But $V_1'+V_t=V_g'-\phi_g+V_t$. Thus we have

$$V_g' - \phi_g + V_t = \lambda(V_g - \phi_g + V_t). \tag{13}$$

By the same argument, the corresponding equation for the plate is

$$V_p' - \phi_p + V_t = \lambda(V_p - \phi_p + V_t). \tag{14}$$

Evidently $V_t$ acts as though $\phi_g$ and $\phi_p$ were reduced by an amount equal to $V_t$.

The potential of the space just outside the cathode has been assumed as the origin of $V$ and hence zero. The cathode potential $V_c$ is at a potential $\phi_c$ volts above zero. Hence the usual grid potential $e_g=V_g-V_c=V_g-\phi_c$. Similarly, the plate potential $e_p=V_p-V_c=V_p-\phi_c$. Substituting these expressions for $V_p$ and $V_g$ into (13) and (14) gives

$$e_g' + (\phi_c - \phi_g) + V_t = \lambda[e_g + (\phi_c - \phi_g) + V_t] \tag{15}$$

$$e_p' + (\phi_c - \phi_p) + V_t = \lambda[e_p + (\phi_c - \phi_p) + V_t]. \tag{16}$$

Denoting $[e_g+\phi_c-\phi_g+V_t]$ by an equivalent grid potential $e_{g0}$ and $[e_p+\phi_c-\phi_p+V_t]$ by $e_{p0}$, then in order that $V+V_t$ vary everywhere in the same ratio, $e_{g0}$ and $e_{p0}$ must vary so that their ratio is constant. This ratio

[10] I. Langmuir and K. T. Compton, "Electrical discharges in gases," *Rev. Mod. Phys.*, vol. 3, pp. 192–257; April, 1931. (See page 251.)

is defined as

$$L = \frac{e_{g0}}{e_{p0}}. \tag{17}$$

Hence along any line of constant $L$ the grid and plate currents vary as the 3/2 power of the voltage measured from an origin displaced from the actual origin of $e_p$ and $e_g$ by voltages $\Delta e_p = \phi_p - \phi_c - V_t$ and $\Delta e_g = \phi_g - \phi_c - V_t$, respectively. This rule may be upset if there is any considerable secondary emission from either the plate or grid, or if the path of the electrons at any point makes an angle with the lines of force much different from zero. The rule also fails if $V$ is small.

The various potentials used in the preceding equation are shown in Fig. 5 as related to an assumed potential distribution along one path in a triode. The curve for $V$ is the actual potential whereas the curve for $V+V_t$ gives the potential distribution which would give the same currents if the initial velocities were zero. This curve is shown dotted in the vicinity of the cathode because in this region the values of $V$ are too small to permit the approximations to be applied.

For all triodes the constant total-current graphs, examples of which are shown in Fig. 1, are remarkably straight and parallel over a considerable region. Within this region the total current can therefore be expressed in the form

$$i_p + i_g = B\left(e_{g0} + \frac{e_{p0}}{\mu}\right)^n, \tag{18}$$

where $B$ is a constant for any one tube and $\mu$ is the negative of the slope of the constant $i_p+i_g$ lines. The exponent $n$ is as yet undetermined.

If now in (18) we factor out $e_{p0}/\mu$, we have

$$(i_p + i_g) = B\left(\frac{e_{p0}}{\mu}\right)^n (1 + \mu L)^n. \tag{19}$$

The theoretical discussion just presented proves that if $L$ remains constant the current must vary as the 3/2 power of the equivalent plate potential $e_{p0}$. Hence $n$ must be 3/2.

The simple form of (19) applies over the region where the constant total-current lines are straight. As $e_{p0}$ decreases the graphs depart from their straight course. The reason for this departure is obvious. When $e_{p0}$ is less than $e_{g0}$ the electrons slow down as they approach the plate. The slower the electrons the greater the space charge. The increasing space charge between the grid and plate as $e_{p0}$ approaches zero acts as a shield between grid and plate and reduces that contribution to the field at the cathode caused by the plate potential. Consequently a larger plate potential is required to maintain the same total current from the cathode.

When the plate potential becomes so low that electrons are turned back, some pass through the grid toward the cathode to be again reversed in direction. Some electrons may oscillate back and forth through the grid never reaching either plate or cathode until finally they hit grid wires. This action adds to the space charge between cathode and grid. Consequently in this case *both* grid and plate potentials must be increased over those values which would give the same total current from the cathode if the space-charge distribution remained the same as for the straight portion of the constant-current curves. This condition when *both* grid and plate potentials are increased occurs only when the potential $e_{p0}$ is very nearly zero or is negative or if a potential minimum develops between grid and plate which causes the space potential somewhere in this region to be zero.

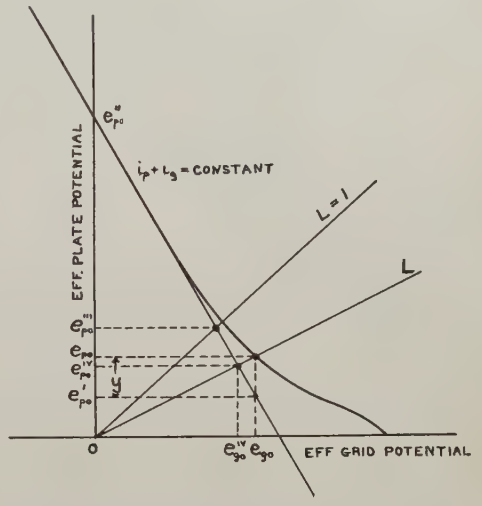


Fig. 6—Constant-cathode-current curve for a triode.

Referring to Fig. 6, $e'_{p0}$ is the plate potential for a grid potential of $e_{g0}$ which would give the assumed $i_p+i_g$ if there were no abnormal increase in space charge between grid and plate. Actually, the plate potential must be increased to $e_{p0}$ to overcome the effect of this space charge. Very often when $L$ is greater than unity, secondary emission from the plate to the grid increases this space charge and this increases $e_{p0}$.

The equation of the straight line given in (18) becomes

$$i_p + i_g = B\left(e_{g0} + \frac{e'_{p0}}{\mu}\right)^{3/2}. \tag{20}$$

Substituting $e'_{p0} = e_{p0} - y$ gives

$$i_p + i_g = B\left(\frac{e_{p0}}{\mu}\right)^{3/2}\left(1 - \frac{y}{e_{p0}} + \mu L\right)^{3/2}. \tag{21}$$

The theoretical treatment shows that the parenthesis must be a function only of $L$, hence

$$\frac{y}{e_{p0}} = f(L). \tag{22}$$

Equation (21) can be written in a slightly different

form which is better for the purposes of this discussion; i.e.,

$$i_p+i_g=B\left(\frac{e_{p0}}{\mu}\right)^{3/2}(1+\mu L)^{3/2}\left(1-\frac{f(L)}{1+\mu L}\right)^{3/2} \quad (23)$$

$$=B\left(\frac{e_{p0}}{\mu}\right)^{3/2}(1+\mu L)^{3/2}F(L). \quad (24)$$

The theoretical discussion shows that not only is $i_p+i_g$ a function only of $e_{p0}$ and $L$, but $i_p$ and $i_g$ singly

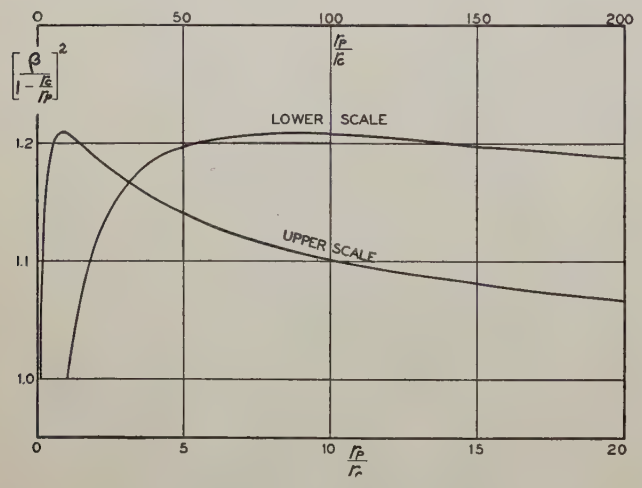


Fig. 7—Graph of $\dfrac{\beta}{\left[1-\dfrac{r_c}{r_p}\right]^2}$ versus $\dfrac{r_p}{r_c}$ for a cylindrical diode.

are also functions only of $e_{p0}$ and $L$ as indicated by the following expressions:

$$i_p = B\left(\frac{e_{p0}}{\mu}\right)^{3/2}(1+\mu L)^{3/2}F_p(L) \quad (25)$$

$$i_g = B\left(\frac{e_{p0}}{\mu}\right)^{3/2}(1+\mu L)^{3/2}[F(L)-F_p(L)] \quad (26)$$

$$= B\left(\frac{e_{p0}}{\mu}\right)^{3/2}(1+\mu L)^{3/2}F_g(L). \quad (27)$$

It follows directly that the ratio of plate current to grid current is also only a function of $L$. This law for the ratio of plate to grid current was recognized to hold approximately for the uncorrected grid and plate potentials by Tank[11] and Lange[12] nearly twenty years ago, and has been investigated by others since.[13–16] All theoretical derivations of the division of current between plate and grid neglect the effects of space charge, initial velocities of emission, and secondary emission, and assume an equipotential plane cathode for plane triodes. The results are interesting but necessarily only an approximation, especially for values of $L$ greater than unity.

The author has spent considerable effort in the attempt to express $F(L)$, $F_p(L)$, and $F_g(L)$ in empirical analytical forms. Although some degree of success has been attained the author feels that any reasonably simple analytical forms cannot be expected to fit all cases sufficiently well to justify their use, and a much better way is to express these functions graphically for each tube as will be explained later.

The constant $B$ in (25), (26), and (27), called by Kusunose[17] "perveance," comprises certain fixed constants and certain factors dependent upon the geometry of the tube. Some information about these factors can be determined by the following argument. The space current of a plane diode is given by Langmuir's expression

$$i=\frac{1}{9\pi}\sqrt{\frac{2e}{m}}\frac{e_{p0}^{3/2}}{x_{cp}^2}S_p \text{ plane diode} \quad (28)$$

where $S_p$ is the area of the plate, $x_{cp}$ is the distance from cathode to plate, and $e_{p0}$ has the same significance as in the first part of this paper. For a cylindrical diode the familiar corresponding expression is

$$i=\frac{2}{9}\sqrt{\frac{2e}{m}}\frac{e_{p0}^{3/2}l}{r_p\beta^2} \text{ cylindrical diode} \quad (29)$$

where $l$ is the length of the cylindrical plate and $r_p$ is the radius of the plate. The factor $\beta$ is the series

$$\beta=\log\frac{r_p}{r_c}-\frac{2}{5}\left(\log\frac{r_p}{r_c}\right)+\frac{11}{120}\left(\log\frac{r_p}{r_c}\right)\cdots \quad (30)$$

where $r_c$ is the radius of the cathode cylinder. Equation (29) can be written in the equivalent form

$$i=\frac{1}{9\pi}\sqrt{\frac{2e}{m}}\frac{e_{p0}^{3/2}S_p}{x_{cp}^2\left(\dfrac{\beta}{1-\dfrac{r_c}{r_p}}\right)^2}. \quad (31)$$

Equation (31) is the same as (28) for the plane diode except for the factor

$$\left(\frac{\beta}{1-\frac{r_c}{r_p}}\right)^2,$$

which is a function only of $r_p/r_c$. This factor is plotted in Fig. 7 and is seen to range between 1 and 1.21. It may advantageously be considered to be divided into $S_p$ to give an effective area as compared to the plate

[11] F. Tank, "Zur Kenntnis der Vorgänge in Elektrodenröhen," *Jahr. der Draht. Tel. und Tel.*, vol. 20, pp. 82–87; August, 1922.
[12] H. Lange, "Die Stromverteilung in Dreielektrodenröhren und Ihre Bedeutung für die Messung der Voltaspannung," *Zeit. für Hochfreguenz.*, vol. 34, pp. 105–109; April, 1928; and pp. 133–140; May, 1928.
[13] D. M. Myers, "Division of primary electron current between grid and anode of a triode," *Proc. Phys. Soc.*, vol. 49, pp. 264–278; May, 1937.
[14] B. D. H. Tellegen, "De Grootte van der Emissiestroom in een Triode," *Physica*, vol. 5, pp. 301–315; October, 1925.
[15] B. D. H. Tellegen, "De Grootte van der Roosterstrom in een Triode," *Physica*, vol. 6, no. 3, pp. 113–116; 1926.
[16] Karl Spangenberg, "Current division in plane-electrode triodes," Proc. I.R.E., vol. 28, pp. 226–236, May, 1940.
[17] Yuziro Kusunose, "Calculation of characteristics and the design of triodes," Proc. I.R.E., vol. 17, pp. 1706–1749; October, 1929.

area of an equivalent plane diode having the same distance from cathode to plate. Evidently from Fig. 7 a cylindrical diode conducts less current than a plane diode of the same plate area and $x_{cp}$.

Consider a diode having a cross section as shown in Fig. 8 (a). This may be considered as a plane diode and cylindrical diode in parallel where $x_{cp}$ is the same for each. The equivalent plane diode will have an effective plate area somewhat less than the actual area because of the cylindrical portion. If the diode is of the form shown in Fig. 8(b), we can divide the plate into various portions each of which has some factor which divided into the actual area gives the effective plate area. If the distance from cathode to plate is different for the different portions, a normal $x_{cp}$ denoted by $x_0$ can be factored out as indicated in the following equation:

$$i_p = \frac{1}{9\pi}\sqrt{\frac{2e}{m}}\,\frac{e_{p0}^{3/2}}{x_0^2}\,\Sigma\,\frac{S_p}{\left(\frac{x_{cp}}{x_0}\right)^2 f} \qquad (32)$$

where $f$ is the factor different for each portion of the plate. The sum may be an integral, but in any case the expression is made up of geometrical factors and has the dimensions of an area. It can be considered as the area of an equivalent plane diode for which the distance between cathode and plate is $x_0$. Denoting this equivalent area by $S_{p0}$, the plate current of any diode is represented by

$$i_p = \frac{1}{9\pi}\sqrt{\frac{2e}{m}}\,\frac{e_{p0}^{3/2}}{x_0^2}\,S_{p0}. \qquad (33)$$

If the tube structure is plane, it is shown elsewhere[18] that a grid and plate having potentials $e_{g0}$ and $e_{p0}$ substituted for the plate of the diode gives the same


Fig. 8—Cross section of diodes.

field at the cathode in the absence of space charge provided the distances from cathode to grid and plate, $d_g$ and $d_p$, satisfy the following equation.

$$x_{cp} = d_g\left[1 + \frac{1}{\mu}\,\frac{d_p}{d_g}\right], \qquad (34)$$

and provided $e_{p0}$ for the diode is replaced by $e_{g0}+e_{p0}/\mu$. Equation (34) is the first approximation and is sufficiently accurate in most cases when the grid wires block off only a small fraction of the total grid area.

The next step commonly taken is to postulate that if the space-charge-free field at the cathode is the same for the triode and the equivalent diode, the space current from the cathode as limited by space charge will be the same in the two cases. This step is an approximation which is good only under certain conditions. If the electrons near the cathode and as far out as the potential minimum experience the same net force in the two cases, the acceleration of the electrons and the space-charge distribution in the vicinity of the cathode will be the same. Hence the potential distribution in the vicinity of the cathode will be the same, giving the same potential minimum as illustrated in Fig. 9(a). Under this condition the current will be the same in the two cases. But the net force on an electron near the cathode is the difference of the force due to the

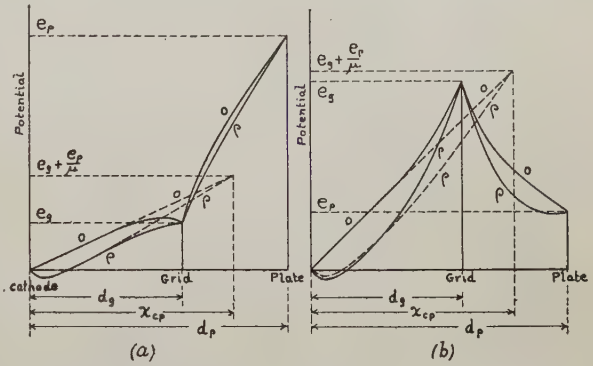


Fig. 9—Potential distributions in a triode and in the equivalent diode.
Curves marked 0—without space charge
Curves marked $\rho$—with space charge.
(a) $e_p > e_g$. (b) $e_p < e_g$.

space-charge-free potential gradient and the integral of the force from the space charge throughout the space. Although the former component of force remains constant when $e_{g0}+e_{p0}/\mu$ is the same, the distribution of space charge varies considerably, especially for low values of $e_{p0}$ when a large space charge develops between grid and plate. This condition is illustrated in Fig. 9(b), a condition when the triode current is not the same as for the equivalent diode.

Over the region where the constant $i_p+i_g$ lines are straight, that is, for values of $L$ less than about 1/2, the approximation is good as attested by the straightness of the lines, and the triode and equivalent diode give the same space current from the cathode. In this region of the characteristic curves the principal portion of the space charge is located near the cathode.

For a cylindrical structure the relation between the radii of the grid and plate cylinders $r_g$ and $r_p$ and the radius of the equivalent diode $r_d$ is given by the following approximation:[18]

$$\log\frac{r_d}{r_c} = \log\frac{r_p}{r_c}\left[1 + \frac{1}{\mu}\,\frac{\log\frac{r_p}{r_c}}{\log\frac{r_g}{r_c}}\right]. \qquad (35)$$

If a triode has the shape represented in Fig. 8(a), where it is composed of plane and cylindrical portions,

[18] W. G. Dow, "Fundamentals of Engineering Electronics," John Wiley and Sons, New York, N. Y., p. 41.

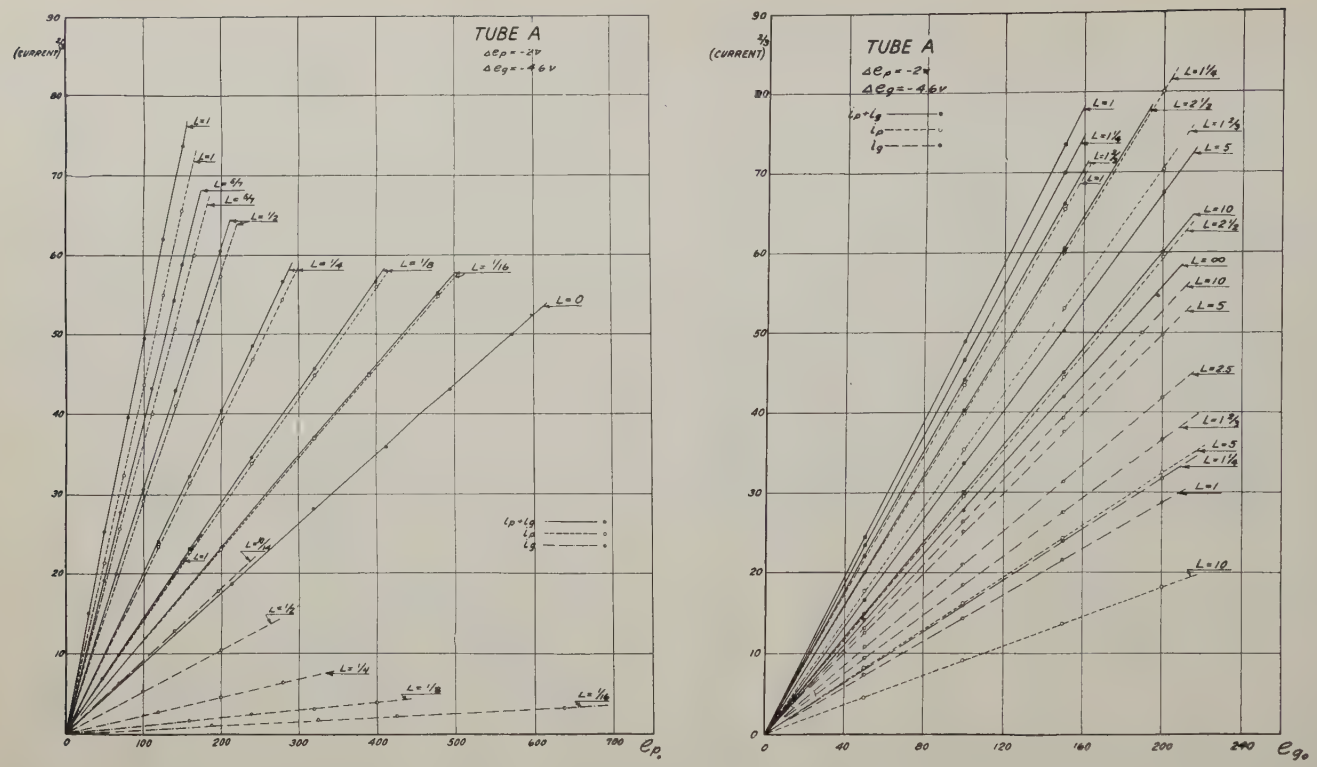


Fig. 10—Graphs of $i_p^{2/3}$, $i_g^{2/3}$, and $(i_p+i_g)^{2/3}$ versus $e_{p0}$ and $e_{g0}$ for a triode.

the distance from cathode to the equivalent-diode plate will be slightly different as calculated from (34) and (35) when the distances from the cathode to the grid and plate are the same for both portions. The cylindrical portion, however, can be reduced to an equivalent plane portion having any chosen $x_0$ by assigning the proper effective plate area.

Generally, tubes are predominantly either plane or cylindrical in structure. They can then be reduced to the equivalent plane or cylindrical diode, and the ratio between the effective plate area and the actual plate area is an interesting design factor. There is some advantage for comparison of various tubes in reducing all tubes to the equivalent plane diode as expressed by (33). The dimensionless ratio $S_{p0}/x_0^2$ is the effective plate area of a plane diode having a cathode-to-plate distance of 1 centimeter. Denote this quantity by $S_1$.

The perveance $B$, called "constant" everywhere above, in (25), (26), and (27) is related to $S_1$ by the following relation:

$$B = \frac{1}{9\pi}\sqrt{\frac{2e}{m}}S_1 \quad \text{or}$$

$$= 2.331 \times 10^{-6} S_1 \text{ (in practical units)} \qquad (36)$$

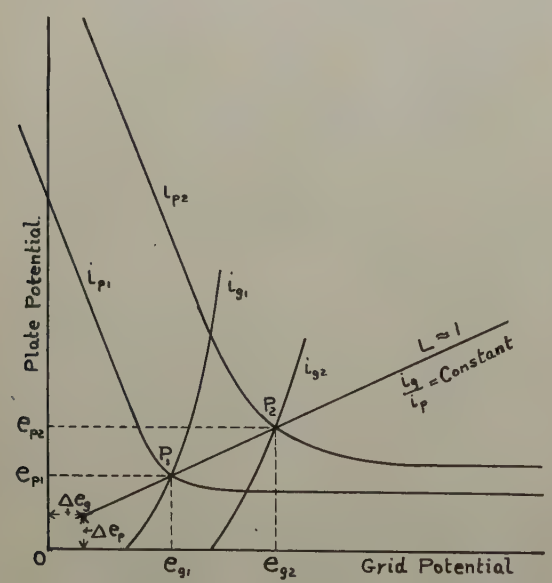


Fig. 11—Method of determining $\Delta e_p$ and $\Delta e_g$.

## Experimental Tests

The theoretical deductions given above are satisfactorily supported by experiments made on a number of tubes of plane and cylindrical form and having values of $\mu$ ranging from 4 to 25. For example, the principle that all currents vary as $e_{p0}^{3/2}$ along a line of constant $L$ is confirmed by the linearity of the graphs of the several currents raised to the 2/3 power against $e_{p0}$ as illustrated for one of the tubes in Fig. 10. The tube for these results showed no appreciable secondary emission. When secondary emission exists that part of the current contributed by secondary electrons does not follow the principle and the graphs depart from linearity.

The analytical expressions are given in terms of $e_{p0}$ and $e_{g0}$. Hence before the experimental results can be plotted the displacement of the origin by the small potentials $\Delta e_p$ and $\Delta e_g$ must be determined. These small

voltage displacements have been previously defined as follows:

$$\Delta e_p = e_p - e_{p0} = \Phi_p - \Phi_c - V_t \qquad (37)$$

$$\Delta e_g = e_g - e_{g0} = \Phi_g - \Phi_c - V_t. \qquad (38)$$

One procedure for determining $\Delta e_p$ and $\Delta e_g$ which has worked satisfactorily is the following: Since secondary emission is practically absent on the $L$ line for unity, this line is best suited to this test. The actual plate voltage $e_p$ is chosen so that when $e_g$ has the same value $i_p$ is, say, 1/25 of the saturation current. The value of $i_g$ is also measured so as to obtain the value of $i_{g1}/i_{p1}$. This point is illustrated by $P_1$ in Fig. 11.

$$\Delta e_p = \frac{e_{p_1}\left(\frac{i_{p_2}}{i_{p_1}}\right)^{2/3} - e_{p_2}}{\left(\frac{i_{p_2}}{i_{p_1}}\right)^{2/3} - 1} \qquad (40)$$

$$\Delta e_g = \frac{e_{g_1}\left(\frac{i_{p_2}}{i_{p_1}}\right)^{2/3} - e_{g_2}}{\left(\frac{i_{p_2}}{i_{p_1}}\right)^{2/3} - 1}. \qquad (41)$$

The entire static-characteristic curves such as those shown in Fig. 1 can now be represented by a very simple graph as illustrated in Fig. 12. In this diagram

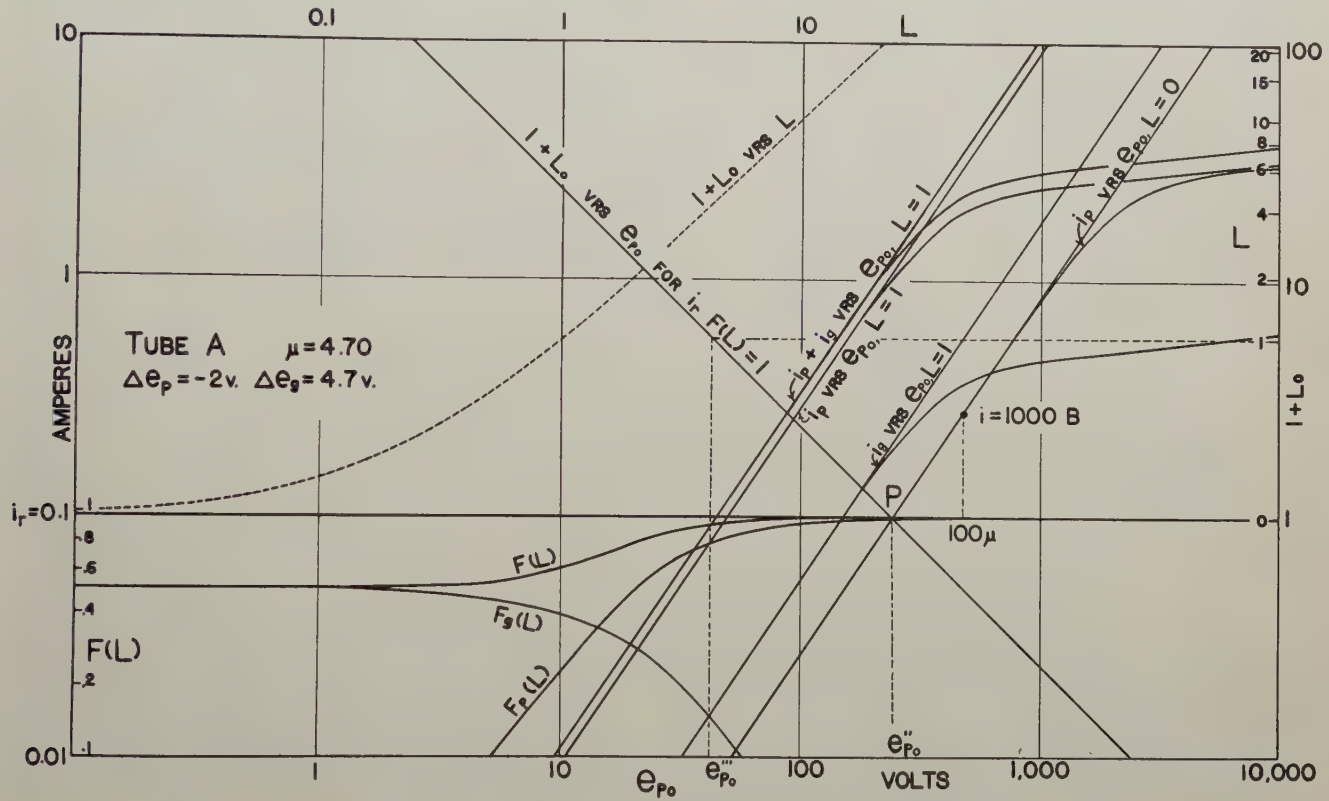


Fig. 12—Log-log chart of the static curves for tube A.

A second point $P_2$ is then determined for which $i_{g2}/i_{p2}$ is the same as for $P_1$. Since the power dissipation at the electrodes is small these measurements can be made with steady currents. If secondary emission is pronounced, lower values of $i_p$ and $i_g$ may be used to advantage.

The two points thus determined lie on a straight line which projected passes through the origin of $e_{p0}$ and $e_{g0}$. The value of $L$ for this line in general differs slightly from unity but is sufficiently near to render the effects of secondary emission inappreciable. Obviously then

$$\left(\frac{i_{p_2}}{i_{p_1}}\right)^{2/3} = \frac{e_{p0_2}}{e_{p0_1}} = \frac{e_{p_2} - \Delta e_p}{e_{p_1} - \Delta e_p}. \qquad (39)$$

A similar relation holds for the grid voltages. From these relations we obtain

the abscissa scale at the bottom gives values of $e_{p0}$ and the ordinate scale at the left gives values of $i_p$. At the right is a second ordinate scale of $1+\mu L$, or $1+L_0$ where $L_0=\mu L$. Also on this same scale the values of $L$ are marked off as shown. The value of $1+L_0$ can be determined directly from the dotted curve plotted to $L$ as read on the upper horizontal scale.

The current having the same ordinate as $L=0$ in Fig. 12 will be called the "reference current" denoted by $i_r$, and is conveniently taken as the value for the lower boundary of the decade below the decade in which saturation current falls.

Equation (24) can be expressed in logarithmic form as follows:

$$\log \frac{(i_p + i_g)\mu^{3/2}}{B} = \frac{3}{2}\log e_{p0} + \frac{3}{2}\log (1 + L_0) + \log F(L). \qquad (42)$$

If we consider first only the straight-line portions of the constant $i_p+i_g$ lines including the straight-line extensions as shown in Fig. 6 for one line, log $F(L)$ is zero. Plotting $1+L_0$ against $e_{p0}$ for a constant total space current equal to $i_r$ gives a 45-degree line as shown in Fig. 12. This line intersects the $L=0$ horizontal (log $(1+L_0)=0$) at the value of $e_{p0}$ corresponding to

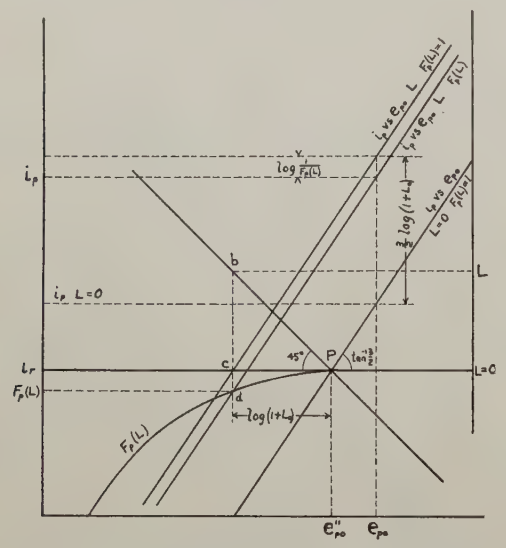


Fig. 13—Log-log chart showing use of $F_p(L)$ curve.

the intersection of the line of constant $i_p+i_g$ equal to $i_r$ with the plate-voltage axis (indicated in Fig. 6 by point $P$) at a plate potential of $e_{p0}''$. The value of $e_{p0}''$ is, by (42),

$$e_{p0}'' = \mu\left(\frac{i_r}{B}\right)^{2/3}. \tag{43}$$

This 45-degree line also passes through the point $L=1$ at a plate potential of $e_{p0}''$ as shown in Fig. 6. This point is generally a more convenient point to determine experimentally in order to locate the 45-degree line.

A straight line drawn through point $P$ and having a slope of 3/2 represents (42) when $L$ is zero and $F(L)$ is unity, and gives directly $i_p+i_g$ versus $e_{p0}$ for $L=0$. Since $i_g$ is zero because $F_g(L)$ is zero for $L=0$, this line also gives $i_p$. The intersection of this line with an ordinate at value of $e_{p0}$ equal numerically to $100\mu$ gives a value of $i_p$ which is numerically equal to $1000B$. This is the simplest way of determining the perveance $B$ from the chart. In the case of Fig. 12, $B$ comes out to be $2.7\times10^{-4}$(ampere/(volt)$^{3/2}$), giving $S_1=116$ square centimeters.

For any value of $L$ greater than zero the three functions of $L$ in (24), (25), and (27) have values other than unity or zero and their effect upon the currents must be taken into account. The explanation is made by referring to Fig. 13. The line already described, giving $i_p$ versus $e_{p0}$ for $L=0$ and $F(L)=1$, and the 45-degree line both passing through point $P$, are shown. The current for any other $L$ is obtained, according to (42), by adding to any ordinate of the line for $L=0$ and $F(L)=1$ the constant length representing 3/2 log $(1+L_0)$ and subtracting the constant length log $1/F_p(L)$. Selecting the particular value of $L$ or $1+L_0$ on the right scale, a projection line is drawn to the 45-degree line at point $b$ and then downward to the $L=0$ horizontal at point $c$. A line drawn through $c$ and having a slope of 3/2 gives the $i_p$-versus-$e_{p0}$ line for the selected $L$ but assumes $F_p(L)$ to be unity. The vertical displacement between this line and the line for $L=0$ is evidently 3/2 log $(1+L_0)$.

The vertical displacement downward of the line just obtained by the distance log $(1/F_p(L)$ is obtained by drawing a line with slope of 3/2 through point $d$, where $d$ lies on a curve for $F_p(L)$ obtained by plotting $F_p(L)$ on the special left ordinate scale against point $c$ for the value of $L$. This straight line through $d$ gives the actual plate current versus $e_{p0}$ for the constant $L$ chosen.

Curves for $F(L)$ and $F_g(L)$ are also drawn as shown in Fig. 12 and are used for determining the lines giving the variation of the particular current with $e_{p0}$ for constant values of $L$. The construction is shown in Fig. 12 for $L=1$. This is commonly called the "diode line."

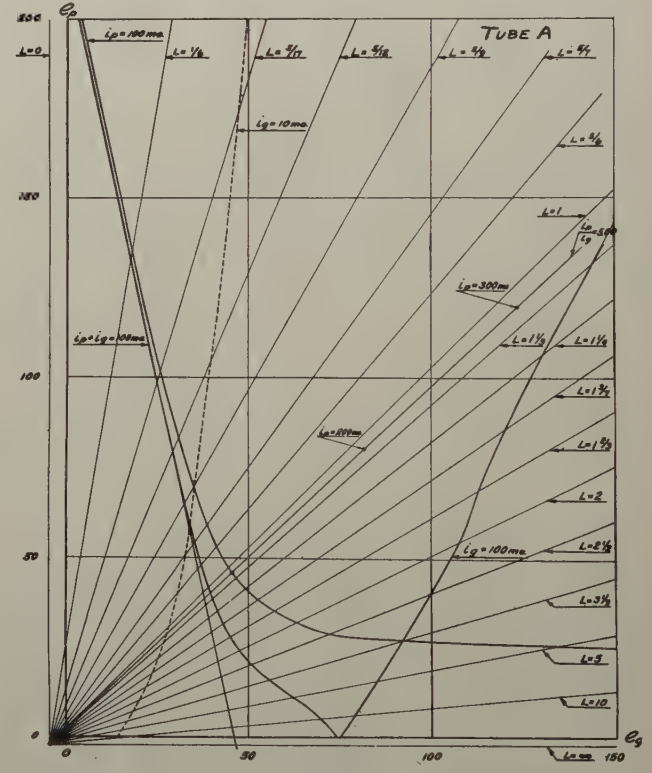


Fig. 14—Curves of constant $i_p+i_g$, $i_p$, and $i_g$ for tube A.

The entire family of plate-current characteristics of a tube is given by the chart just described if the single curve $F_p(L)$ and the point $P$ are known. Similarly the entire family of grid-current curves can be derived from the single curve for $F_g(L)$.

The experimental data for plotting a complete chart shown in Fig. 12 are easily taken. First the values of $\Delta e_p$ and $\Delta e_g$ are determined by the method described

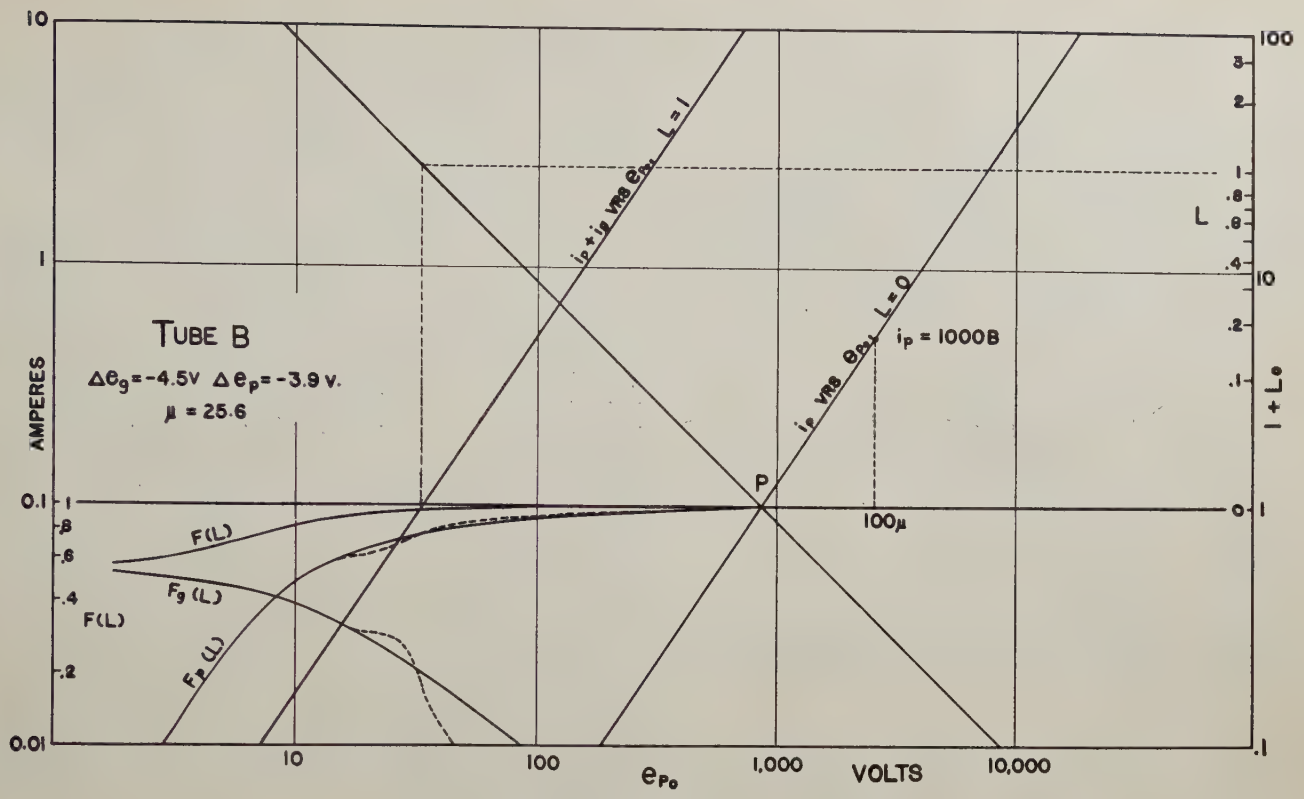


Fig. 15—Log-log chart of the static curves for tube B.

earlier although for approximate results these small corrections may be neglected or estimated. Next the constant-current curves for $i_p+i_g$, $i_p$, and $i_g$ for the value of $i_r$ are obtained and plotted as shown in Fig. 14. These data may be obtained by an instantaneous method[2] or, since $i_r$ is small, these data may be taken by the direct-current method. The cathode should be equipotential or operated on alternating current, the plate and grid return being connected to a mid-tap on the transformer. There is little difference between the data for these two conditions of the cathode except at low plate and grid voltages. There is also shown on Fig. 14 a constant-grid-current curve for $i_r/10$ which is freer from secondary emission and may be used to advantage in finding the normal shape of $F_g(L)$. The straight portion of the $i_p+i_g$ curve is extended as shown in Figs. 6 and 14. The slope of this line gives $\mu$. A number of $L$ lines are then drawn as shown in Fig. 14. The several functions can be determined by the method to be described for $F(L)$. Referring to Fig. 6, the intersections of the $L$ line with the extended $i_p+i_g$ line and the curve are determined as represented by $e_{p0}^{IV}$, $e_{g0}^{IV}$, and $e_{p0}$, $e_{g0}$. Then

$$F(L) = \left(\frac{e_{p0}^{IV}}{e_{p0}}\right)^{3/2} = \left(\frac{e_{g0}^{IV}}{e_{g0}}\right)^{3/2}. \qquad (44)$$

In case the intersection with the grid curve for $i_r/10$ is used, the value of $F(L)$ is obtained by multiplying the 3/2 power of the voltage ratio by 10. The values of the several functions are then plotted to abscissas determined by projecting $L$ from the right scale to the 45-degree line.

Normally these curves for the three functions are smooth as shown in Fig. 12. Secondary emission distorts the $F_p(L)$ and $F_g(L)$ curves in opposite directions in regions above and below $L=1$, as shown for tube $B$ in Fig. 15. Generally the functions for no secondary emission can be fairly accurately drawn in as smooth curves passing through the points for $L=1$ and joining onto the extremities of the curve. As already stated the grid curve for $i_r/10$ is much freer of secondary emission and helps to determine the correct shape for $F_g(L)$ except for very large values of $L$. Also the relation $F(L)=F_g(L)+F_p(L)$ is of assistance in determining the true shapes of these curves.

The three dots on the $L$ line slightly below the $L=1$ line in Fig. 14 are the points for $i_p=100$, 200, and 300 milliamperes used in determining the values of $\Delta e_p$ and $\Delta e_g$.

The straight lines of Fig. 12, having a slope of 3/2, obviously take no account of saturation but give the current versus $e_{p0}$ for infinite emission. If the actual space current $i_p+i_g$ versus $e_{p0}$ for a constant $L$ be plotted, a curve of the shape shown by the upper graph of Fig. 16 is obtained. Bell, Davis, and Gossling[19] point out that this curve has essentially the same shape if the temperature of the filament is reduced, as shown by the dotted line. It is, therefore, possible to obtain this curve for reduced filament current so that the electrode dissipations remain within safe limits and then move a template, cut out to fit the curve, upward

[19] J. Bell, J. W. Davis and B. S. Gossling, "High power valves: Construction, testing and operation," *Jour. I.E.E.* (London), Wireless Section, vol. 13, pp. 177–199; September, 1938.

along the 3/2-power line to the position corresponding to full emission of the cathode. Full saturation can be determined by direct measurement using some instantaneous method such as that referred to, or by calculation from the emission equation.[20]

The particular saturation curve shown in Fig. 16 is for a tungsten filament. Saturation is quite definite but incipient saturation starts at currents which may be as low as one quarter of saturation value. Bell,

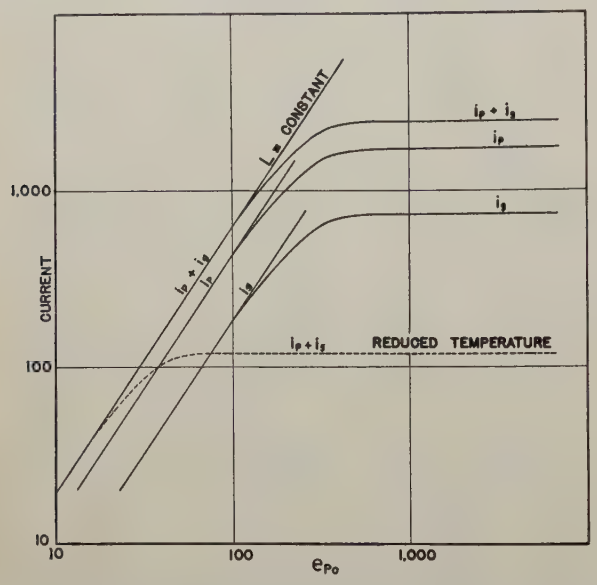


Fig. 16—Current-saturation curves for a tungsten cathode.

Davis, and Gossling explain this departure from the straight line as caused partly by local saturation or shielding of parts of the filament as in a coiled filament, and partly by the Schottky effect. It would seem then that the shape of this saturation curve would depend upon the geometry of the tube and upon the type of filament. This is true, but for any type of cathode the shape is remarkably constant. The thoriated and oxide-coated filaments show less marked saturation and often an earlier departure from the straight line as shown by the saturation curves of Fig. 12.

It is obvious that all of the $i_p+i_g$ lines for various values of $L$ must saturate at the same level of current. Hence the template for the saturation curve can be shifted *horizontally* for the various $i_p+i_g$ lines.

For any given $L$ there are three lines for $i_p+i_g$, $i_p$, and $i_g$ as shown in Fig. 12 for $L=1$. Along the straight part, the sum of $i_p$ and $i_g$ must equal $i_p+i_g$. It is evident that if the template is shifted *vertically* so as to be tangent to the three straight lines at the same value of $e_{p0}$, and so that the vertical distance between any pair of lines is the same throughout, the saturation curves thus constructed give the same division of current between plate and grid as for the straight region where the currents are space-charge limited. That the space current should divide in the same ratio in the saturation region as in the space-charge region is by no means evident but experimentally this seems to be the case at least approximately. It is of little importance, however, whether or not the same law of division holds in the saturation region because the tube is seldom used so that current reaches saturation, but the region approaching saturation is of practical importance and in this region the law of division seems to hold accurately enough for practical purposes.

A convenient scheme for reading values from the chart will now be described. The saturation curve may be drawn only on the straight line through $P$ having a slope of 3/2 as shown in Fig. 12, i.e., the line for $i_p$ versus $e_{p0}$ for $L=0$. This curve following down along the straight portion of $P$, is traced on a sheet of transparent paper or celluloid. The horizontal and vertical lines through $P$ are also traced. This tracing can then be moved so that the intersection point of the three lines is made to coincide with the point on the curve for the function of current division corresponding to the chosen value of $L$, as, for example, over point $d$ in Fig. 13 if $i_p$ along the $L$ line is desired. The vertical and horizontal lines aid in lining up the tracing.

It has been pointed out that the 45-degree line through $P$ as shown in Fig. 12 is a constant-current curve for $i_r$ assuming $F(L)$ is unity. The actual constant-$i_p$ line for the value $i_r$ can be derived by the simple construction shown in Fig. 17. The projection

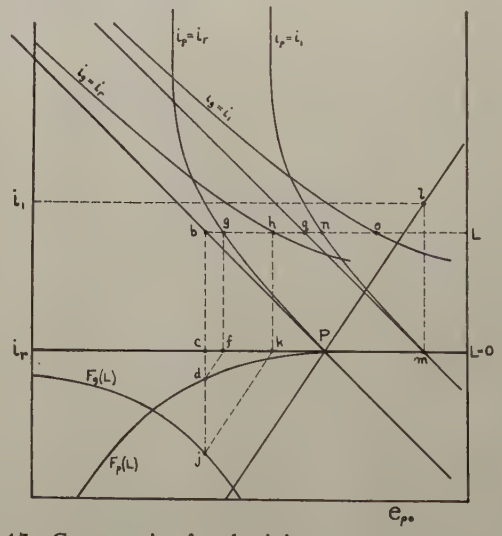


Fig. 17—Construction for obtaining constant-current lines.

from $L$ to $b$, and thus downward to $c$ and $d$, has been described with reference to Fig. 13. Now projecting from $d$ to $f$ along a line of slope 3/2, and then upward to $g$ on the horizontal to $b$ gives the actual $e_{p0}$ required for the chosen $L$ to give the plate current $i_r$. Projection from $j$ to $k$ and then to $h$, gives the actual $e_{p0}$ for a grid current of $i_r$. A continuation of this process gives curves of constant $i_p+i_g$, $i_p$, and $i_g$ for a value $i_r$ as shown in Fig. 17 and in Fig. 18 for tube $A$. For any other constant-current line such as $i_p=i_1$, projection at the $i_1$ level to $l$ on the 3/2 line through $P$ and then downward to $m$ gives the intersection point for a new 45-degree constant-$i_1$ line if $F(L)$ were unity. The actual constant-plate-current line for $i_1$ can be obtained by spacing off from the 45-degree line the distance $qn$ equal to the distance $bg$. Similarly for the grid-current

[20] I.R.E. Standards on Electronics, 1938.

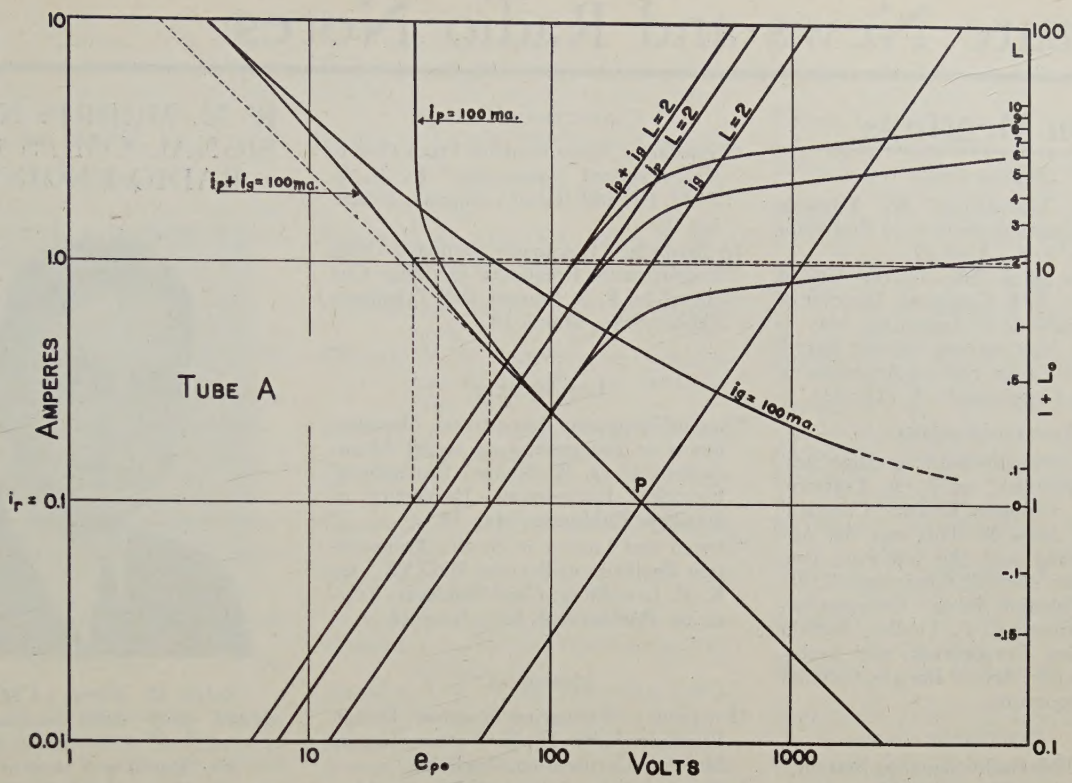


Fig. 18—Log-log chart for constant-current lines for tube *A*.

line, distance *qo* is the same as distance *bh*. It is obvious then that all of the constant-plate-current curves are obtained by moving the curve for $i_r$ horizontally the distance *Pm*. Similarly the constant $i_p+i_g$ and $i_g$ curves for other values of current are obtained by shifting the curves for $i_r$ horizontally by the proper distance. This suggests a simple scheme for deriving all of the constant-current curves. The curves shown in Fig. 18 for $i_r$ can be traced on a transparent paper and then shifted horizontally to obtain other constant-current curves. Unfortunately, however, the constant-current lines cannot be made easily to take account of saturation of the cathode.

The chart of the type shown in Figs. 12 and 15 has a number of uses. First, it can be constructed, as already suggested, from data for constant-current lines for a single value $i_r$. These data can be taken at low power. The rest of the curves can be derived from the chart, the chart furnishing an easy scheme of extrapolation. It is convenient to read off the values of current used in the calculation of tube performance without the necessity of constructing the usual constant-current curves on the $e_p-e_g$ plane. A second application of the chart is as a means of comparison of tubes. The amplification factor and the plate area of the equivalent plane diode are indicated on the chart, as already described. For example, tubes *A* and *B* whose charts are shown in Figs. 12 and 15 are of approximately the same size and have the same maximum plate dissipation of 100 watts, yet tube *B* has an effective diode plate area for 1 centimeter spacing of 221 square centimeters as compared with 116 for tube *A*. The division of current between plate and grid as it varies with *L* is shown and comparison can be made for various tubes. The values of $F_p(L)$ and $F_g(L)$ at $L=1$ is an important condition for which a comparison can be made. For example, tube *B* shows a larger fraction of current going to the grid at $L=1$ than is the case for tube *A*. The value of $F(L)$ is in general smaller for tube *A* than for tube *B* showing that the space charge which builds up between grid and plate for low values of $e_{p0}$ has more effect in reducing space current in tube *A*, as would be expected because of its lower value of $\mu$. Other uses for this type of chart may occur to the reader.

## Conclusion

In presenting the material in the charts in this paper, the results on only two tubes have been given. Actually, a great many tubes have been tested both with cylindrical and plane plates, and in every case the approximate laws given above have fitted the experimental results. As already stated, secondary emission, if present to any considerable degree, will cause deviation from the extrapolated results, so that if the data on any tube are taken at low power where secondary emission is inappreciable, the extrapolated results for higher values will be those which would exist if secondary emission were absent. The author feels that the method presented is sufficiently accurate to be of practical value.

## Acknowledgment

The author wishes to express his appreciation for the accurate and painstaking work of Dr. R. I. Sarbacher who made the observations for much of the study described in this paper.

# Institute News and Radio Notes

## Section Meetings

BUENOS AIRES

"Frequency Modulation" by Eduardo Labin, Fabrica Argentina de Productos Electricos, S. A., April 29.

"Impressions of a Trip to the United States," by A. T. Cosentino, Director of Communications of Argentina, May 8.

"Frequency Modulation—Second Part," by Eduardo Labin, Fabrica Argentina de Productos Electricos, S. A. May 22.

BUFFALO-NIAGARA

"Impedance Measurements at High and Low Frequencies" by F. A. Lidbury, President, Oldbury Electro Chemical Company, May 20. This was the Annual Meeting and the following new officers were elected: Chairman, F. H. Scheer, Colonial Radio Corporation; Vice Chairman, L. F. Fiedler, Buffalo Broadcasting Corporation; and Secretary-Treasurer, Arnold Bartels, Colonial Radio Corporation.

CINCINNATI

"The Subaudible Radio Signaling System," by Arthur Van Dyck, President, Institute of Radio Engineers, May 19.

CONNECTICUT VALLEY

"Impedance Measurements From One to One Hundred Megacycles," by R. F. Field, General Radio Company, February 19.

"A Secondary Frequency Standard Using Regenerative Frequency-Dividing Circuits," by F. R. Stansel, Bell Telephone Laboratories, March 19.

LOS ANGELES

"Radio-Frequency Impedance Measurements at Frequencies up to 60 Megacycles," by J. K. Nunan, Professor of Electrical Engineering, University of Southern California, May 19.

"Design and Layout of Studio Transmission Facilities of Station W6XYZ," by K. U. Landsberg, Chief Engineer, Television Productions, Inc., June 23.

MONTREAL

"Frequency-Modulation Receiver Design Principles," by D. E. Foster, Rogers Majestic Corporation, April 29.

Inspection Trip to Dorval Airport, May 20.

## GRIMES AND GILLIES BECOME PHILCO VICE PRESIDENTS

DAVID GRIMES

JOSEPH HARRY GILLIES

*David Grimes (A'20–M'28) was born on May 28, 1896, in Minneapolis, Minnesota. He received a bachelor of science degree in engineering from the University of Minnesota in 1919.*

*He served as chief radio officer at Kelly Field, Texas, during World War I. After the war, he joined the American Telephone and Telegraph Company as a research engineer in telephony. In 1922 he established a consulting engineering organization. In 1930 he entered the License Laboratory of the Radio Corporation of America as a license engineer and four years later, entered the services of the Philco Corporation.*

*After having charge of the home-radio-set engineering, he was appointed chief engineer in 1939. He was recently elected Vice President in charge of engineering.*

*Joseph Harry Gillies (M'37) was born in Philadelphia, Pennsylvania, on July 31, 1909.*

*In the four years before 1929 when he entered the employ of the Philco Corporation, he worked for several radio manufacturers. He was placed in charge of the Production Development Department in 1934 and became Assistant Works Manager in 1938. He was appointed Works Manager in the next year and has recently been elected Vice President in charge of radio production.*

## R. M. MORRIS NAMED SIGNAL CORPS CHIEF RADIO ENGINEER

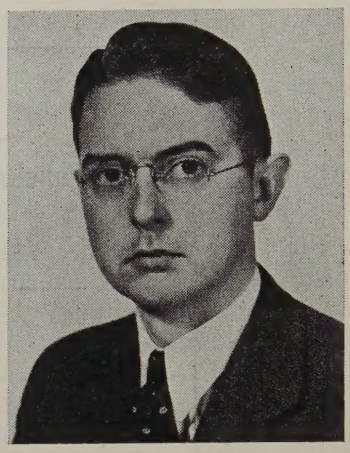

*Robert M. Morris (A'26) has been named chief radio engineer of the United States Army Signal Corps.*

*Mr. Morris was born in Washington, D. C., on January 18, 1902. He attended Western Reserve University and the Case School of Applied Science.*

*His first employment was with the Western Electric Company. In 1924, he became a member of the original staff of WEAF when that station was established by the American Telephone and Telegraph Company.*

*When the National Broadcasting Company was formed in 1927, he was named Chief Development Engineer, a title which he held until 1941 when he was made business manager of the NBC Radio-Recording Division. He is now on leave of absence to serve the Government in his new position.*

PITTSBURGH

"Lock-in Tubes for High-Frequency Applications," by W. R. Jones, Director of Commercial Engineering, Hygrade-Sylvania Corporation, May 11. Annual Meeting at which the following new officers were elected: Chairman, D. A. Myer, KDKA; Vice chairman, B. R. Teare, Carnegie Institute of Technology; and Secretary-Treasurer, A. P. Sunnergren, West Penn Power Company, June 8.

SAN FRANCISCO

"The New NBC Studios," by Messrs. Greaves, Phelan, and McIlwain, National Broadcasting Company, April 15.

"Electrical Concepts at Extremely High Frequencies" by Simon Ramo, General Electric Company, May 7.

TORONTO

"Service Problems of the Radio Industry Under Wartime Conditions." The first part was presented by L. Jackson, Canadian Westinghouse Company, and the second part by G. J. Irwin, Philco Corporation, of Canada, Ltd. This was

the Annual Meeting and the officers elected were: Chairman, T. S. Farley; Vice Chairman, R. G. Anthes, University of Toronto; and Secretary-Treasurer, L. C. Simmonds, of A. C. Simmonds and Sons, May 11.

TWIN-CITIES

"The Army Signal Corps, Its Functions and Procedure," by C. A. Jacobson, U. S. Signal Corps, May 27.

WASHINGTON

"Modern Cathode-Ray Tubes" by L. B. Headrick, RCA Manufacturing Company, Inc., April 29.

"Radio Direction Finding" by G. V. Eltgroth, Bendix Radio Division, June 8.

## Membership

The following admissions to Associate grade were approved on July 1, 1942.

Adams, E. L., Miami Valley Broadcasting Corp., Dayton, Ohio
Affias, I. M., 3339 Hull Ave., New York, N. Y.
Atkinson, C., Jr., Naval Research Laboratory, Washington, D. C.
Banthorpe, C. H., 12 Leigh Ave., Ilford, Essex, England
Bartlett, G. W., 261 Whitman St., New Bedford, Mass.
Bencan, W. L., 300 Cooper St., Camden, N. J.
Burkhalter, A. H., 2 Rector St., New York, N. Y.
Carpenter, A. G., Jr., 382 Warburton Ave., Yonkers, N. Y.
Crass, H. J., Jr., 3333 N. Marshfield Ave., Chicago, Ill.
Crooks, W. R., 8015 Leonard St., Philadelphia, Pa.
DePaul, V. A., 495 Prince Arthur W., Montreal, Que., Canada
Dossett, M. H., 857 Burlington Ave., Frankfort, Ind.
Dowdell, J. T., 16 Scott St., Utica, N. Y.
Dubbs, B., 1151 Stratford Ave., Bronx, N. Y.
Easley, R. L., 1722 Marion St., Columbia, S.C.
Ellis, C. A., 101 W. Central St., Natick, Mass.
Ellison, D. R., 3 Rod Rd., Alden, N. Y.
Espy, W. D., Ridgewood Ave., Waterford, Conn.
Gegenheimer, W. C., Box 223, Pequannock, N. J.
Gervais, W. A., International Telephone and Radio Labs., 67 Broad St., New York, N. Y.
Glaser, R. A., National Research Council, Ottawa, Ont., Canada
Hall, C. F., 1730 Highland Ave., Troy, N. Y.
Hanson, A. N., 565 N. Grant St., Hinsdale, Ill.
Hart, B. L., 101 General Heath Ave., White Plains, N. Y.
Heck, J. R., Box 91, Barrackville, W. Va
Hymans, S. J., 5046 W. Washington Blvd., Chicago, Ill.
Jacobsen, I. R., B&K Television, 190 N. State, Chicago, Ill.
Jarvis, J., 29 Forest Rd., Dumont, N. J.
Jessup, C. M., Detached 4 Communication Sq. c/o 37 Air Base Sq., Army Air Base, New Orleans, La.
Kelly, R. E., 4329 Montgomery Ave., Bethesda, Md.
Kilkenny, I., 306 E. Maumee Ave., Angola, Ind.
Lain, P. A., 224 Lyn Haven Dr., Alexandria, Va.
Lehr, P., 148-25-88th Ave., Jamaica, L.I., N. Y.
Luk, Y. K., 318 S. Market St., Troy, Ohio
Malchow, M. E., 458 Berwick Ave., Town of Mt. Royal, Que., Canada
Malone, W. H., Radio Station WGTM, Wilson, N. C.
McLean, H. H. Lakeview, Windsor Junction, N. S.
Mentzer, J. R., 11 Cedarwood Rd., Catonsville, Md.
Millen, T. I., 69 Anderson Ave., Toronto, Ont., Canada
Mills, J. E., "Officer's Mess," R.A.F. Station, Cronwell, Lincs., England
Nieter, T., 1101 College Ave., Racine, Wis.
O'Donnell, R. V., 1017 Putnam Ave., Brooklyn, N. Y.
Parker, W. E. D., "Kaygor," Worlebury Park, Weston-S-Mare, Somerset, England
Porsch, A. W., 220 W. Fourth St., Emporium, Pa.
Quade, H. G., 5211–5215 Washington Ave., Houston, Tex.
Ricks, J. B., 1236 Forest Ave., Wilmette, Ill.
Ruehl, G. C., Jr., 1 Tanglewood Rd., Catonsville, Md.
St. Petery, L. B., 1048 Dancy St., Jacksonville, Fla.
Shick, N. E., Oldfield Rd. at Lee Dr., Fairfield, Conn.
Schindler, R. W., 6813 Charles Ave., Parma, Ohio
Sloughter, G. S., 5 Catherine St., Bestal, N. Y.
Spitz, C. E., 2238 W. Jackson St., Phoenix, Ariz.
Stockman, H., Cruft Lab., Harvard University, Cambridge, Mass.
Teplany, A. J., 3626 Hildana Rd., Shaker Heights, Ohio
Vogel, W. W., 6120 Wolcott Ave., Chicago, Ill.
Walker, W. F., 1745 Catalpa Rd., Cleveland, Ohio
Warren, M., Jr., Louisville Pike, Maryville, Tenn.
Whealy, J. E., 222 Tegler Bldg., Edmonton, Alta., Canada
Wineer, W. A., 33 Maple St., Islip, L.I., N. Y.
Zurcher, L. A., Sycamore Ave., Shrewsbury, N. J.

# Contributors

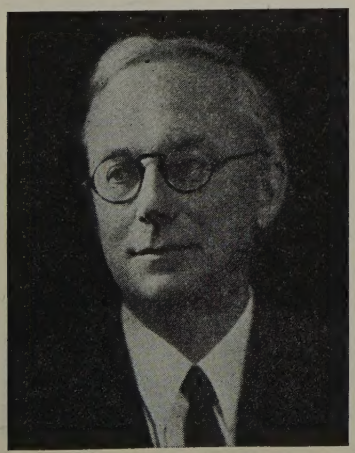

E. L. CHAFFEE

Emory Leon Chaffee (M'17–F'21) received his B.S. degree from Massachusetts Institute of Technology in 1907, and his A.M. and Ph.D. degrees from Harvard University in 1908 and 1911, respectively, He is a Fellow of the American Physical Society, American Academy of Arts and Sciences, and a member of the International Scientific Radio Union. He is Rumford professor of physics, Gordon McKay professor of physics and communication engineering, and director of Cruft Laboratory, Harvard University.

❖

George L. Haller (A'28–M'36) was born on May 8, 1907, at Pittsburgh, Pennsylvania. He received the B.S. degree in electrical engineering from Pennsylvania State College, 1927; the E.E. degree in 1934; and the M.S. degree in Physics, 1935. He was a radio engineer at KDKA from 1927 to 1929; engineer with E. A. Myers and Sons, 1929 to 1933; graduate assistant, Pennsylvania State College, 1933 to 1935. He has been with the War

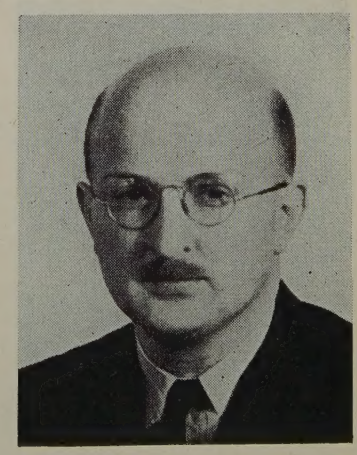

GEORGE L. HALLER

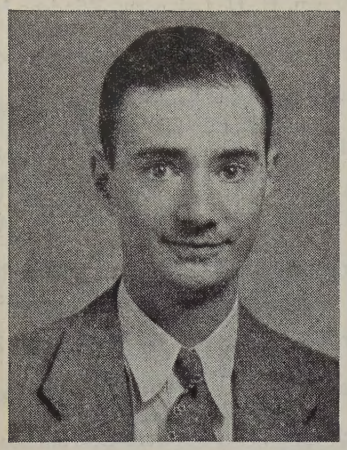

GROTE REBER

Department, Aircraft Radio Laboratory, since 1935, becoming a Major in the Signal Corps in 1942. Major Haller is a member of Sigma Xi, Tau Beta Pi, Sigma Pi Sigma, Eta Kappa Nu, and Pi Mu Epsilon.

❖

Grote Reber (A'33) was born on December 22, 1911. He received the B.S. degree from Armour Institute of Technology in 1933. He was a radio engineer for General Household Utilities in 1933 and 1934 and was with the Stewart Warner Corporation from 1935 to 1937. Mr. Reber attended the University of Chicago during 1938, and in 1939 he went with the Research Foundation of Armour Institute of Technology. He returned to Stewart Warner in 1941 to aid the war program. He is an associate member of the American Rocket Society and the Chicago Astronomical Society.

❖

Hans Salinger (A'37) was born in Berlin, Germany, on April 1, 1891. He received the Ph.D. degree from the University of Berlin in 1915. From 1919 to 1929 he was a research associate at the Reichpostzentralamt in Berlin and from 1929 to 1935, professor at the Polytechnical Institute and the Heinrich Hertz Institut für Schwingungsforschung in Berlin. From 1936 to 1942 Dr. Salinger was with the Farnsworth Television and Radio Corporation. He is an Alumni Member, University of Pennsylvania Chapter of Sigma Xi.

HANS SALINGER

❖

Charles F. Sheaffer (A'36) was born at Shawnee, Oklahoma, on December 30, 1907. Since 1923 he has been active as a radio amateur and experimenter. From 1927 to 1934 he was chief engineer of the Oklahoma Broadcasting Company. From 1934 to 1942 Mr. Sheaffer was a member of the engineering staff of the Tulsa Broadcasting Company, operators of KTUL. Since February of 1942, he has been employed as a radio engineer with the United States Signal Corps.

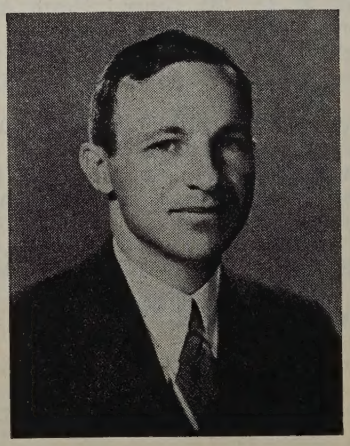

*Brown Dunkins Photo Reflex*

C. F. SHEAFFER

❖

Lynne C. Smeby (A'27–M'42) was graduated from the University of Minnesota in 1928. In 1929 he was appointed chief engineer of WRHM, now WCTN, in Minneapolis and the next year he became technical supervisor of KSTP in Saint Paul. In 1935 Mr. Smeby became technical supervisor of WXYZ, Detroit; WOOD-WASH, Grand Rapids; and the Michigan Radio Network. In 1939 he joined the International Telephone and Telegraph company and was assigned to Puerto Rico to renovate station WKAQ at San Juan, install a coastal-harbor radiotelephone system, and develop a police radio system for the Island. In December of the same year he joined the National Association of Broadcasters in the capacity of Director of Engineering, resigning in 1942 to join a civilian group working for the Army Signal Corps in Washington. Mr. Smeby is a member of the Board of Editors of the Institute of Radio Engineers and with Dr. W. L. Everitt conducted the Annual Ohio State Broadcast Engineering Conferences.

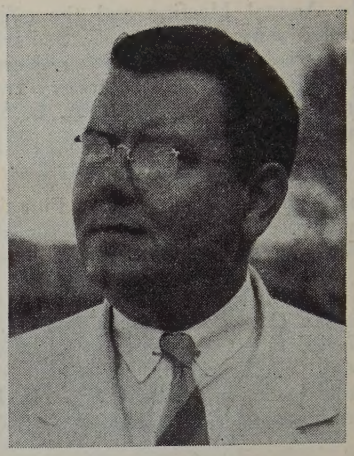

LYNNE C. SMEBY

❖

Carl E. Smith, (A'30–M'39) was born near Eldon, Iowa on November 18, 1906. He received the B.S. degree in electrical engineering from Iowa State College in 1930. From then until the summer of 1931 he was a student engineer for the RCA Victor Company, Inc., in Camden, New Jersey, and took evening postgraduate work at the University of Pennsylvania. A year of postgraduate study at the Ohio State University resulted in the M.S. degree in electrical engineering in 1932. In the summer of 1932 he joined the technical staff of the United Broadcasting Company, became assistant chief engineer in 1936, and chief engineer in 1941. In 1936 he received the professional degree of electrical engineer from the Ohio State University for research work on broadcast transmitter antenna design. In 1935 the Smith Practical Radio Institute was founded by Mr. Smith. Since then he has written all of the textbooks published by the institute. He is a member of the American Institute of Electrical Engineers, and a registered professional engineer in the State of Ohio.

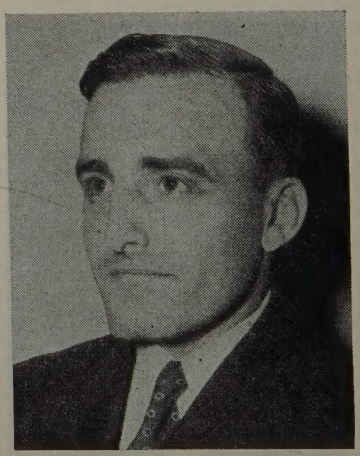

CARL E. SMITH